Alma Mater Studiorum - Università di Bologna

SCUOLA DI SCIENZE

Dipartimento di Chimica Industriale "Toso Montanari"

Corso di Laurea Magistrale in

Chimica Industriale

Classe LM-71 - Scienze e Tecnologie della Chimica Industriale

Synthesis of heteroleptic Cu(I) complexes based on quinolin-yl-1*H*-1,2,3-triazole

Tesi di laurea sperimentale

CANDIDATO

Luisa Luci

RELATORE

Prof. Letizia Sambri

CORRELATORE

Dr. Claudia Bizzarri

Anno Accademico 2017-2018

Acknowledgments

I would like to express my deep gratitude to Dr. Claudia Bizzarri, my research supervisor, for her patient guidance, motivation, enthusiastic encouragement and useful critiques of this research work. Her guidance helped me in all the time of research and writing of this thesis. I could not have imagined having a better advisor and mentor.

I would also like to thank Professor Letizia Sambri, for her advice and assistance during my internship and thesis.

My grateful thanks are also extended to Professor Stefan Bräse, who hosted me in his research group.

Special thanks also to my labmates Sophie and Dimtry for useful and constructive recommendations on this project and funny moments during my internship.

Finally, I wish to thank my parents and friends for their support and encouragement throughout my study.

Table of contents

1- Introduction

"Our Earth is like a giant spaceship which travels in the immensity of the Universe, […], Earth does not consume its energetic resource to move but needs a lot of energy to transport a large number of passengers". [1]

As we all know, the number of people in the world is increasing (see **Fig. 1**) and therefore also the global energy demand; each of us wants to reach the economic welfare but to do it we need a lot of energy. [1,2]

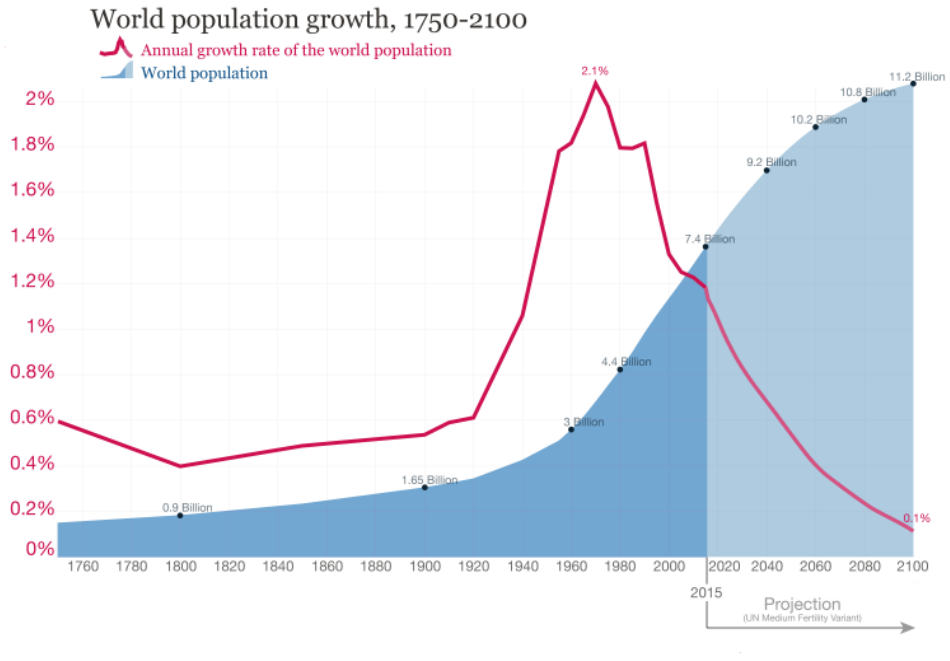

Figure 1: World population, from1750 to 2015 and projections until 2100. [2]

By now, fossil fuels provide most of the global primary energy supply. In fact, the British Petroleum Company's (BP) statistical review of global energy of June 2018 reports that the main energy sources are still oil and coal, and only a little percentage are renewable (as shown in **Fig. 2**). [3]

Moreover, world primary energy consumption grew by 2.2% in 2017. This growth was below average in Pacific Asia, the Middle East and South and Central America but above average in other regions. [3]

These sources are not eternal; it is well recognised in the scientific community that the shortage of fossil raw materials is a big problem. [1,5]

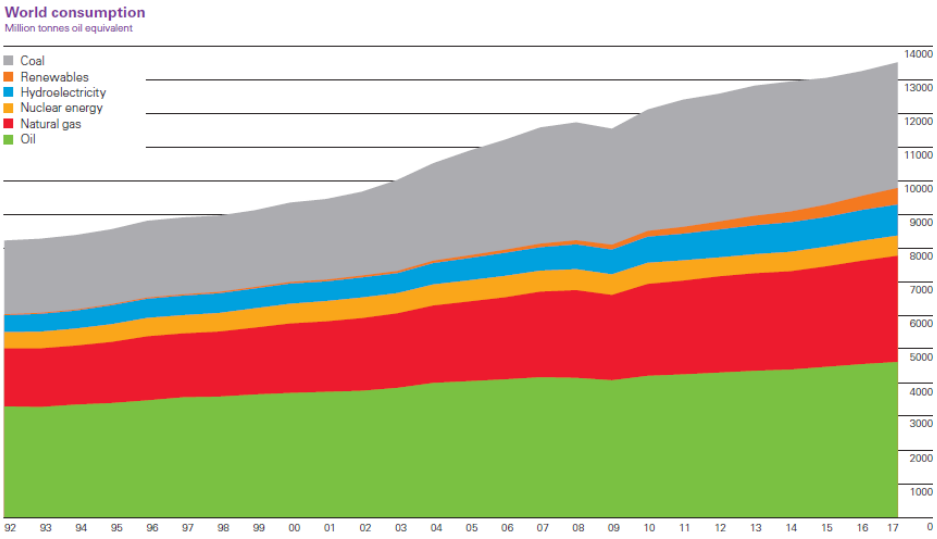

Figure 2: Global supply of commercially traded primary energy, from BP 2017. [3]

The increasing of energy consumption, in fact, is also causing the rise of carbon dioxide (CO_2) concentration in the atmosphere, recognized as the most abundant greenhouse gas, causing serious environmental problems like global climate change. [4]

Thus, an energy transition from fossil fuels to renewable fuels is necessary. Although it has been started, this transition is a long and difficult process. This need has led to an increase in research and development of renewable resources. Examples of renewable resources are: solar energy, wind, geothermal energy and water energy as tide and wave; among these the first one is by far the largest and most available.

The focus in this work is on solar energy and in particular on how to store it in the form of chemical bonds as occurs in photosynthesis.

1.1Solar energy [1,5]

Solar energy is the only inexhaustible, renewable and carbon-neutral source available on our earth and is so abundant to replace fossil fuels.

The earth surface received 90 PW in a year, while the rate of energy consumption of our civilisation is smaller (17.2 PW in 2014).

However, this energy is not always available because of the circadian cycle between day and night, the different season and weather condition; therefore, to use this energy we have to convert it into useful energy forms like electricity, heat and fuels.

1.1.1 *Natural photosynthesis* [6a,7]

Nature has always used solar energy to produce its own "fuels" through a process called photosynthesis, in plants, algae or some bacteria.

Chlorophyllian photosynthesis is a natural process used by plants to produce chemical energy using sunlight, water and CO_2. The heart of this process is the splitting of water by sunlight into oxygen and hydrogen equivalents. The oxygen is released in the atmosphere as waste, while the hydrogen equivalents are used to reduce CO_2 into sugars. The process is not easy and therefore needs different steps (see **Fig. 3**).

In the first step, the light dependent reactions take place. Inside plant cells, light is stored thanks to pigments like chlorophyll and carotenoids, which allow the plant to absorb the solar energy and to transfer it to the reaction centres, where charge separation takes place. Through a multistep redox reaction, in which water is oxidized thanks to a catalytic centre called "water oxidizing centre" (WOC), energy is transported and used to produce the energy-rich molecule adenosine triphosphate (ATP) and nicotinamide adenine dinucleotide phosphate (NADPH), which acts as hydrogen carrier.

The products of the first step are then used in the second step: the light independent reactions. Here the enzyme RubisCO captures CO_2 from the atmosphere and thanks to ATP and NADPH converts CO_2 into sugars, through a process called Calvin cycle.

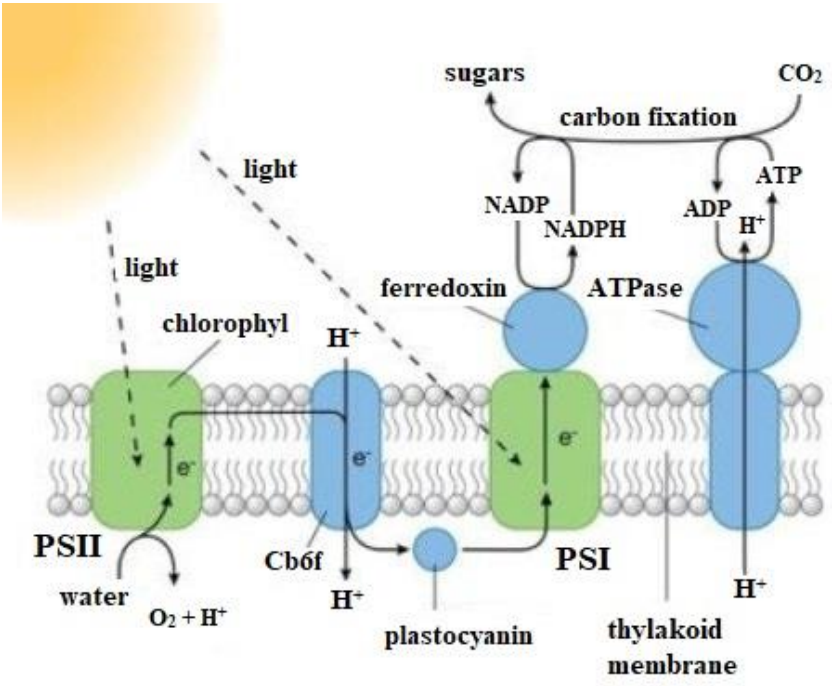

Figure 3: Schematic representation of the natural photosynthesis inside a chloroplast cell. [8]

1.1.2 *Photovoltaic* [1,5]

In the last years, photovoltaic systems have been extensively developed. These systems convert photons into electrical energy. Example of photovoltaic systems are silicon solar cell, dye-sensitised solar cells (DSSC) and organic photovoltaic (OPV). The first ones were developed 60 years ago and have good efficiency of energy conversion about 15-20%. [5] In the last 15 years the use of these systems has grown, but there are several problems that have to be overcome. For example, the problem to store and transport energy, the expensive price because of the high cost of construction. Moreover, these systems cannot be use in future since they are built with element such as In, Ga, Se which are not abundant on earth crust.

The future of photovoltaic technology may be DSSC and OPV systems, which can offer good performance, low requirement in term of raw materials and are economic and easy to recycle. Nevertheless, they are still not competitive and suffer of lower efficiency (about 8%), [5] stability and lifetime.

Photovoltaic systems seem to be a good way to reduce the use of fossil fuels, but, it is also necessary to take into account that sun light is dilute, in fact, the efficiency of the energy converted into electricity is still too low, taken into account that its power density that comes on earth surface annually is about 170 Wm^{-2}. Therefore, photovoltaics is enough to power houses with the sunlight intercepted by its roof, but not enough to power facilities with high energy-use as industries, refinery or skyscraper.

1.1.3 *Biomass* [1,5]

The end product of photosynthesis is biomass. This can be seen as a renewable fuel, easy to store and transport, that is burned to produce energy, like heating, to generate electricity or to produce bio-gas. The use of biomass is mainly localized in the undeveloped regions such as Africa and India.

Biofuels are considered carbon neutral, because return, after burning, to the atmosphere the CO_2 they used to grow. Actually, we have to consider that also the operation of harvest and transport need energy and produce CO_2, that there is no a real planned regeneration and that often the high production results in massive deforestation, with negative effect on climate. Moreover, the first generation of biomass are obtained from edible feedstock, so there is also a competition with food production.

The second generation of biofuels (from non-edible stocks) seems to give a solution, but this technology is still in its early days.

1.1.4 *Artificial solar fuels*

Fossil fuels are nothing else than products of anaerobic fermentation of the photosynthesis of millions of years ago. For that reason, they cannot be considered renewable. [5]

Instead of storing sunlight as electricity, as in the case of photovoltaics, it is possible to convert solar light into useful chemical energy. In these last years, an increasing number of scientists, inspired by nature, is engaged to search for a valuable way to use light to produce artificial solar fuels. [7,9]

In particular, the water splitting reaction of natural photosynthesis has inspired the design and the synthesis of catalyst capable of storing multiple redox equivalent and driving reaction as water splitting into molecular hydrogen and oxygen or CO_2 reduction to carbon monoxide, methanol or methane.

Since CO_2 reduction is more difficult from a kinetic point of view, [5] many scientists focused on the water splitting.

The development of this process has great importance because hydrogen seems to be the ideal renewable fuel. Hydrogen has, in fact, high energy power per mass and don't have a negative impact on environment because water is the only by-product of its combustion. Unfortunately, its application is limited for lack of technology. The use of hydrogen presents many problems for the storage, since it cannot be liquefied at ambient conditions and is highly flammable. [10]

One alternative to hydrogen could be solar fuels based on CO_2 reduction. In this case water is the best reducing agent and hydrogen donator, but reduction using molecular hydrogen is also a good method to convert CO_2 into useful product as formic acid, methanol or methane. The most efficient catalysts for this method are based on iridium (Ir), ruthenium (Ru) or rhodium (Rh). [14] The high challenge in this field is to find a good catalyst that is sensitive to the low concentration of CO_2 in the atmosphere. [5,10]

A schematic comparison between the water splitting and CO_2 reduction is shown below in **Table 1**.

Photocatalytic H_2O reduction	Photocatalytic CO_2 reduction
H_2 generation from water, single product	Low CO_2 solubility in water, more possible products
Simple mechanism	Mechanism involving several e^- and H^+ transfers
H_2 diffusing out of the liquid phase	Product in contact with the photocatalyst with decomposition
Thermodynamically uphill	Thermodynamically less favourable than H_2 production

Table 1: Comparison between H_2O and CO_2 reduction. [10]

To achieve these goals, scientists have been trying to obtain a less complicate but efficient process to produce simple fuels, once the natural photosynthetic processes are carefully studied and fully understood. [7,9]

1.2- Reduction of CO_2

Through the development of new systems for the reduction of carbon dioxide, artificial photosynthesis can be used to solve both problems, the increasing energy demand and the rise of carbon dioxide in the atmosphere.

In fact, CO_2 is not only the most abundant greenhouse gas produced by anthropogenic activities and by the use of fossil fuels, but it is also an abundant and cheap carbon feedstock.

In order to find new renewable sources and to re-establish the global CO_2 balance, we should start to see it as a resource, instead of a waste.

The challenges are high. In fact, the use of CO_2 presents some difficulties: this molecule is thermodynamically and kinetically very stable, for this reason, reduction of CO_2 requires a lot of energy. [11] Moreover, the reduction of carbon dioxide requires multistep reactions with multiple electron transfer. In fact, these methods such as electrocatalysis, photocatalysis or reduction thanks to a reducing agent can be used to convert CO_2 into carbon monoxide, formic acid, methane, methanol (at the moment only with low efficiency) depending on the final oxidation state and reaction pathway (see **Scheme 1**). These products have a higher energetic content and can be easily stored, transported and used in the existing facilities.

As said before, reduction of CO_2 is not easy, a single electron reduction of CO_2 requires a lot of energy and this is due in part to the rearrangement from a linear to a bent structure. Proton-assisted electron transfer have more favourable energies, because thermodynamically more stable molecules are produced. [12,13]

$$CO_2 + e^- \rightarrow CO^{\bullet -} \qquad E'^\circ = -1.90V.$$
$$CO_2 + 2H^+ + 2e^- \rightarrow CO + H_2O \qquad E'^\circ = -0.53V$$
$$CO_2 + 2H^+ + 2e^- \rightarrow HCO_2H \qquad E'^\circ = -0.61V$$
$$CO_2 + 6H^+ + 6e^- \rightarrow CH_3OH + H_2O \qquad E'^\circ = -0.38V$$
$$CO_2 + 8H^+ + 8e^- \rightarrow CH_4 + 2H_2O \qquad E'^\circ = -0.24V$$

Scheme 1: CO_2 reduction potentials vs NHE at pH= 7, 25°C. [13]

1.3 Photocatalytic systems

Photoactivated reduction of CO_2 uses solar energy to activate CO_2. These techniques are more attractive in terms of sustainability than the previous ones. [16] The photocatalytic systems can be distinguished between heterogeneous and homogeneous systems.

1.3.1 *Heterogenous systems* [10,17a]

There are different artificial photocatalytic systems for CO_2 reduction based on heterogeneous systems like, for example, bulk semiconductor photocatalysts based on metal oxides, sulphides or nitrides such as TiO_2 (the most used), ZnS and CdS. Since their quantum yield, selectivity and absorption in the visible light are low, their properties are improved thanks to co-catalysts based on noble metals (for example Au nanoparticles).
Other types of heterogeneous systems are the matrix dispersed photocatalysts, in which the photoactive material is linked to an inert matrix.

1.3.2 *Homogeneous systems*

Photocatalytic homogeneous systems based on transition metal complexes seem to be effective, to act selectively and with good yield in the reduction of CO_2.

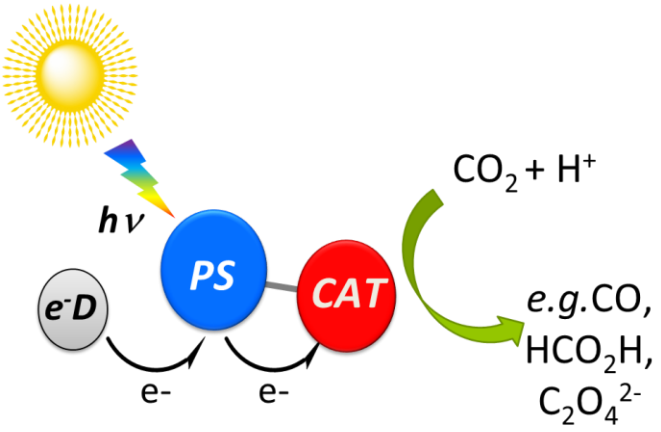

Figure 4: Schematic representation of the components of photocatalytic reduction of CO_2.

Typical photocatalytic systems for CO_2 reduction consist in a photosensitizer (PS), a catalyst (CAT) and a sacrificial electron donor (e^-D) (see **Fig. 4**). The PS absorbs light and mediates the electron transfer from e^-D to the CAT. The catalyst should gain at least two electrons to activate CO_2 and produce CO or formic acid. One of the main challenges of this field is to convert CO_2 in higher reduced molecules, like methanol or methane. [17]

It is also possible to build multinuclear systems in which the light absorber and the catalyst are the same supramolecule. [18]

The photocatalytic reactions may follow two different pathways, the reductive quenching cycle and the oxidative quenching cycle, shown below, in **scheme 2** and **scheme 3**, respectively.

In both cases the PS is promoted to the exited state.

- Reductive quenching cycle:

$$PS + h\nu \rightarrow PS^*$$

$$PS^* + e^-D \rightarrow PS^-$$

$$PS^- + CAT \rightarrow CAT^- + PS$$

$$CAT^- + CO_2 \rightarrow CAT + products$$

Scheme 2: Schematic representation of the reductive photocatalytic cycle. [17a]

The reductive quenching cycle takes place when the excited state of PS is first quenched from the electron donor; then, the reduced PS is responsible for the reduction of the catalyst, generating the active state of the catalyst and the PS back in its ground state. The CAT is now

able to bind CO_2 and to proceed with the catalytic mechanism to release the product and regenerate the catalyst.

- Oxidative quenching cycle:

$$PS + h\nu \rightarrow PS^*$$
$$PS^* + CAT \rightarrow CAT^- + PS^+$$
$$CAT^- + CO_2 \rightarrow CAT + products$$
$$PS^+ + e^-D \rightarrow PS$$

Scheme 3: Schematic representation of the oxidative photocatalytic cycle. [17a]

In the oxidative quenching cycle, the excited state of the PS undergoes electron transfer process directly with the CAT. The remaining oxidized PS species (PS^+) will then be reduced back to PS by the sacrificial electron donor.

1.3.3- *Catalyst*

The catalyst should be stable and highly sensitive to the CO_2 gas, also in low concentration like the atmospheric one. Example of good catalysts based on earth abundant metals for CO_2 reduction are conjugated metallomacrocycles such as corrins, corroles, porphyrins with a Co or Fe centre, Co(III) or Ni(II) macrocycle such as (Ni(cyclam)), where cyclam is 1,4,8,11-tetraazacyclotetradecane, as depicted in **Figure 5**. [11,17a]

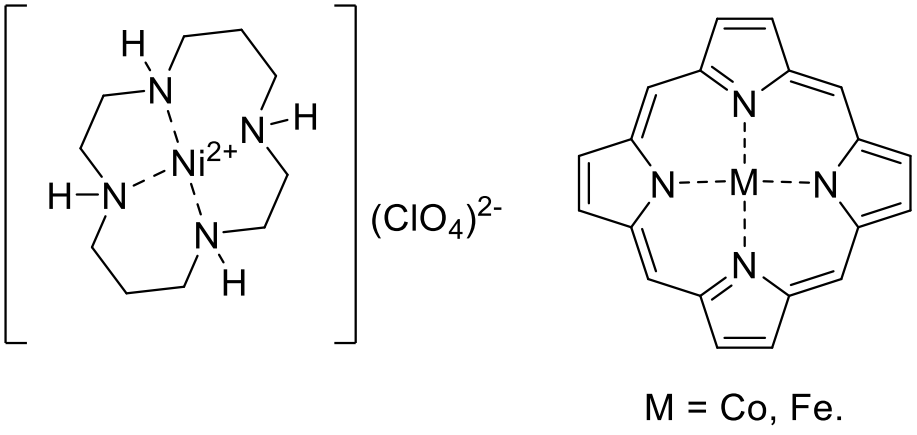

Figure 5: Structure of examples of catalyst for reduction of CO_2.

It has been shown that iron porphyrins can act as PS and CAT at the same time and are among the most efficient for the reduction of CO_2 to CO, with turnover numbers (TONs) up to 30 and catalytic selectivities (CSs) to CO of 85%. [19]

1.3.4 *Sacrificial Electron donor*

The sacrificial electron donor provides the required electrons and has the right redox potential to easily reduce the PS or the CAT.

As e^-D can be used triethylamine (Et_3N), triethanolamine (TEOA) or ascorbic acid (see **Fig. 6**). [6a]

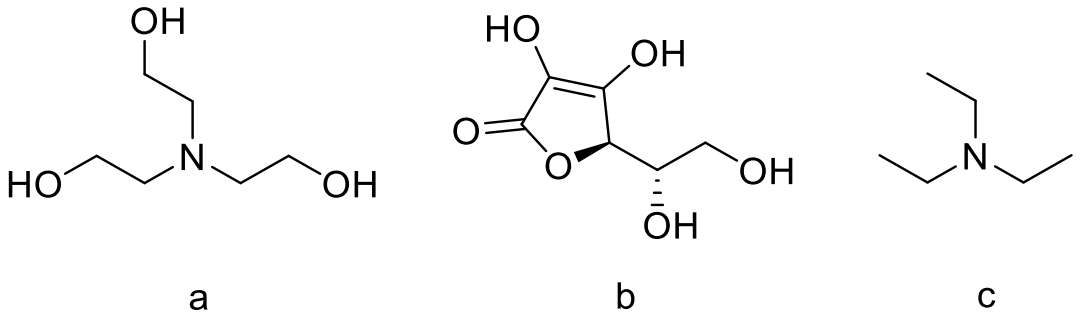

Figure 6: Structure of possible sacrificial electron donor: **a**) triethanolamine, **b**) ascorbic acid, **c**) triethylamine.

1.3.5 *Photosensitizer*

A good photosensitizer should have a higher absorption at a particular wavelength in the visible region than the other species of the system, a long-lived excited-state lifetime and high photostability. [20]

It is well known that there are good photosensitizers based on ruthenium [20] or iridium complexes with polypyridine ligands. Although they work well, now the research trend is to find good PS based on less expensive and easily available complexes, based on earth abundant metal centres, such as copper, zinc, cobalt, nickel. [21]

The first CO_2 photocatalytic reduction example was published by Lehn and co-workers in the 80's. They used $[Ru(bpy)_3]Cl_2$ as photosensitizer, where (bpy) is 2,2'-bipyridine (structure in **Fig. 7**), $CoCl_3$ as catalyst and triethanolamine (TEOA) as sacrificial electron donor in aqueous solution, this system showed a quantum yield (Φ_{co}) of 0.012.[6a,11]

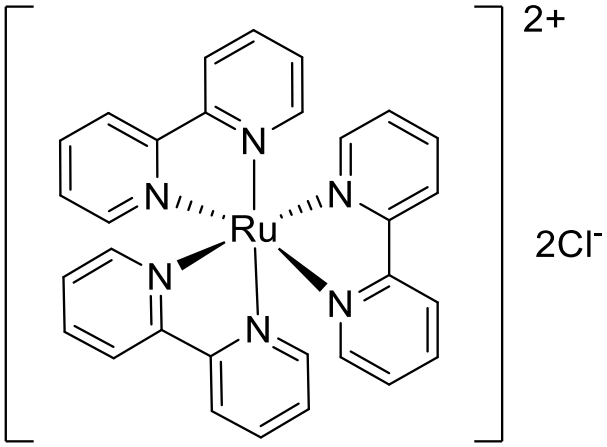

Figure 7: Chemical structure of $[Ru(bpy)_3]Cl_2$.

Some years later, the same group used $[Re(bpy)(CO)_3Cl]$as PS and as CAT, since it absorbs visible light and allows the catalytic reduction of CO_2 with Φ_{co}=0.14 and good selectivity. [6a] The main problem of this system is that this molecule absorbs mostly in the UV region (λ_{exc} = 355 nm). [6b] For realistic applications, such as utilization of solar photons, absorption in the visible region is desired; therefore, other studies were done in order to increase the absorption in visible light. Ishitani and co-workers have used a bridging ligand to covalently attach the catalyst to $[Ru(bpy)3]^{2+}$ photosensitizer, which absorbs strongly in the visible, in order to create a supramolecular dyad complex. [6a,11] These dyads exhibited significantly better performance than the previous one with Φ_{co}= 0.12 high selectivity, [6a] but they show low activity and easily decomposition. [10,11]

More and more scientists have been studying the development of new photocatalytic systems with a practical utility, in which the PS is based on earth abundant metal-complexes, supporting large-scale fuel production. [21]

In this area, Cu(I) complexes seem to be a good alternative to Ru(II). [13,22] Showing interesting emission properties these complexes find already application as component in organic light-emitting diodes (OLEDs) [23] and light-emitting electrochemical cells (LECs). [24] It has already been shown that they act as good photosensitizers for hydrogen generation from water as well as photo-redox catalysts in organic reactions. [25]

The aim of this work is to follow this route to design and synthesise new PS based on Cu(I) complexes for the photocatalytic reduction of carbon dioxide.

1.4 Copper

Copper is a transition element in the 11th group of the periodic table, [Ar] $3d^{10}4s^{1}$.

It forms a rich variety of compounds usually with oxidation number +1 and +2. For their photochemical and photophysical properties, Cu(I) complexes are of great interest in this scope. The behaviour of Cu(I) complexes is due to their closed shell electronic configuration, the full d orbitals (d^{10}) bring to a symmetric delocalisation of the electronic charge favouring the tetrahedral symmetry in order to minimize electrostatic repulsion. This configuration does not permit d-d metal centred electronic transition (MC), which are non-emissive. Such transitions are permitted in Cu(II) complexes (d^{9}), which often have square planar geometry, causing strong absorption in the visible region. [26]

Anionic Cu(I) complexes do not show particular photophysical properties, while cationic ones show an interesting behaviour. In fact, the latter exhibit luminescence originating from metal-to-ligand charge transfer (MLCT) state, when empty π orbitals are easily accessible, with high molar extinction coefficient (ε), long lifetime (τ), intense luminescence. [26]

First studies of Cu(I) complexes were done in the 1970's regarding $[Cu(phen)_2]^+$ and its derivatives, where (phen) is 1,10-phenanthroline,[27] having Cu(I) a strong tendency to bind those ligands. Cu(I) complexes of this type generally have distorted tetrahedral geometries and prefer to adopt a D2 structure (as shown in **Fig. 8**), depending on size, chemical nature and position of the substituents. [27,28] These complexes absorb in the UV region by intense ligand-centred (LC) transition and have moderate absorption in the visible area, due to MLCT transitions. Nevertheless, improvement of the photoluminescence quantum yield is not easy.[28]

After excitation of the electronic ground state of this kind of complexes, the lowest ^{1}MLCT state is populated, this excited state can relax to the ground state by radiative decay, with emission of radiation (fluorescence), or undergo, by a non-radiative decay, an intersystem crossing (ISC) to the triplet excited state ^{3}MLCT, where phosphorescence can take place.[29]

From the ground state to the excited state the metal changes its formal oxidation state from I to II (see **scheme 4**), with a d^{9} electronic configuration, which undergo a pseudo Jahn-Teller (PJT) distortion with a more flattened structure (see **Fig. 8**). [30]

$$[Cu(I)(L)(L)]^+ \rightarrow [Cu(II)(L^-)(L)]^+$$

Scheme 4: Schematic representation of ground state and excited state of Cu(I) complexes. [29]

Therefore, the Cu(I) excited complex geometry is more similar to a Cu(II) complex. According to the mechanism proposed by McMillin and co-workers [31] flattening distortion create a more accessible metal centre, with the 5th coordination site on the axial position available to possible nucleophilic attack (as depicted in **Fig. 8**) from donor solvents, such as acetonitrile (ACN), *N*,*N*-dimethylformamide (DMF) and methanol (MeOH), or from counterions, such as ClO_4^- and NO_4^-, causing a minor excited state lifetime. [32]

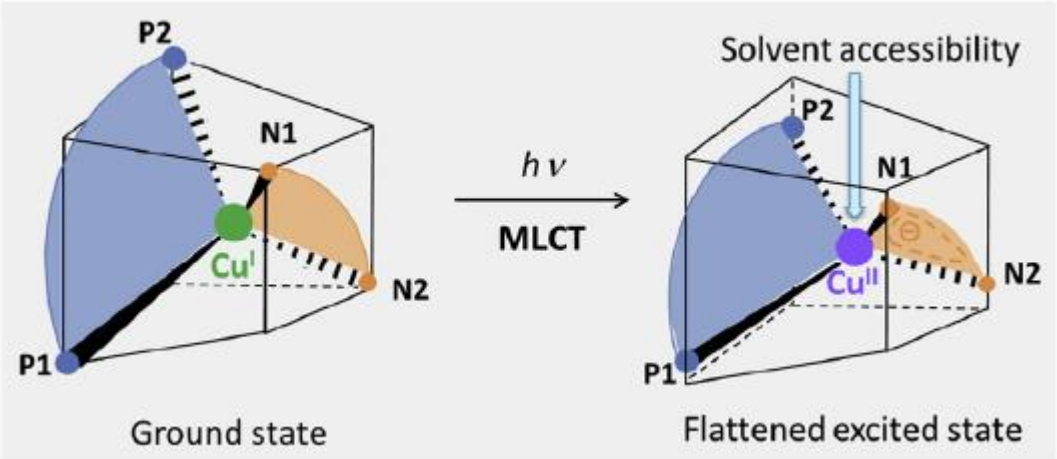

Figure 8: Geometry of the ground state and exited state of Cu(I) complexes. [29]

To suppress this flattening motion, several studies have been reported. [32]

Studying homoleptic and heteroleptic Cu(I) complexes (structures in **Fig. 9**) was found that access to the 5th coordination site is more difficult if the substituents have high steric hindrance, leading to an increase of the photoluminescence quantum yield (PLQY) and luminescence lifetime. [30] Examples of heteroleptic Cu(I) complex are $[Cu(N\hat{}N)(P\hat{}P)]^+$ where (N^N) represents diimine chelating ligands and (P^P) diphosphine chelating ligands.

Phosphines have been always used with transition metal complexes for organic catalysis thanks to their sterical and electronical properties. In fact, these ligands are able to stabilize the tetrahedral geometry and destabilize the square planar coordination in the excited state. [32] Moreover, the phosphines can act as Lewis σ base and donate the lone-pare on the phosphine to the metal centre and but also as π acceptors ligand through back bonding (stronger for phosphine with aril group). [33,34]

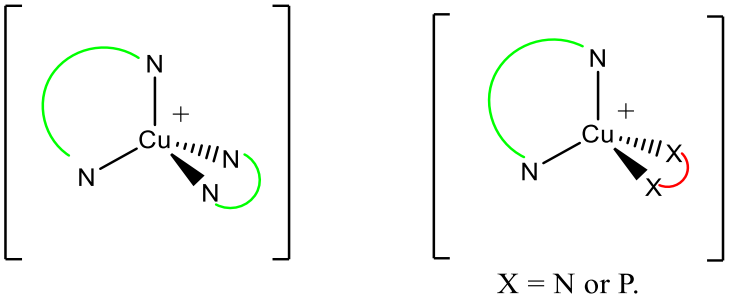

Figure 9: Chemical structure of homoleptic (left) and heteroleptic (right) Cu(I) complexes. [29]

Moreover, heteroleptic copper (I) complexes show an improvement in the emission properties: great emission energy and longer exited state lifetimes. However, since the excited state of these complexes is a ^{3}MLCT state, they are strongly dependent on solvent and oxygen, in fact, oxygen has a triplet ground state which, for the process of "triplet-triplet annihilation", can cause quenching of the emission. [35,36]

To optimize photoluminescence then, it is necessary to have ligands with steric hindrance and electron withdrawing properties. Bulkier ligands cause a less distorted excited state, therefore, an increment of the radiative rate. However, the use of too bulky ligands can cause the opposite effect for the strong ligand-ligand repulsion, and lead to dissociation in solution forming the less constrained homoleptic species. [27,37]

Excitation of $[Cu(N\hat{}N)(P\hat{}P)]^+$ complexes can follow an ultra-fast PJT distortion from the ^{1}MLCT state to the ^{1}MLCT flattened state (see **Fig. 10**) [38]. The deactivation to the ground state can follow radiative or non-radiative decay. The ISC from ^{1}MLCT flattened state to ^{3}MLCT state occurs on a long-time scale compared to Ru or Ir complexes; this process is faster if the geometries of the ^{1}MLCT flattened state and of ^{3}MLCT are similar.

Thermal activated delayed fluorescence (TADF) is observable for these complexes, [39] in fact, when the energies of ^{1}MLCT and ^{3}MLCT state are similar, even at room temperature, the thermal energy is enough to overcome the energy gap and a reversed ISC can occur. Nevertheless, when the temperature is decreased to 77K (or lower) the thermal energy is not enough and the emission comes only from the ^{3}MLCT, at lower energy. Reducing the temperature, in fact, the absorption bands become tight, low emission intensity with bathochromic shift are observed. [39]

The excited state of heteroleptic Cu(I) complexes can be influenced by the nature of the ligand, the temperature, solvents and counter-ions.

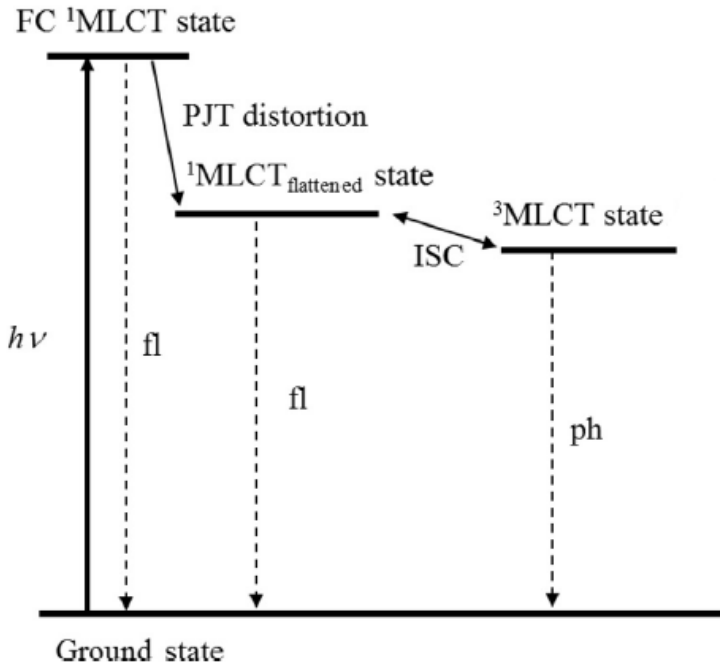

Figure 10: Jablonski diagram for $[Cu(I)(N\hat{}N)(P\hat{}P)]^+$ complexes. [29]

Solvent induced quenching is extinguished by the crowded structure around the metal centre. The introduction of larger and rigid phosphine ligands with high steric hindrance, such as DPEphos, Xantphos (see **Figure 11**), by McMillin and co-workers [40] limited ligand dissociation and quenching by the solvent molecules. It was suggested that this is the case because there is the possibility that also the the oxygen atom present in these P^P forms a weak coordinative bonding with copper. Therefore, this kind of complexes presents a high PLQY, a strong and long-lived emission, even in donating solvents and high stability. [41]

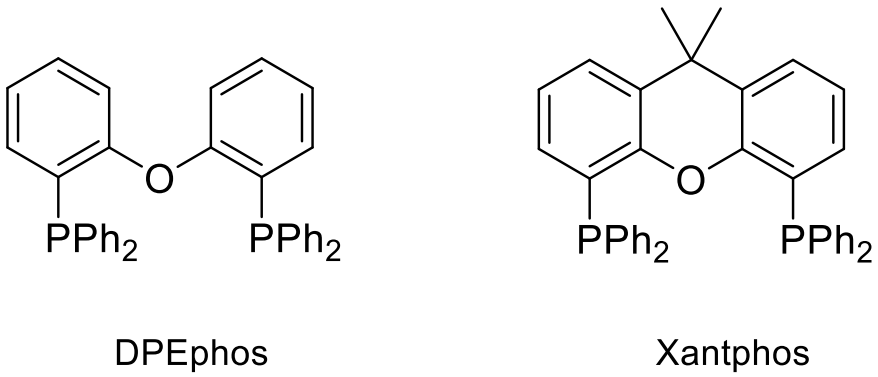

Figure 11: Chemical structure of possible bulky diphosphine-ligands.

Also, sterically demanding diimine ligand can increase the PLQY and luminescence lifetime and increase the absorption in visible light. [42]

Moreover, Cu(I) complexes show a higher photoluminescence quantum yield in the solid state than in DCM solution. Inhibition of the flattening distortion decreases the rate of non-radiative decay and the quenching from counterions is completely stopped.

1.5- Triazole: synthesis and application.

The aim of the thesis is to prepare suitable PS, based on heteroleptic Cu(I) complexes, and enhance their luminescence properties using bulky ligands. As chelating N^N ligand quinolin-yl-1*H*-1,2,3-triazole were studied; these ligands are interesting not only for their sterical properties but also for the easy and cheap way of synthesis.

Organic azides have reached considerable interest; in particular, when industries began to use azides for the synthesis of heterocycles such as triazoles and tetrazoles. In fact, aromatic azides are versatile intermediates with many applications in organic and bioorganic chemistry, such as for example dyes, fluorescent whiteners, photostabilizer of polymers and corrosion inhibitor. [43]

Most azides can be explosive, especially those of low molecular weight. These substances decompose with the release of nitrogen through energetical input as for example pressure, impact, or heat. Therefore, sometimes they can be difficult to handle.

Between the triazoles particular interest is in 1,2,3-triazole: these rings are robust systems that are easily to prepare and functionalize.

In this work the focus was on 1,4-disubstituted-1,2,3-triazole and 4,5-disubstituted-1,2,3-triazole, as shown in **Figure 12**.

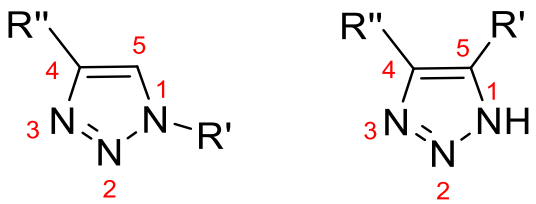

Figure 12: Structure of 1,4-disubstituted (left) and 4,5-disubstututed (right) triazole. [44]

Triazoles with unsubstituted ring nitrogen atom have special interest, in fact, they can form charged or neutral Cu(I) complexes.

They have three thermodynamically stable tautomers (see **Fig. 13**). They exist in equilibrium in solutions and have very close values of Gibbs energy. [45] Experimental and theoretical studies indicated that the first tautomer, 1*H*-isomer, is more stable in solution, while 2*H*-isomer is more stable in gas phase. [46]

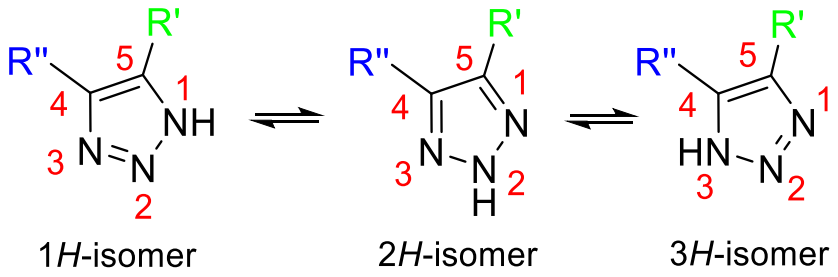

Figure 13: Tautomers of 4-5-disubstituted-1,2,3-triazole, with R' different from R''. [44]

1,3-Dipolar cycloaddition of substituted azides to alkynes is a common approach to obtain 1*H*-1,2,3-triazoles. Huisgen was the first one to establish mechanistic details of this reaction. [47]

1.5.1 *Thermal 1,3-Dipolar Cycloaddition of Azides to Alkynes: Huisgen reaction.*

Although, thermodynamically, the cycloaddition of alkynes to azides is exothermic, the high activation barrier is responsible for the low reaction rate, which implies that the reaction should be performed at high temperatures. [44]

A general procedure is to heat the reactants at reflux in toluene, benzene, or alcohols, or to heat them in DMF or dimethyl sulfoxide (DMSO). A disadvantage of this method is that high temperatures shift the thermodynamic equilibrium, which often leads to a mixture of the two regioisomers (1,4 and 1,5-disubstituted-1,2,3-triazole, see **Fig. 14**) when using asymmetric alkynes. [48] The regioselectivity strongly depends on electronic and steric effect of the substituents on the alkyne.

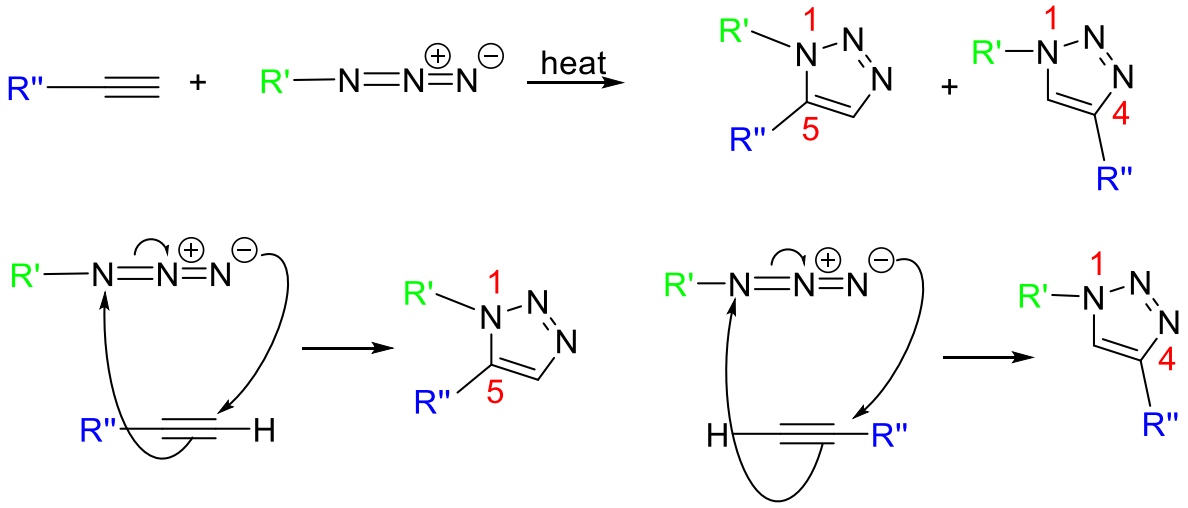

Figure 14: Mechanism of thermal 1,3-Dipolar Cycloaddition. [49]

The Huisgen cycloaddition is the reaction of a dipolarophile (as alkenes or alkynes) with a 1,3-dipolar compound (a molecule containing one or more heteroatoms) that leads to 5-membered heterocycles. As depicted in the above mechanism (**Fig. 14)**, two π-electrons of the dipolarophile and four electrons of the dipolar compound participate in a concerted, pericyclic shift. [49]

1.5.2 *Copper-catalysed azide alkyne 1,3 cycloaddition (CuAAC): Sharpless reaction.*

The group of Sharpless modified the Huisgen method. [50] They observed that the reaction of aliphatic azides with terminal alkynes is accelerated by copper ions, moreover also the regioselectivity is improved. [51]

The active Cu(I) catalyst can be generated from Cu(I) salt or *in-situ* generated Cu(I) from Cu(II) salt using sodium ascorbate as the reducing agent.

This reaction introduced the term “click chemistry”, which describes reactions that are easy to perform, take place under mild conditions, form complex structures with exclusive regioselectivity and with very high yields. Pure products can be isolated by simple filtration or extraction. [52]

The special aspect of this reaction is that it is bio-compatible and takes place particularly well in aqueous media. [53]

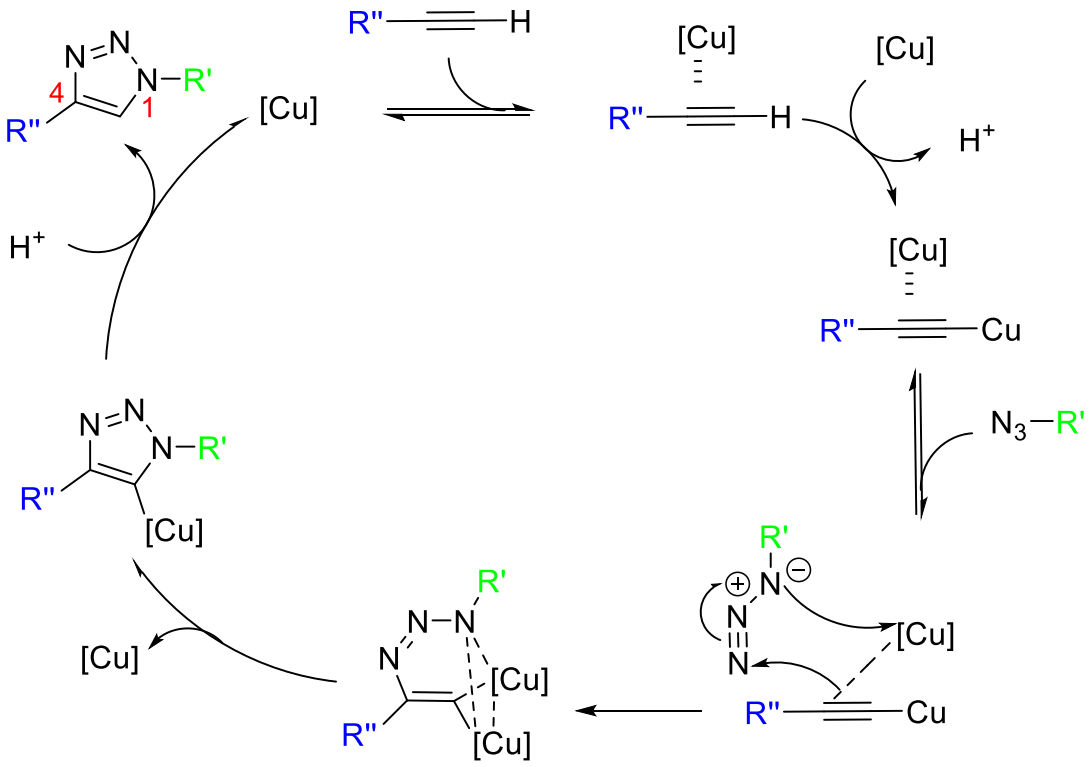

Figure 15: Mechanism of the copper-catalysed Azide-Alkyne Cycloaddition. [54]

In the mechanism depicted in **Fig. 15**, first, copper (I) coordinates to π electrons of the alkyne compound. After deprotonation by a base (that can be the solvent itself), a copper-acetylide molecule is formed (the reaction is possible only for terminal alkynes). Coordination of the azide to copper-acetylide is followed by the cyclization to produce the triazole ring. Finally, protonation releases the free triazole molecule. [54]

2- Aim of the thesis

The aim of the thesis is the synthesis and detailed characterisation of mono and di-nuclear Cu(I) complexes that can be used as PS in artificial photosynthesis.

Heteroleptic Cu(I) complexes are a more sustainable and economic alternative to noble metal complexes. Moreover, they showed to have good luminescence properties and long-lived excited states. For these reasons, they can be used as photosensitizer.

Previous studies, performed in the group where this work was done, showed that heteroleptic Cu(I) complexes based on pyrid-yl-1*H*-1,2,3-triazole have interesting characteristic to act as PS for the photocatalytic reduction of carbon dioxide. [55] Moreover, it has been shown that the presence of a methyl group in *alpha* to the nitrogen atom of the pyridine increases the structural rigidity and therefore allow an increase in the quantum yield in solution of these complexes. [55]

In order to increase the stability and the absorption in visible light of the PS, new Cu(I) complexes based on quinolin-yl-1*H*-1,2,3-triazole were synthesised. To study the possible cooperative effects between the metal centres on the luminescence behaviour, dinuclear complexes were prepared. The respective mono-nuclear Cu(I) complexes were also synthesised for comparison. To study the influence of the π-conjugation in the properties of the new complexes, spacers with different degrees of electronic communication were investigate (**Fig 16**).

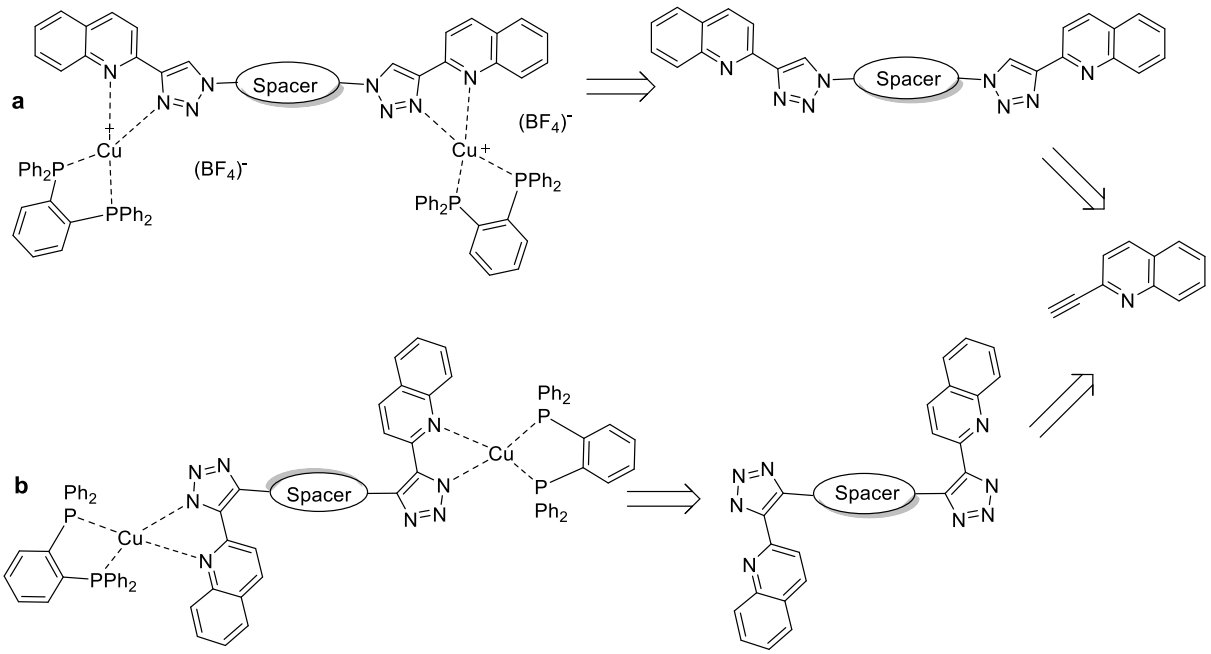

Figure 16: General structures of the complexes synthesised in this work: **a**) based on 1,4-disubstituted triazole; **b**) based on 4,5-disubstituted triazole.

For a better understanding of their excited state and electronic process, photophysical and electrochemical investigations were done. The properties of the new PS will be compared with those based on pyridine triazole and those present in the literature.

In future the most promising ones will be evaluated in photocatalytic reduction of CO_2.

3- Results and Discussion

3.1 Synthesis of the starting material

In earlier studies, performed in the research group where this work was done, mononuclear and binuclear heteroleptic Cu(I) complexes using bis [(2-diphenylphosphino)phenyl] ether (DPEPhos) and pyrid-yl-1*H*-1,2,3-triazole as chelating ligands were synthesised.[55]

These compounds showed good luminescence in solution at room temperature with long-lived excited states.[55] Moreover, bimolecular quenching experiments of these complexes with the catalyst Ni(cyclam)Cl_2 inspire their use as photosensitizers for the photoreduction of carbon dioxide. In this study it has been also shown, that a methyl group in *alpha* to the nitrogen atom of the pyridine (see **Fig. 17**) increases the structural rigidity and therefore the steric hindrance in the excited state, allowing an increase in the quantum yield in solution of these complexes.[55]

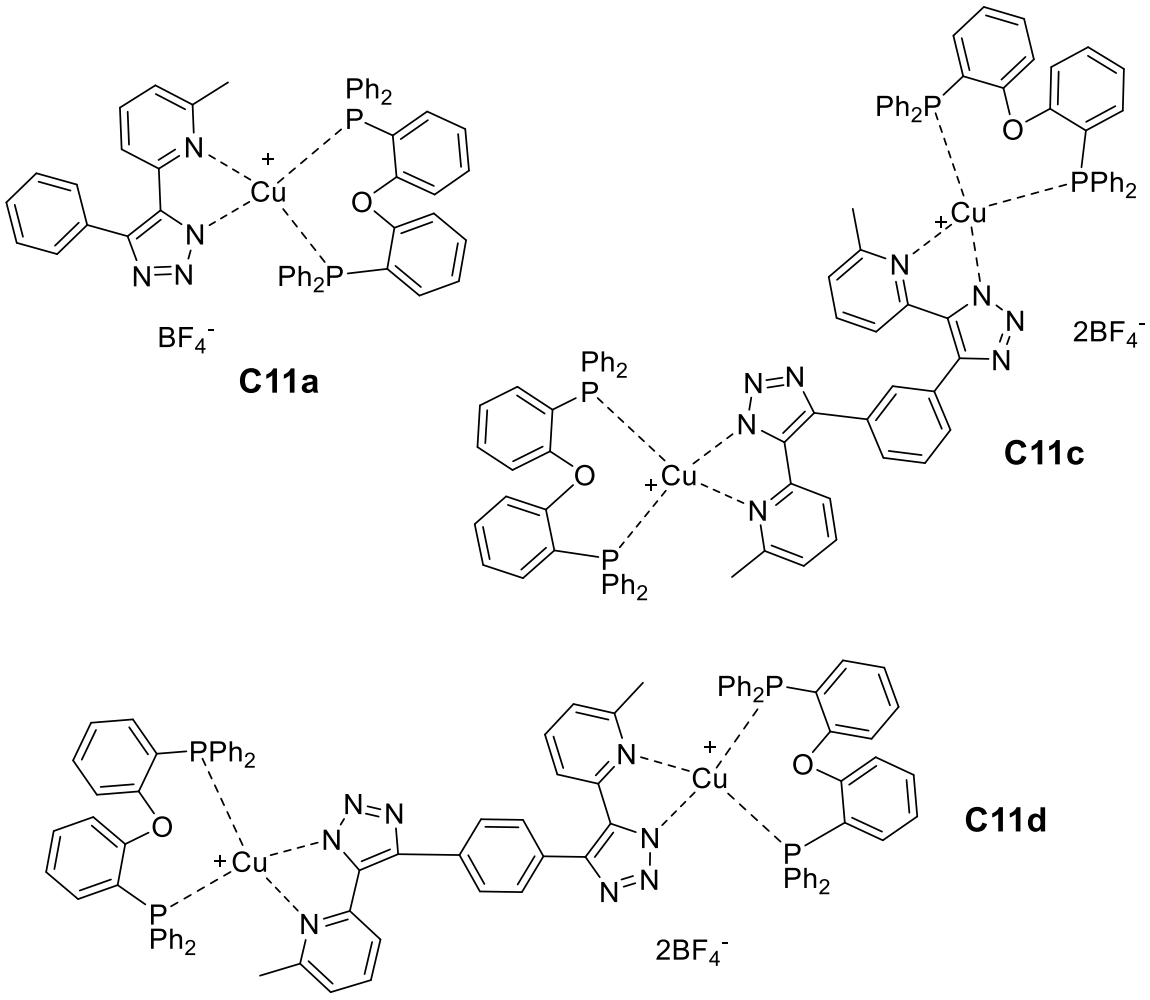

Figure 17: Structure of the mononuclear complex based on pyridyl-*1H*-1,2,3- triazole, **C11a, C11c, C11d**.

Based on these observations, the focus in this work was to increase the absorption of visible light and tune the luminescence properties in new heteroleptic Cu(I) complexes.

To do this, chelating ligands based on quinol-2´-yl-*1H*-1,2,3-triazole were chosen.

Quinoline is an aromatic heterocyclic compound containing a benzene ring fused with a pyridine ring (see **Fig. 18**).

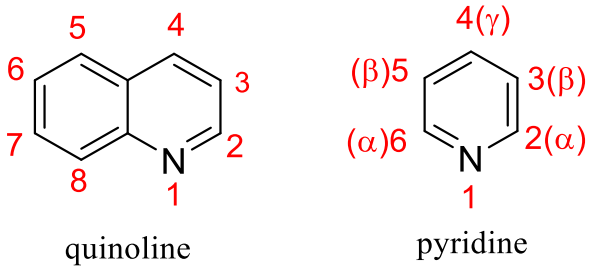

Figure 18: Chemical structure of quinoline and pyridine.

To obtain a quinolin-2'-yl-1*H*-1,2,3-triazole, it is necessary a two-step synthesis.[56]

The first step is a Sonogashira cross-coupling between 2-bromoquinoline **1** (commercially available and easy to handle) and trimethylsilylacetylene **2**, in order to obtain a protected 2-ethynylquinoline (see **Scheme 5**). The Songashira coupling requires anhydrous and anaerobic conditions, therefore the reaction was carried out under argon atmosphere, using dry-diisopropylamine (DIPA) as solvent, which acts as non-nucleophilic base, at room temperature in order to avoid the breaking of the triple bond.

Step 1:

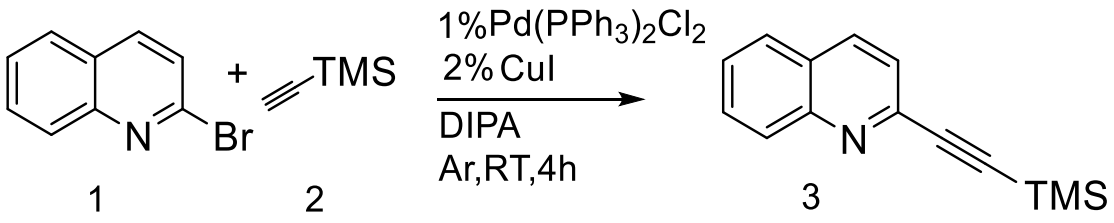

Scheme 5 Synthesis of 2-((trimethylsilyl)ethynyl)quinoline **3,** TMS = $Si(CH_3)_3$.

After filtration and evaporation of the solvent the product was analysed by ^{1}H-NMR and was all used for the next step to remove the protecting group. Therefore, the product **3** is treated

with potassium carbonate (K_2CO_3) and methanol (MeOH) at room temperature (see **Scheme 6**). [56]

Step 2:

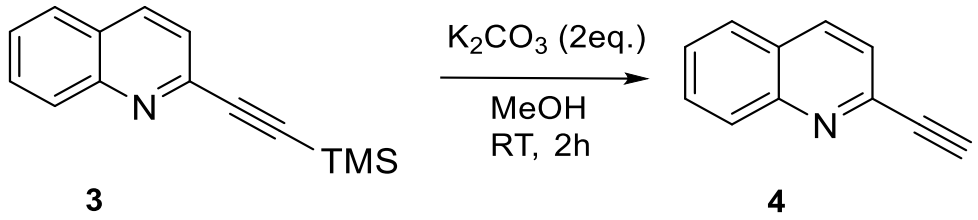

Scheme 6: Synthesis of 2-ethynylquinoline **4,** TMS = $Si(CH_3)_3$.

The product **4** was purified via silica gel chromatography using as eluent a solution of cyclohexane and ethyl acetate 1:1, and analysed by ^{1}H-NMR. When not directly used, it was stored in the fridge because the triple bond is unstable and may undergo polymerization.

The compound **4** was always obtained with good yields between 58-72%.

The study mentioned above showed also that binuclear complexes based on pyridine triazole, have a longer excited-state lifetime than the mononuclear compounds, which appears to be due to electronic interaction between the two metal centres. [55]

For this reason, in order to evaluate, also in the new compounds, the influence of the electronic communication between the metal cores of binuclear complexes, different spacers with diverse degree of π-conjugation were studied (see **Fig. 19**).

We expect to see an influence on the luminescent properties according to the degree of conjugation of the bridging systems, or according to the geometry (e.g. the spatial orientation of the metal centres) even when the bridging ligand is not conjugated.

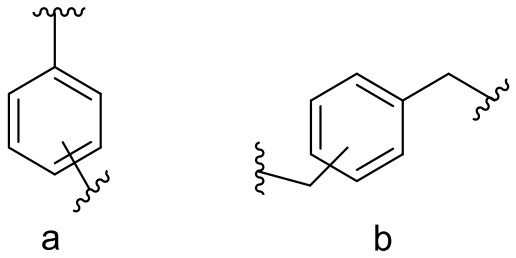

Figure 19: Bridging unit used in the following synthesis, **a**) phenyl group, **b**) benzyl group.

3.2 Synthesis of the ligands.

Several ligands were synthetized in this work, and for sake of simplicity, all compounds with similar structure were collected into groups.

Group 1:

The first group collects the ligands, consisting of mono- and bis- 1,4-disubstituted-triazole with a benzyl group as spacer.

The following compounds were synthesized through a "click-Sharpless" reaction using sodium azide (NaN_3). [57]

The reaction was carried out at room temperature using a solution of ethanol (EtOH) and water (H_2O) 7:3 as solvent. As depicted in **Scheme 7**, a copper (II) salt, $CuSO_4 \cdot 5 \cdot H_2O$, was used as pre-catalyst and sodium ascorbate as reductive agent. Thus, the Cu(I) active catalyst was formed *in situ*.

The reaction leads selectively to 1,4-disubstituted triazole.

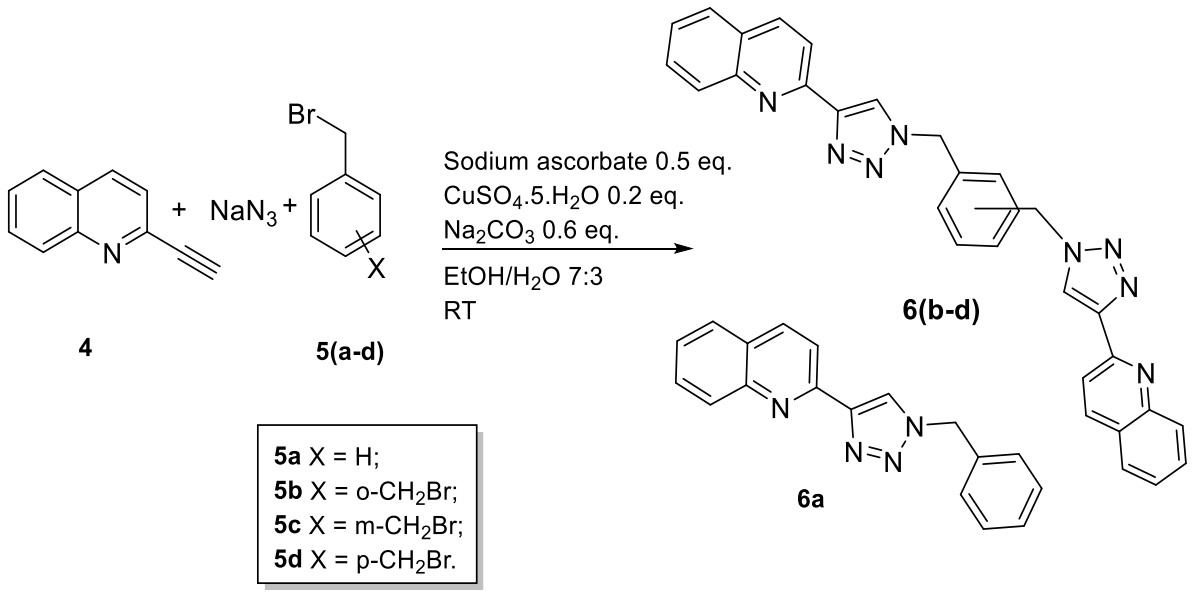

Scheme 7: Synthesis of bis((4'-(quinolin-2''-yl)-1'*H*-1',2',3'-triazol-l'-yl)methyl)benzene ligands.

Sample	Substitution	Yield
6a	mono	82%
6b	Orto	19%
6c	meta	41%
6d	para	17%

Table 2: Name, substitution and yield of the ligands of the first group.

The products **6 a-d** were obtained with different yields between 17%-82% (see **Table 2**)
In fact, the reaction led selectively to the desired regioisomer the mono-triazole was isolated without further purification (compound **6a)**. When the product was a bis-triazole, the purification was necessary because other sideproducts could be formed (e.g. not completed reaction products, see **Fig. 20**). Therefore, they were purified with chromatographic column using silica gel as stationary phase and as eluent dichloromethane (DCM) and 1% of MeOH. The increase of the polarity was necessary for the desired products, since 1,2,3-triazole rings are very polar. The products were characterized by ^{1}H-NMR.
At this point the focus was not on the improvement of the yield, but on the search of an appropriate synthesis for these ligands and on the best purification method.

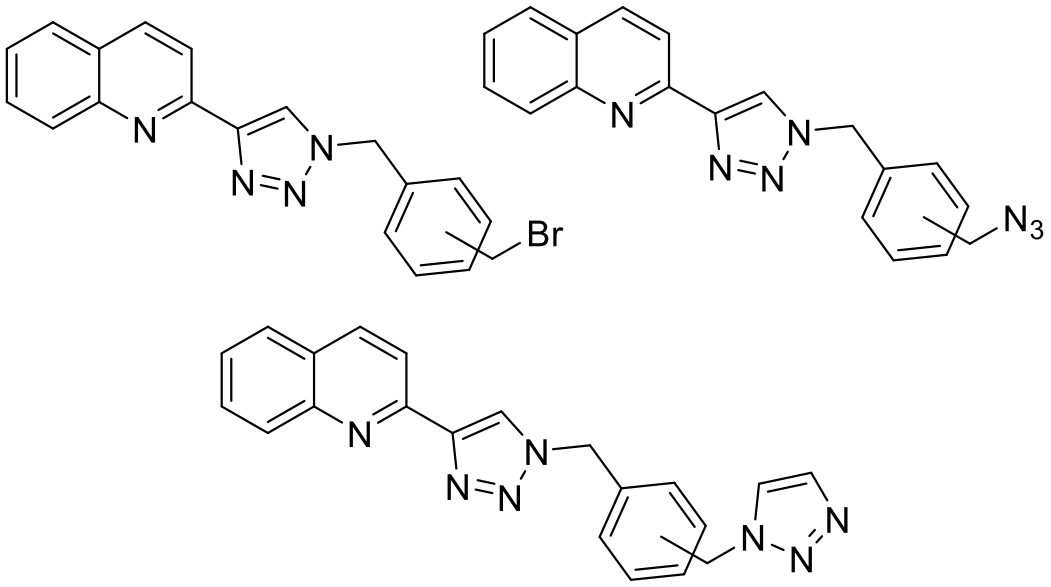

Figure 20: Possible sideproducts of reaction depicted in **Scheme 7**.

Group 2:

The second group collects the ligands, consisting of mono and bis- 4,5-disubstituted-triazole with a phenyl group as spacer.

The 4,5-disubstituted-triazole ligands were obtained through a two-step synthesis. [56]

As first step a Sonogashira coupling to form the intramolecular triple bond, carried out under argon atmosphere, this time with high temperature (see **Scheme 8**).

Step 1:

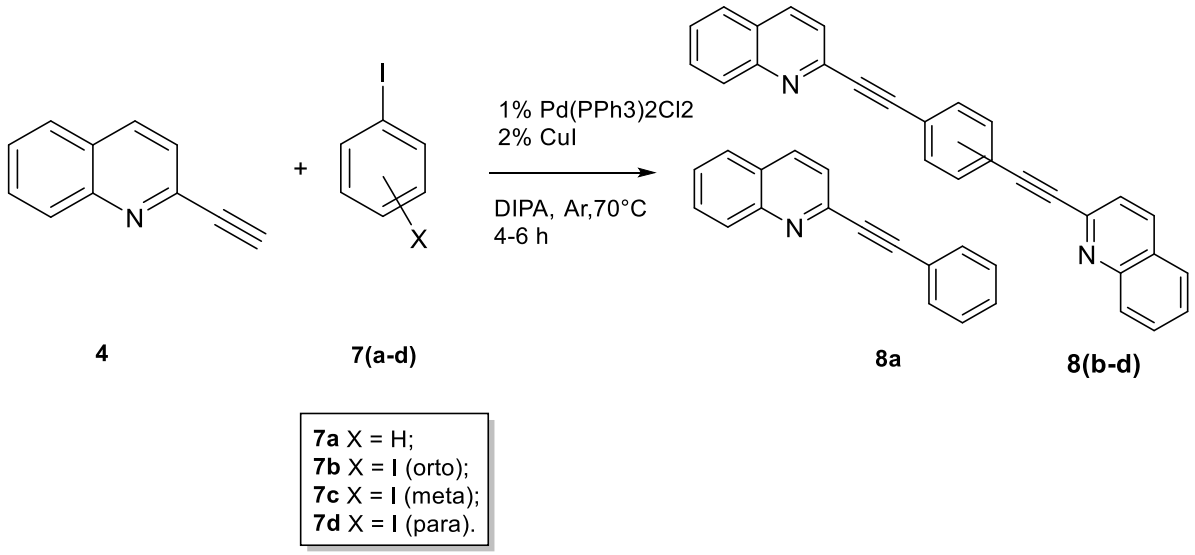

Scheme 8: Synthesis of bis(quinolin-yl-ethynyl)benzene pre-ligands.

Sample	Substitution	Yield
8a	mono	98%
8b	orto	14%
8c	meta	42%
8d	para	42%

Table 3: Name, substitution and yield of the pre-ligand of group 2.

The products **8(a-d)** were purified via silica gel chromatographic column using DCM + 1% of MeOH as eluent and obtained with high yield for the mono-substituted pre-ligand and with 30%-40% of yields for the di-substituted (see **Table 3**). After purification the compounds **8** were used for the next step: a thermal 1,3-cycloaddition or Huisgen reaction, using trimethyl, silyl, azide (TMS-N_3) in *N*,*N*-dimethylformamide (DMF) at high temperature (110°C), as depicted in **Scheme 9**.

Step 2:

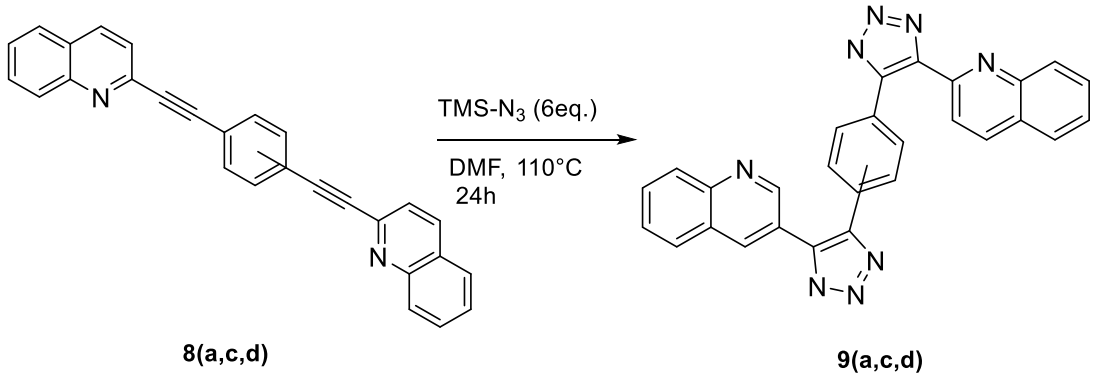

Scheme 9: Synthesis of bis(5'-(quinolin-2''-yl)-1'*H*-1',2',3'-triazol-4'-yl)benzene ligands.

Sample	Substitution	Yield
9a	mono	89%
6c	meta	60%
6d	para	88%

Table 4: Name, substitution and yield of ligands of the second group.

Since TMS-N_3 is very volatile (boiling point 52 °C), the addition of this reagent was done at the very beginning of the reaction, at room temperature and some equivalents more were added during the reaction. To help the reaction keeping the reagent inside the flask, an argon pression was needed. During the work-up, the trimethylsilyl group was removed.

As mentioned in the introductive part, the Huisgen method is a good approach to obtain 4,5-disubstituted triazoles, since the azide was linked only to a TMS group, the presence of other stereoisomers was not a problem. If protonation occurs, different tautomers can be seen. The product **9(a,c,d)** were obtained with good yields between 60%-89% (see **Table 4**). Despite many efforts, the reaction to obtain the product **9b** (structure in **Fig. 21**) was not successful. Probably the cycloaddition of azide to the alkynes was not possible or very difficult for the high steric hindrance.

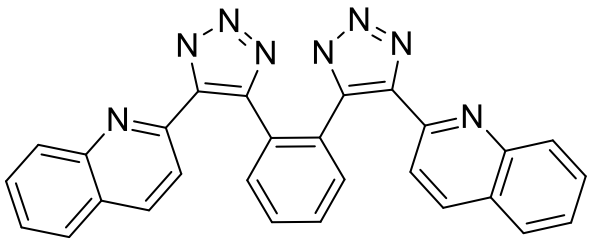

Figure 21: Possible structure of the ligand **9b**.

Group 3:

The third group collects the ligands with a 1,4-triazole, but, in this case, a phenyl group as spacer, instead of a benzyl as we have seen in group 1.

This kind of ligands would have been very interesting for the high π-conjugation of the system. Since the reaction for the first group of ligands worked well the same Click-Sharpless method was followed (**scheme 10**), [57], but unlike the previous reaction, in this case, the synthesis showed some difficulties.

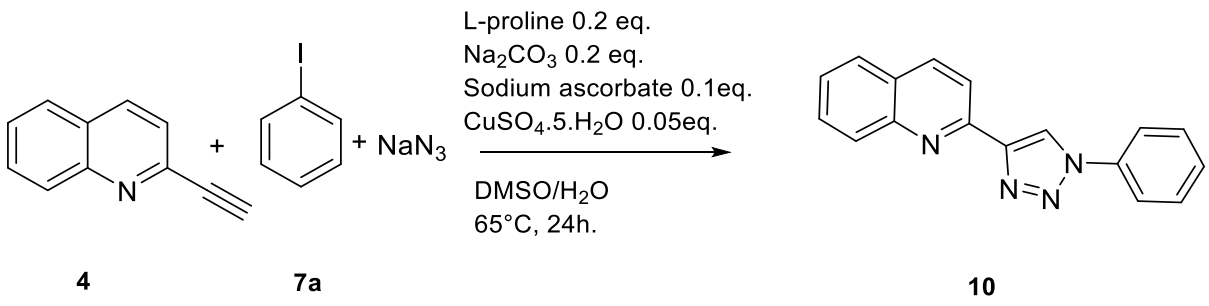

Scheme 10 Synthesis of 2-(1''-phenyl-1'*H*-1',2',3'-triazol-4'-yl)quinoline, first method.

The final product **10** had a lot of impurities. Purification via chromatographic column, using first DCM and then increasing slowly the percentage of MeOH was not enough. Since the product and the by-product had a very similar behaviour (e. g. 2-(quinolin-2´-yl)-*1H*-1,2,3-triazole) and no solvent mixture was found to separate them, a preparative TLC with inverse phase and DCM as solvent was used.

This technique allowed the separation of the fractions but only few milligrams of the pure product were obtained. The amount was not enough to proceed with complexation.

Since the formation of the aromatic azide could have been the problematic step, a new synthetic method was followed, see **Scheme 11.** [58]

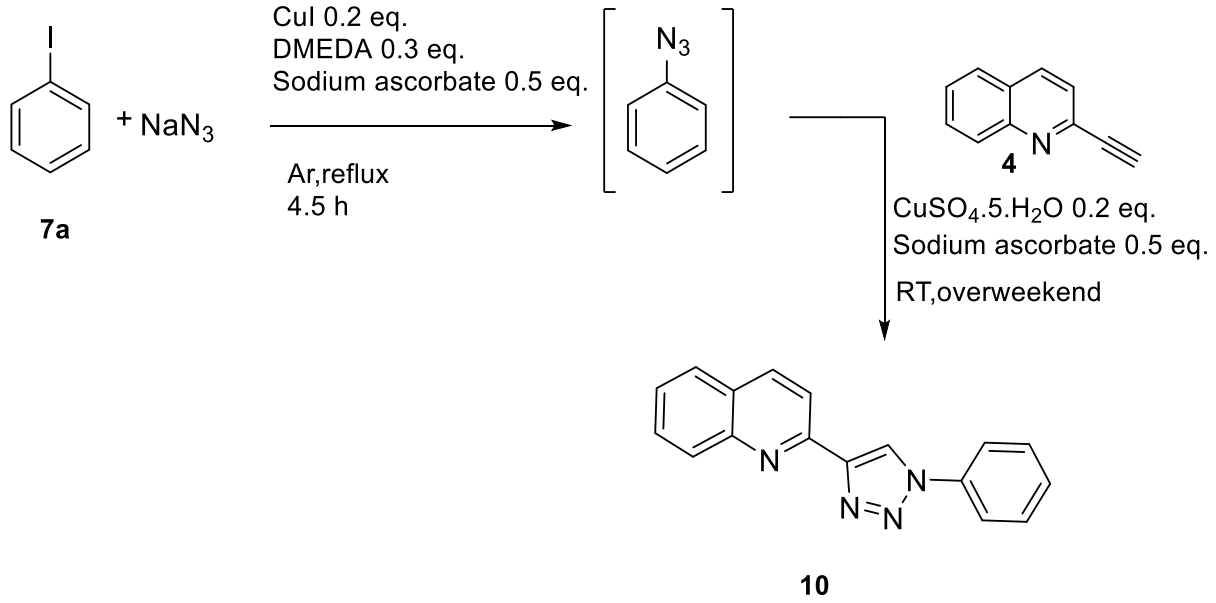

Scheme 11 Synthesis of 2-(1''-phenyl-1'H-1',2',3'-triazol-4'-yl)quinoline, second method.

Also in this case, the reaction led to different products and the purification was not easy; the product was obtained only after purification *via* a preparative TLC in reversed phase silica.

Since these ligands could have been very interesting, even if the reaction lead to very low yields, the synthesis of the disubstituted triazole was tested more times, but without good results. Other synthetic approaches might be studied in the future.

3.3 Synthesis of the Cu(I) precursor.

Since Cu(I) is an economic alternative to Ru(II), to obtain compounds suitable as photosensitizers heteroleptic copper (I) complexes were synthetized.

The precursor tetrakis (acetonitrile)copper(I) tetrafluoroborate (**11**) was synthesised according to literature procedures. [59]

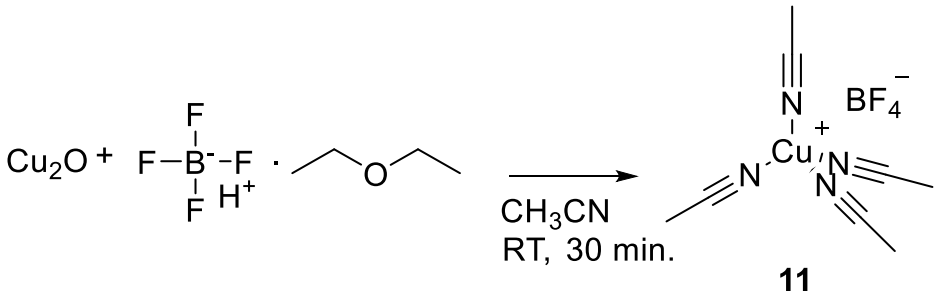

11

Scheme 12 Synthesis of Tetrakis(acetonitrile)copper(I) tetrafluoroborate.

The reaction of copper(I) oxide with tetrafluoroboric acid is strongly exothermic, therefore, the acid was added slowly with constant stirring. The heat generated is necessary to solubilise copper(I) oxide.

Since Cu(II) is not soluble in warm solution, filtration was enough to remove it. The green/blue solution was then cooled in a freezer and a white powder crystallized out of solution. The pure tetrakis(acetonitrile) copper(I)tetrafluorophosphate **11**, was then dried in vacuum and stored under argon.

3.4 Synthesis of the Cu(I) complexes.

As already mentioned in the introduction, the phosphine ligands can influence the photoluminescence properties and the stability of the Cu(I) complexes. Therefore, in order to increase the steric hindrance of the excited state and avoid the coordination by solvent molecules, in their excited state, bis[(2-diphenylphosphino)phenyl] ether **12** (DPEPhos) was chosen as chelating ligand. As the precursor used is a tetrafluoroborate (BF_4) salt (**11**), the charged complexes have BF_4^- as counterion.

To synthesize the complexes, the diphosphine ligand DPEPhos was reacted with the tetrakis (acetonitrile) copper (I) tetrafluoroborate.

Since Cu(I) is easily oxidised to Cu(II), the reaction was carried out in dry and freshly distilled DCM under argon atmosphere, see **Scheme 13**.

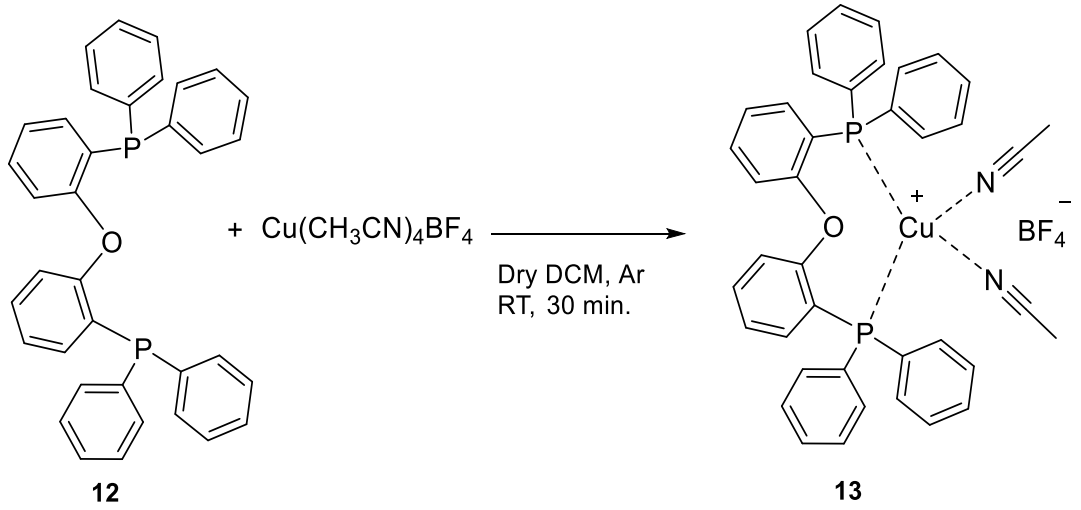

Scheme 13: First step of the synthesis of Cu(I) complexes.

Then, the appropriate number of equivalents of the chelating N^N ligand were added to this solution, as depicted in **Scheme 14**.

Below an example of complexation for the mono-substituted ligand **10**.

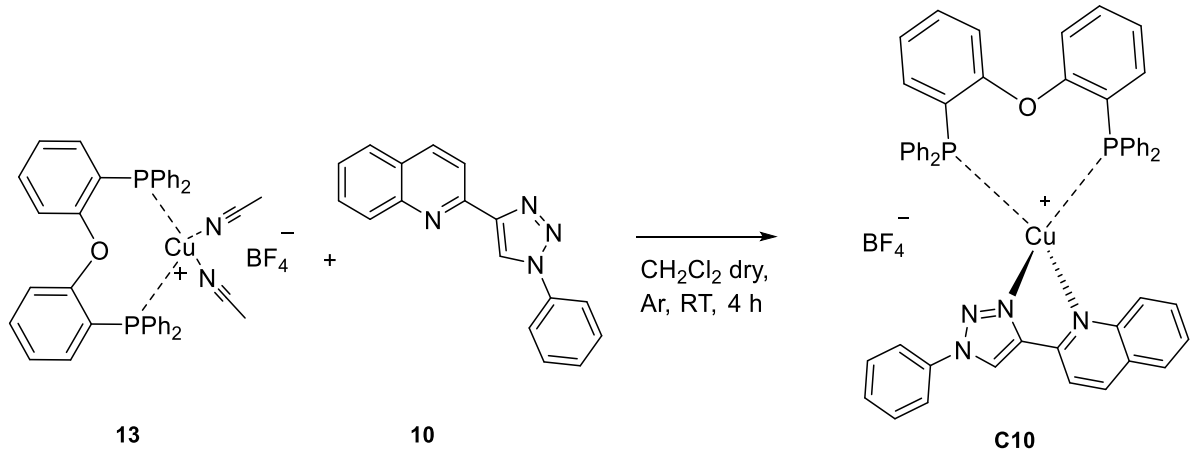

Scheme 14: Synthesis of the Cu(I) complex **C10**.

As shown in the **Scheme 14** when using the neutral 1,4-triazole ligands, the final complexes were salts, and the BF_4^- counterion was present in order to maintain electroneutrality, due to the positively charged Cu(I). On the other hand, in the 4,5-triazole ligands deprotonation of the

triazole ring occurred after purification, affording the negatively charged ligands that, upon coordination with the positively metal core, form neutral complex.

To promote a slow crystallization, the new complexes were purified by recrystallization in cyclohexane. Only for some of them was necessary a further purification via chromatographic column in order to remove the eventual excess of phosphine ligand. All complexes were analysed with ^{1}H-NMR, ^{13}C-NMR, ^{31}P-NMR, high resolution mass and elemental analysis.

In the table below are listed all the new complexes synthesized in this work (see **Table 5**).

Groups	Sample	Substitution	Spacer	Yield
1	C6a	mono	Phenyl	72%
	C6b	orto	Phenyl	91%
	C6c	meta	Phenyl	62%
	C6d	para	Phenyl	94%
2	C9a	mono	Benzyl	56%
	C9c	meta	Benzyl	72%
	C9d	para	Benzyl	30%
3	C10	mono	Phenyl	52%

Table 5: Name, structure and yield of the new Cu(I) complexes.

As described in the introductive section, the presence of bulky chelating ligands is necessary to avoid coordination of the solvent molecules or of counterions on the axial position of the excited state of the formally Cu(II) complex. However, too bulky ligands can lead to an exchange of ligands in solution. In order to study the stability of the complexes in solution, a comparison was done between the ^{1}H-NMR of the complexes directly after crystallisation and the ^{1}H-NMR of the same solution after some weeks.

This test showed that the complexes with 1,4-triazole had great stability in solution.

As shown below, the pick of the first and second NMR of the complex **C6c** are exactly the same. No exchange of ligands nor coordination by solvent is present (see **Fig. 22**).

While, the complexes with 4,5-triazole **C9a, c, d** after some days in solution showed different ^{1}H-NMR with a smaller number and broad picks (see **Fig. 23**); moreover, the presence of a white precipitate, probably a coordination polymer of Cu and the triazoles, was observed inside the tubes.

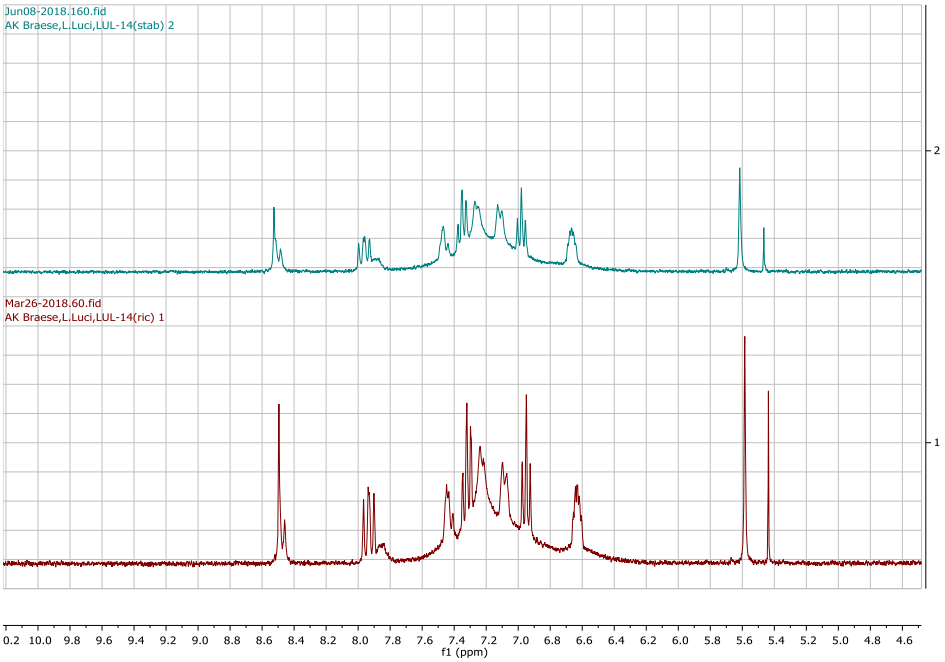

Figure 22: ^{1}H-NMR in CD_3CN of **C6c**, same tube after purification and after 74 days, decrease in intensity is due to the addition of deuterated solvent.

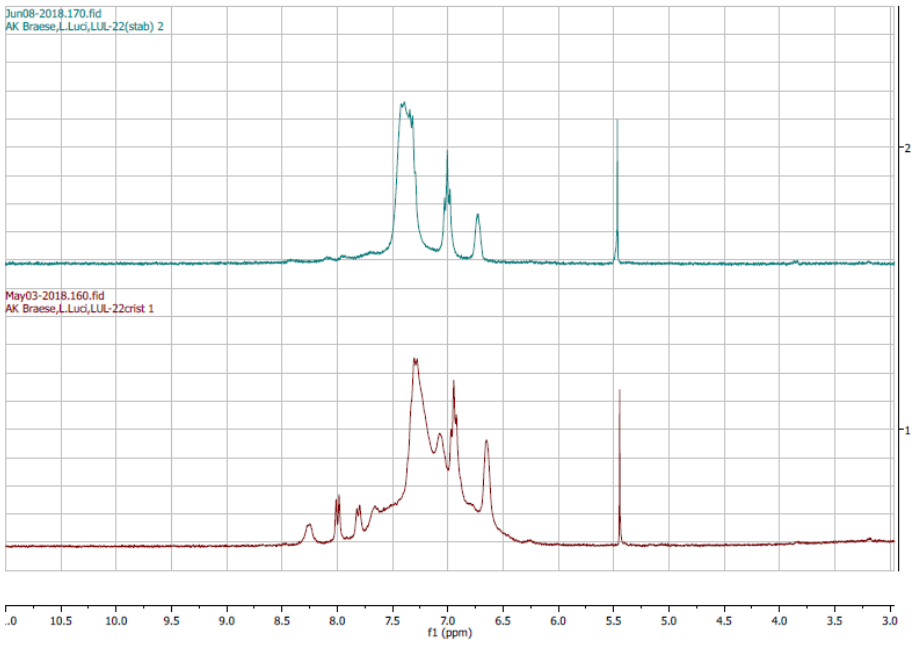

Figure 23: ^{1}H-NMR in CD_3CN of **C9d**, same NMR tube after purification and after 36 days.

3.5 Electronic absorption spectra of the complexes.

Photophysical measurements are of great importance, in fact, they were necessary to evaluate the absorption of visible light of the new complexes.

All complexes were dissolved in DCM as spectroscopic solvent and measured at room temperature.

As shown in the spectra below (**Fig.24**), the absorption profiles of the group 1 complexes are quite similar to each other, while the complexes **C9(a,c,d)** have different profiles (**Fig.25**). Electronic absorption of complex **C10** is also very similar to those of group 1 (**Fig. 26**).

Group 1:

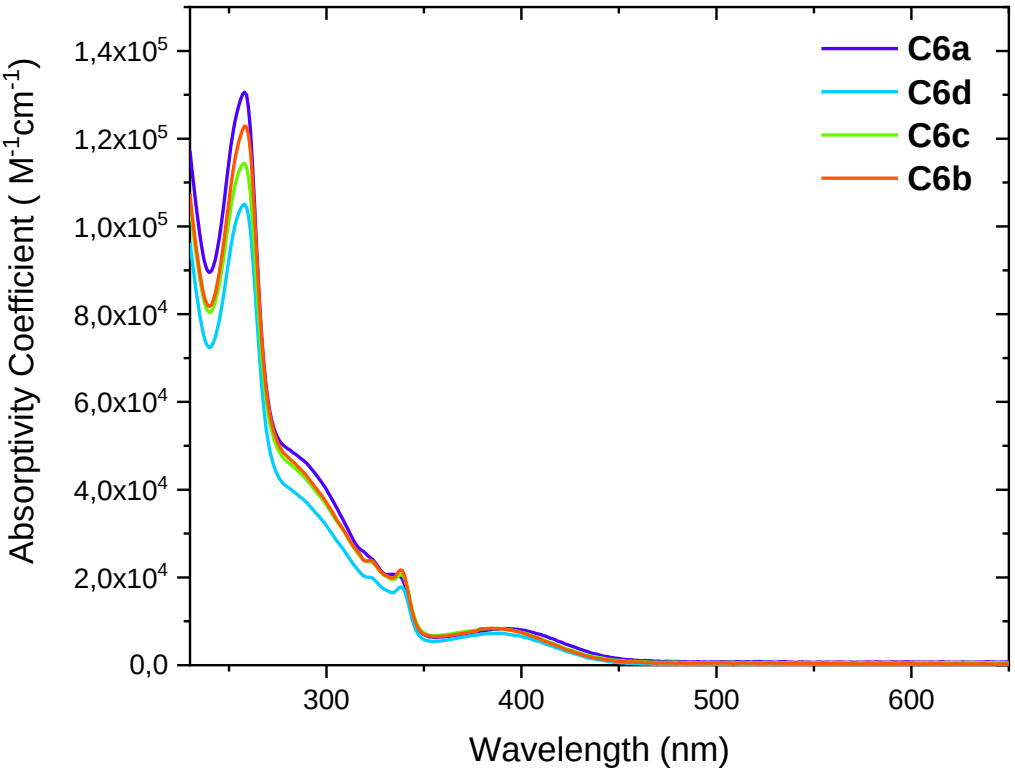

Figure 24: UV-VIS absorption spectra of the complexes **C6a, b, c, d,** [1x10^{-5}M] in DCM, 20°C.

Below are listed the compounds for each group with their absorption maxima and the relative absorptivity coefficient (**Table 6** for Group 1**, Table 7** for Group 2 and **Table 8** for Group3).

Sample	Absorption ^{1}MLCT [nm]	Absorptivity coefficient (ε) [$M^{-1}\cdot cm^{-1}$]
C6a **(mono)**	392	$8.36x10^3$
C6b (**orto)**	380	$8.32x10^3$
C6c **(meta)**	388	$8.45x10^3$
C6d **(para)**	388	$7.25x10^3$

Table 6: Absorption maxima and absorptivity coefficient of the complexes of the first group, conc. [$1x10^{-5}$ M].

The new heteroleptic Cu(I) complexes display intense ligand centre (LC) absorption bands in the UV region, below 350 nm, with high energy, which are assigned to a π → π* transitions centred on the N^N and P^P ligands.

Absorption between 350-450 nm are assigned to metal to ligand charge transfer (MLCT) transitions, from Cu centre to the diimine ligand.

The electron withdrawing effect of the P^P ligand on the metal centre disfavour the Cu → N-N electron donation, leading to a blue shift of the lower energy MLCT transitions compared with those of the homoleptic Cu(I) complexes.

The absorption maxima of the new complexes are shifted in the visible region, while those of the complexes based on pyridine-ligands were around 300-350 nm.[55] In fact, diimine ligands with more electron withdrawing group or increased π-conjugation, lead to a decrease of the HOMO-LUMO energy gap, visualized by a red shift of the optical transitions.

Moreover, even if in the binuclear complexes two chromophore groups are present, no increase in absorption is shown, see **Fig.24** and **Table 6**.

Group 2:

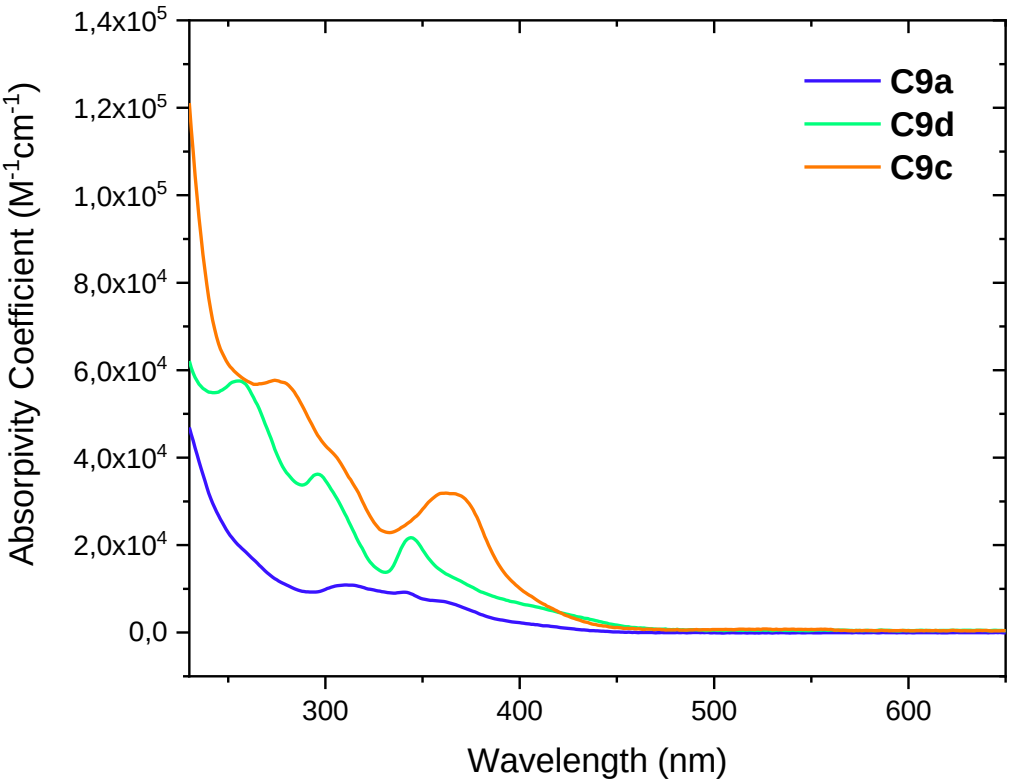

Figure 25: UV-VIS absorption spectra of the complexes **C9 a, c, d,** [1x10^{-5}M] in DCM, 20°C.

The neutral complexes **C9a,b,c** present peculiar absorption spectra. The intensity is high for the binuclear complexes for the presence of two chromophoric units. They have intense ligand centre (LC) absorption bands in the UV region, above 300 nm and exhibit blue-shifted MLCT bands compared with those complexes of group 1 and 3, with absorption maxima of the ^{1}MLCT state around 350 nm.

Sample	Absorption ^{1}MLCT[nm]	Absorptivity coefficient (ε) [$M^{-1}\cdot cm^{-1}$]
C9a **(mono)**	322	9.92x10^3
C9c **(meta)**	401	9.74x10^3
C9d **(para)**	378	9.77x10^3

Table 7: Absorption maxima and absorptivity coefficient of the complexes of the second group, conc. [1x10^{-5} M].

In this case, the presence of two chromophoric groups in the dinuclear complexes is reflected in an increase in the absorption (see **Fig. 25**).

Group 3:

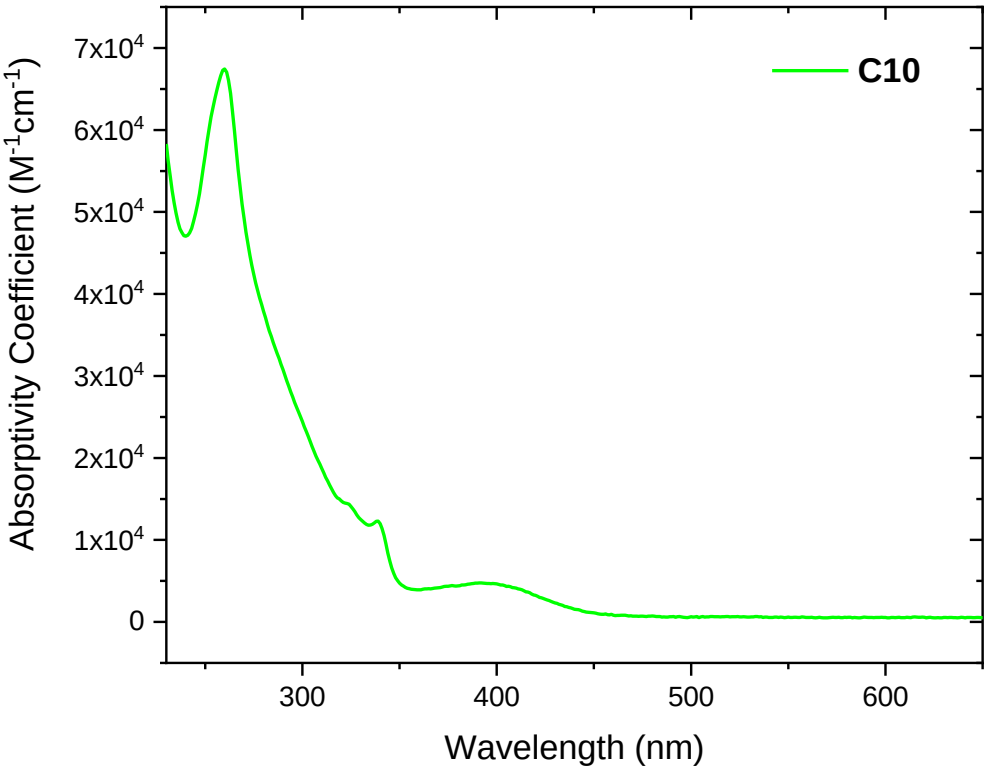

Figure 26: UV-VIS absorption spectrum of the complex **C10,** [1x10^{-5}M] in DCM, 20°C.

Similarly to the first group, the complex **C10** present an absorption spectrum with intense LC absorption bands in the UV region above 350 and MLCT transitions between 350-450 nm.

Sample	Absorption ^{1}MLCT [nm]	Absorptivity coefficient (ε) [M^{-1}·cm^{-1}]
C10 (mono)	392	8.36x10^{3}

Table 8: Absorption ^{1}MLCT and absorptivity coefficient of the complex **C10**, conc. [1x10^{-5} M].

3.6 Emission and excitation spectra.

Excitation and emission measurements were also performed for the new complexes. The measurements were carried out in DCM (spectroscopic grade) at room temperature and were done first in the presence of oxygen and then in solution degassed with argon, in order to have an oxygen-free atmosphere. This technique is the simplest way to distinguish if the emission involves a triplet excited state. In fact, without molecular oxygen, which is a known triplet-state quencher, the emission of the complexes increases (see **Fig. 27**).

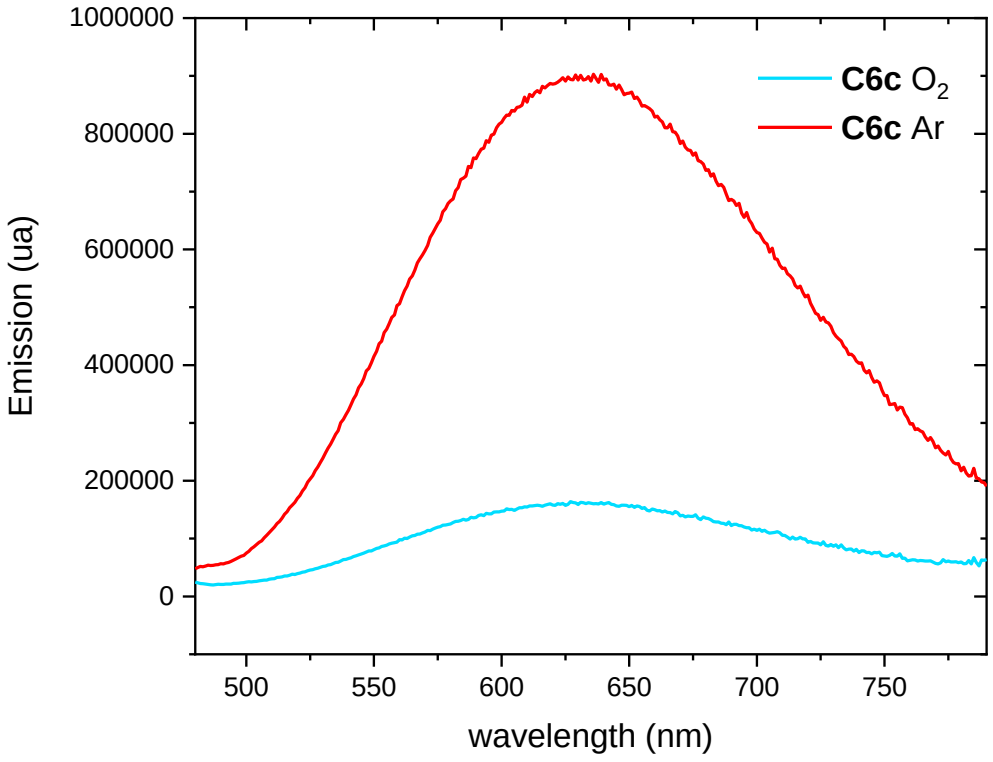

Figure 27: Example of O_2 quenching on the emission of the complex **C6c**.

To act as good photosensitizers, the complexes need to have long-lived excited state (in the range of microseconds), at least long enough to undergo electron transfer to a catalyst (oxidative quenching) or from an electron donor (reductive quenching).

The investigated complexes are luminescent and exhibit unstructured broad emission with large Stokes shifts, typical of an emissive excited state with a dominant metal-to-ligand charge-transfer character. The emission quantum yields measured in argon saturated atmosphere are appreciable.

The excitation spectra were recorded by monitoring the emission maximum of the corresponding complex. Their profiles are very similar to each other and recall the observed absorption spectra.

For any photoluminescent species, the quantum yield (PLQY) of its luminescence is a basic property, and its measurement is an important step in the characterization of the species. Quantum yield is the ratio of photons absorbed to photons emitted. In other words, the quantum yield gives the probability of the excited state being deactivated by emission rather than by another, non-radiative mechanism.

For species in dilute solution it is common to measure the emission spectrum and compare its integrated intensity with the same quantity for a reference system with a known PLQY. [60]

$$PLQY_f^i = \frac{F^i f_s n_i^2}{F^s f_i n_s^2} \cdot PLQY_f^s \qquad \textbf{(eq. 1)}\ [60]$$

Where $PLQY_f^i$ and $PLQY_f^s$ are the PLQY of the sample and that of the standard, respectively; F^i and F^s are the integrated intensities (areas) of sample and standard spectra, respectively.

f_s and f_i are the absorption factor, the fraction of the light hitting on the sample that is absorbed ($f_x = 1^{-(10-Ax)}$, where A = absorbance); the refractive indices of the sample and reference solution are n_i and n_s, respectively. [60]

The excitation wavelengths for sample and reference are the same.

In the new Cu(I) complexes the PLQY is calculated with the **equation 1**, where:

Quantum yield of the reference $Ru(bpy)_3$ in water is 0,028.

The areas of samples and reference is calculated by integrating the relative emission plot in Ar.

The refractive index of DCM (solvent used in the sample) is 1,42416.

The refractive index of water (solvent use in the reference) is 1,332988.

The k radiative and k non-radiative where calculated as:

$$k_{\text{radiative}} = \frac{PLQY}{lifetime} \qquad k_{\text{non radiative}} = \frac{(1-PLQY)}{lifetime}$$

Below are reported the spectra and photochemical data of the new compound.

Group 1:

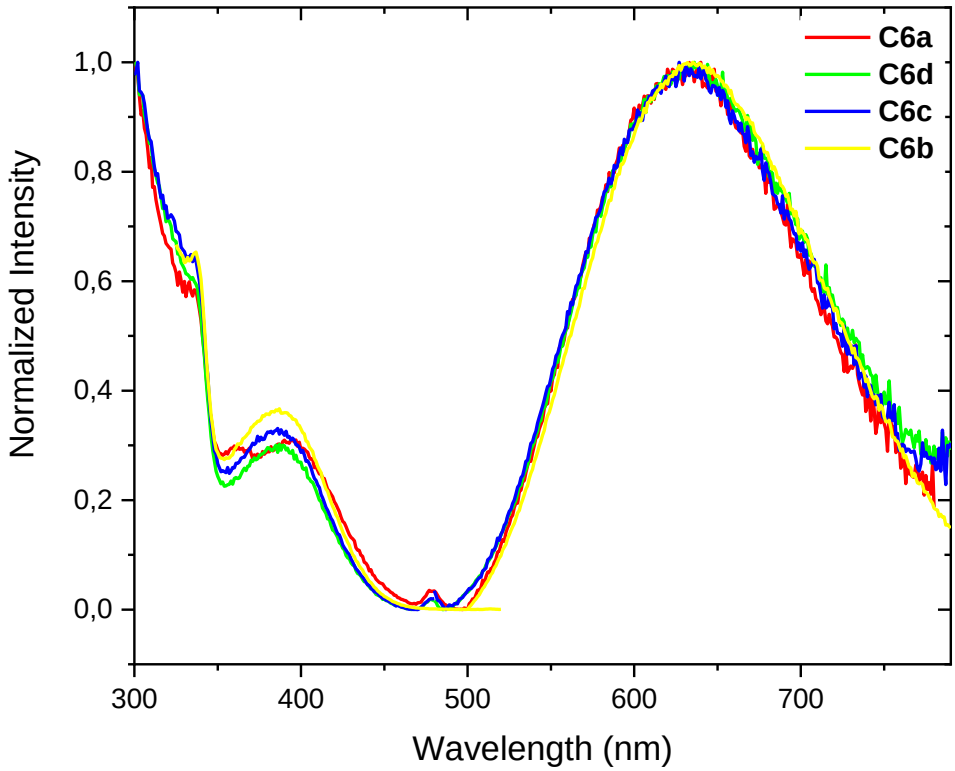

Image 28: Emission (right) and excitation (left) spectra of the complexes of the first group, **C6(a-d),** (λ_{exc}**C6a,c,d** = 420 nm, λ_{exc} **C6b** = 415 nm).

Sample	$\varepsilon_{\lambda abs(350)}$ [$M^{-1}\cdot cm^{-1}$]	$\varepsilon_{\lambda abs(400)}$ [$M^{-1}\cdot cm^{-1}$]	λ_{emis} [nm]	PLQY (%)	τ [µs]	k_r [s^{-1}]	k_{nr} [s^{-1}]
C6a (mono)	$6.95x10^3$	$8.35x10^3$	633	1.0	2.25	$4.48x10^3$	$4.40x10^5$
C6b (orto)	$7.06x10^3$	$7.43x10^3$	635	3.1	1.26	$2.42x10^4$	$7.69x10^5$
C6c (meta)	$7.37x10^3$	$8.40x10^3$	629	1.2	2.65	$4.52x10^3$	$3.73x10^5$
C6d (para)	$5.83x10^3$	$7.26x10^3$	636	1.6	2.31	$7.10x10^3$	$4.26x10^5$

Table 9: Photophysical values of complexes **C6(a-d)** recorded in DCM solution at room temperature.

The complexes of the first group present a long-lived the excited state, which is an important characteristic of PS, and good PLQY. This is higher for the disubstituted complexes, which,

moreover, have a stronger emission, in particular **C6b** (orto) complex, but this is not reflected in the lifetime of the excited state. The increase in quantum yield and lifetimes for the orto-binuclear complexes might reflect the influence of the second metal centre on the photophysical properties (see **Table 9**).

Group 2:

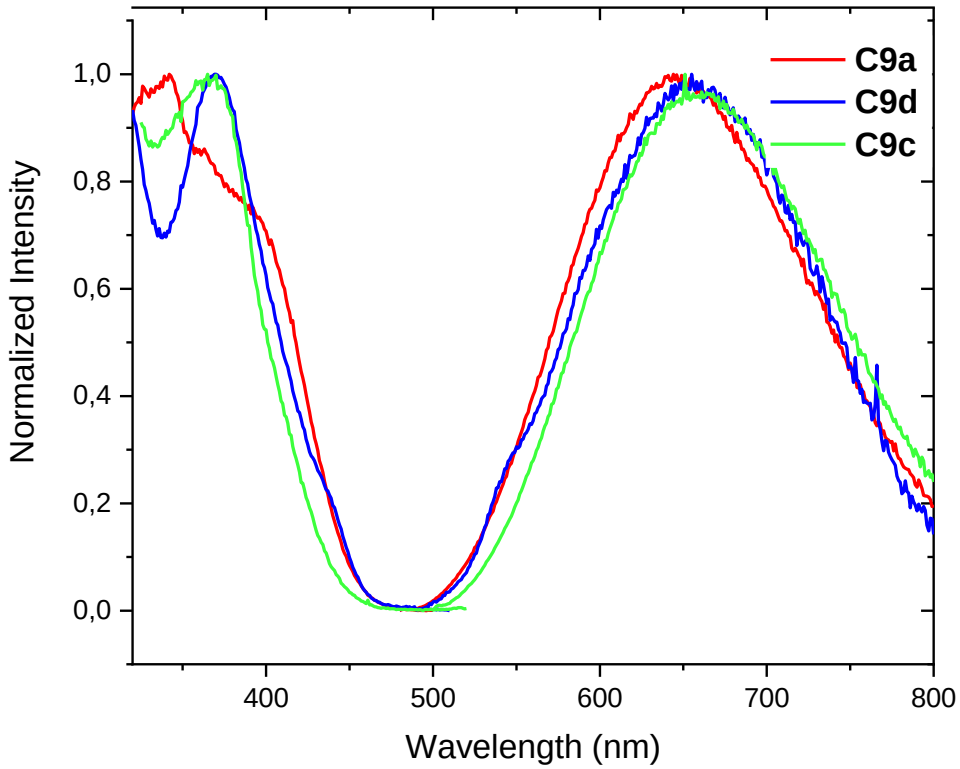

Figure 29: Emission (right) and excitation (left) spectra of the complexes of the second group, **C9a,c,d,** (**λ_{exc}C9a,d** = 420 nm, **λ_{exc}C9c** = 415 nm).

Sample	$\varepsilon_{\lambda abs(350)}$ [$M^{-1}\cdot cm^{-1}$]	$\varepsilon_{\lambda abs(400)}$ [$M^{-1}\cdot cm^{-1}$]	λ_{emis} [nm]	PLQY (%)	τ [µs]	k_r [s^{-1}]	k_{nr} [s^{-1}]
C9a (mono)	$7.71x10^3$	$2.27x10^3$	644	0.6	0.40	$1.51x10^4$	$2.47x10^6$
C9c (meta)	$2.83x10^4$	$1.01x10^4$	664	0.4	0.35	$1.04x10^4$	$2.81x10^6$
C9d (para)	$1.90x10^4$	$6.70x10^3$	655	0.4	0.36	$9.95x10^3$	$2.78x10^6$

Table 10: Photophysical values of complexes **C9(a,c,d)** recorded in DCM solution at room temperature.

The complexes of the second group do not respect the trend of the previous, binuclear complexes have a low PLQY and minor lifetime of the excited state even if the bridging ligand is a phenyl group and also the emission seems to be nearly half of that of the mononuclear complex.

For comparison below are showed the photoluminescence spectra and data of the Cu(I) complexes based on 5-(6'-methyl-pyrid-2'-yl)-*1H*-1,2,3-triazole, which structure is depicted in **Fig. 17**.

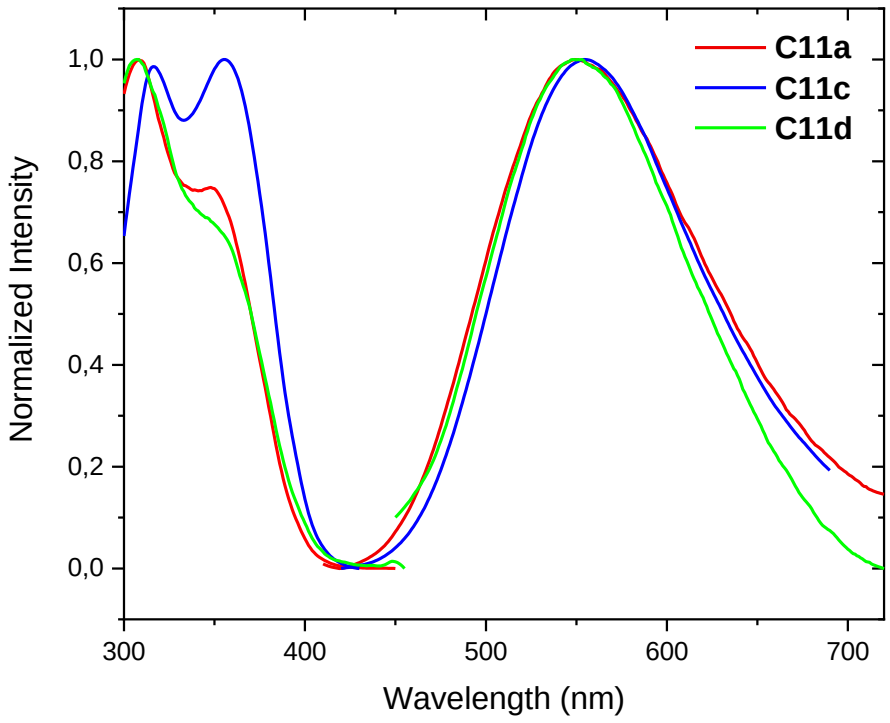

Figure 30: Emission (right) and excitation (left) spectra of the complexes based on 5-(6'-methyl-pyrid-2'-yl)-1*H*-1,2,3-triazole**,** recorded in DCM, at room temperature.[55]

Sample	$\varepsilon_{\lambda abs=350nm}$ [$M^{-1} \cdot cm^{-1}$]	λ_{emis} [nm]	PLQY (%)	τ [µs]	k_r [s^{-1}]	k_{nr} [s^{-1}]
C11a (mono)	3.85 x 10^3	554	5.4	0.88	6.1 x10^4	10.7 x10^5
C11c (meta)	9.04 x 10^3	556	9.9	1.21	8.2 x10^4	7.4 x10^5
C11d (para)	1.63 x 10^4	557	14.2	2.78	5.1 x10^4	3.1 x10^5

Table 11: Photophysical values of complexes based on 5-(6'-methyl-pyrid-2'-yl)-1*H*-1,2,3-triazole recorded in DCM solution at room temperature. [55]

The molar absorptivity at 350 nm is high for more of the quinoline triazole complexes.

The complexes of the second group were supposed to have an improvement in the luminescence properties compared to the methyl-pyridine one; in fact, they have similar structure (see **Fig. 17** and **Scheme 9**), even if the latters are charged complexes (no deprotonation of the ligands occurred). As we expected to see, the former complexes have absorption and emission maxima more shifted in the visible region (see **Table 7** and **10**). Nevertheless, the PLQY and lifetime are much higher for the methyl-pyridine complexes (see **Table 11**) than for the complexes based on quinoline, in particular very low value for the binuclear complexes.

Actually, all the new complexes show lower PLQY and only the compound of the first and third group (see **Table 12**) have a lifetime of the excited state comparable to that the pyridine triazoles complexes, but none of them as high as the **C11a** complex.

Group 3:

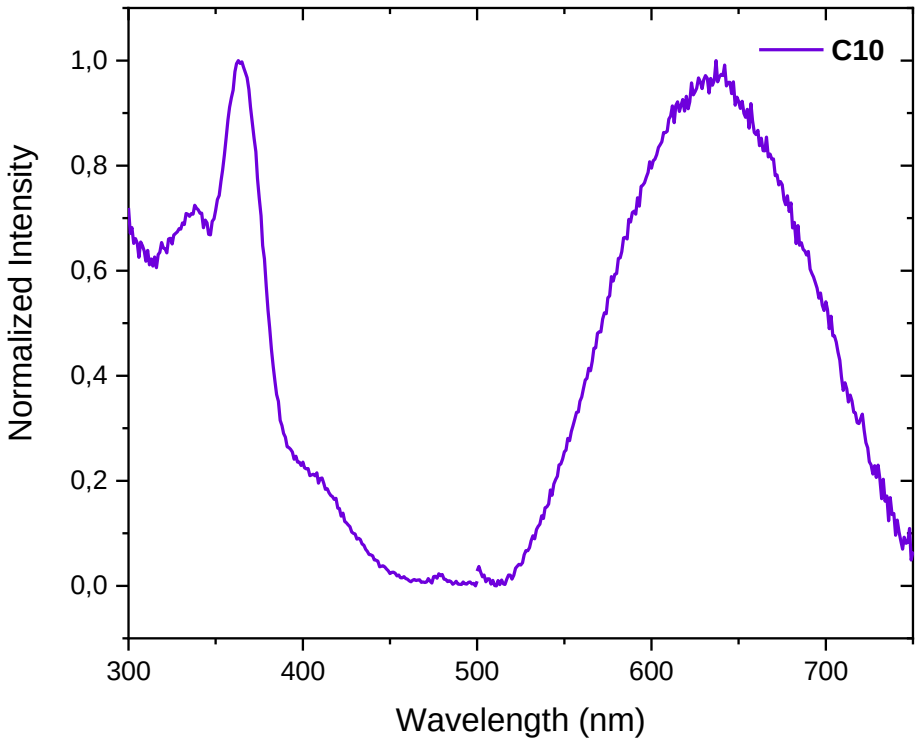

Figure 31: Emission (right) and excitation (left) spectra of the complex **C10, (**λ_{exc} = 420 nm).

Sample	$\varepsilon_{\lambda abs=350nm}$ [$M^{-1}\cdot cm^{1}$]	$\varepsilon_{\lambda abs=400nm}$ [$M^{-1}\cdot cm^{-1}$]	λ_{emis} [nm]	PLQY (%)	τ [μs]	k_r [s^{-1}]	k_{nr} [s^{-1}]
C10	$4.73x10^3$	$4.64x10^3$	642	0.622	2.09	$2.98x10^3$	$4.76x10^5$

Table 12: Photophysical values of complexes **C10** recorded in DCM solution at room temperature.

The complex **C10** have a low PLQY but long lifetime of the excited state, with value similar to that of the first group of complexes.

In conclusion, it is possible to say that the presence of quinoline gives an increase in stability of the exited state, avoiding non-emissive pathways and resulting in a notable emission in solution at room temperature and in a more absorption in visible light; despite that, no improvement in the lifetime of the excited state and in the photoluminescence quantum yield have been found.

This can be rationalized by comparing the 3D structure of the quinoline and the 6-methylpyridine (**Fig. 32**). Although the quinoline has a bulkier structure than a simple pyridine, the planarity of the former heterocycle does not induce a strong steric hindrance as in the case of the methyl substituted in *alpha* to the pyridine. Thus, the luminescence of the Cu(I) complexes based on quinoline is lower.

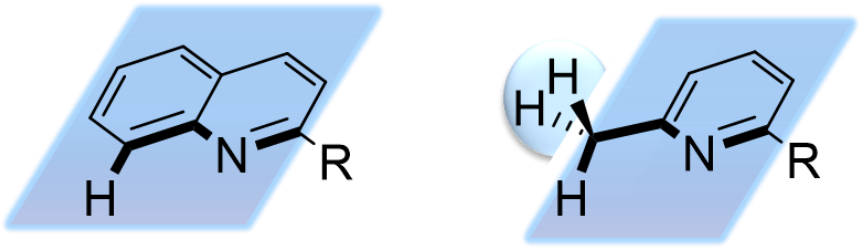

Figure 32: 3D structure of quinoline and the 6-methylpyridine

3.7 Emission in solid state

All complexes are yellow solid and showed high luminescence in solid state under UV light, λ_{exc}=395 nm, (see **Fig. 33** and **34**).

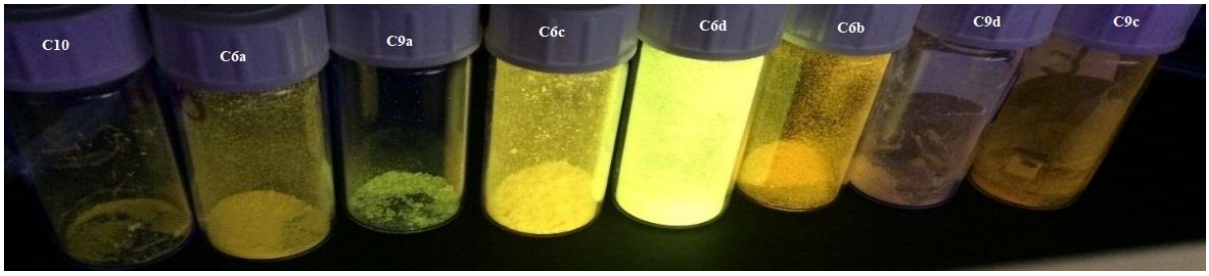

Figure 33: Picture of the new complexes under UV-VIS lamp, λ=395 nm.

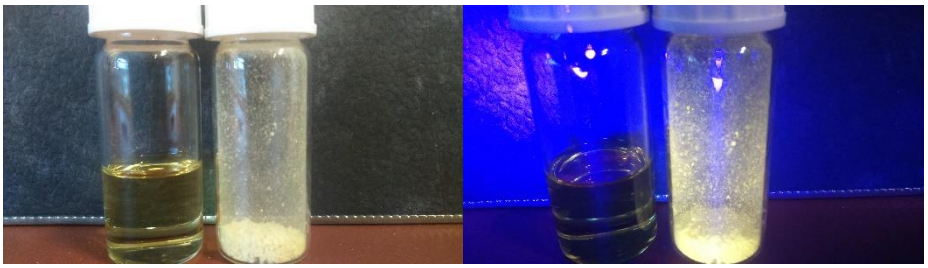

Figure 34: Picture of the complex **C6c** in solution and in solid state, on the left under solar light and on the right under UV-VIS lamp λ_{exc}=395 nm.

Further experiments are needed in order to assess the nature of the emissive state in these Cu(I) complexes. In particular, it would be interesting to see if they are thermally activated delayed fluorescent (TADF) emitters.[39] However, this lays outside the aim of this thesis, therefore it will be investigated in another project.

3.8 Electrochemistry of the mononuclear Cu(I) complexes

The three mono-substituted complexes **C6a**, **C9a**, **C10** were characterised also by cyclic voltammetry, in order to investigate their electrochemical behaviour.

The working and counter electrodes were a platinum disk and a platinum wire, respectively. Since a silver wire was used as the pseudo-reference electrode, ferrocene as internal standard was necessary. The solvent was dry acetonitrile, with 0.1 M concentration of the supporting electrolyte, tetrabutylammonium hexafluorophosphate ($TBAPF_6$).

The redox processes are not reversible. Cyclic first oxidation and the first reduction are quite similar in all three complexes (see **Fig. 35** for complex **C6a**, Fig. **36** for complex **C9a** and **Fig. 37** for complex **C10**).

The oxidation is expected to occur first on the metal site, while a second oxidation process is localised on the chelating diphosphine ligand. The reduction process should be concentrated on the N^N chelating ligands.

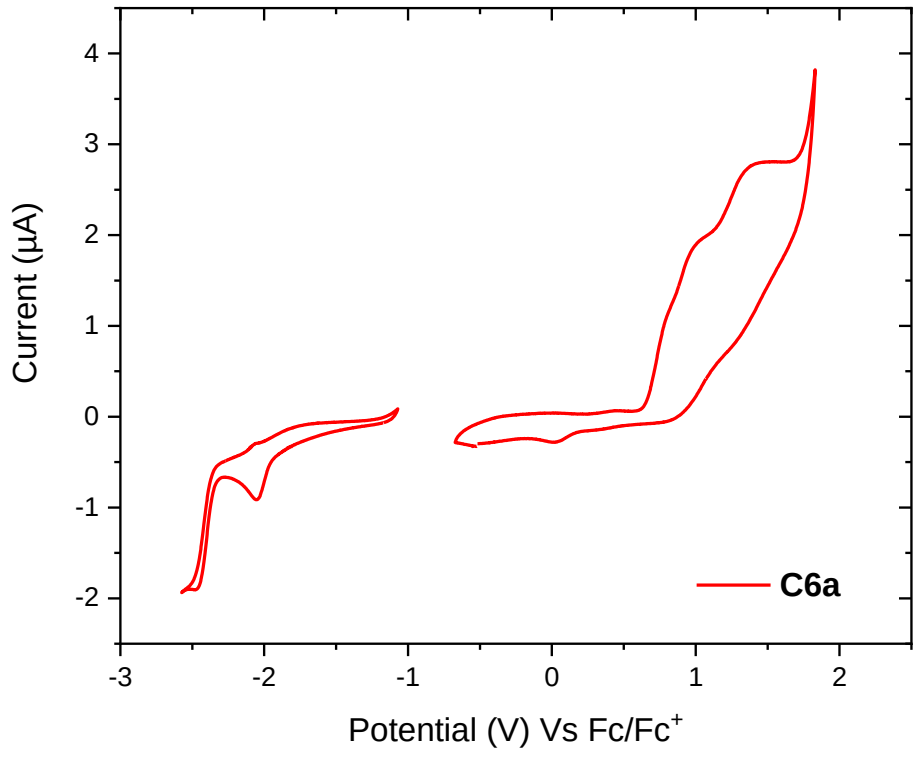

Figure 35: Cyclic voltammetry of complex **C6a**, in acetonitrile (0.1 M $TBAPF_6$), scan rate 100 mV/s.

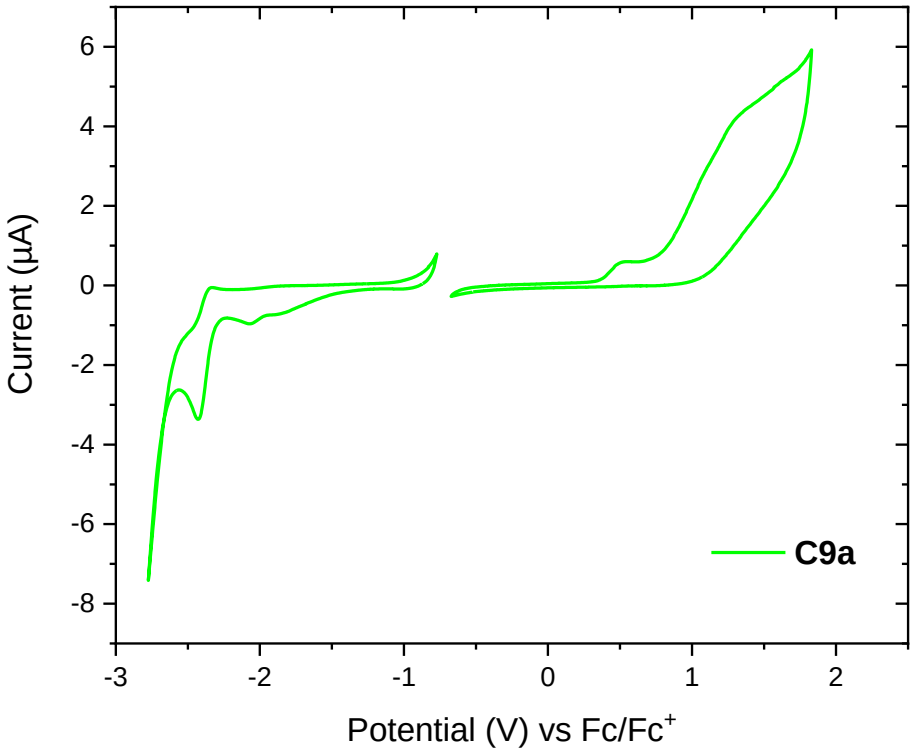

Figure 36: Cyclic voltammetry of complex **C9a**, in acetonitrile (0.1 M $TBAPF_6$), scan rate 100 mV/s.

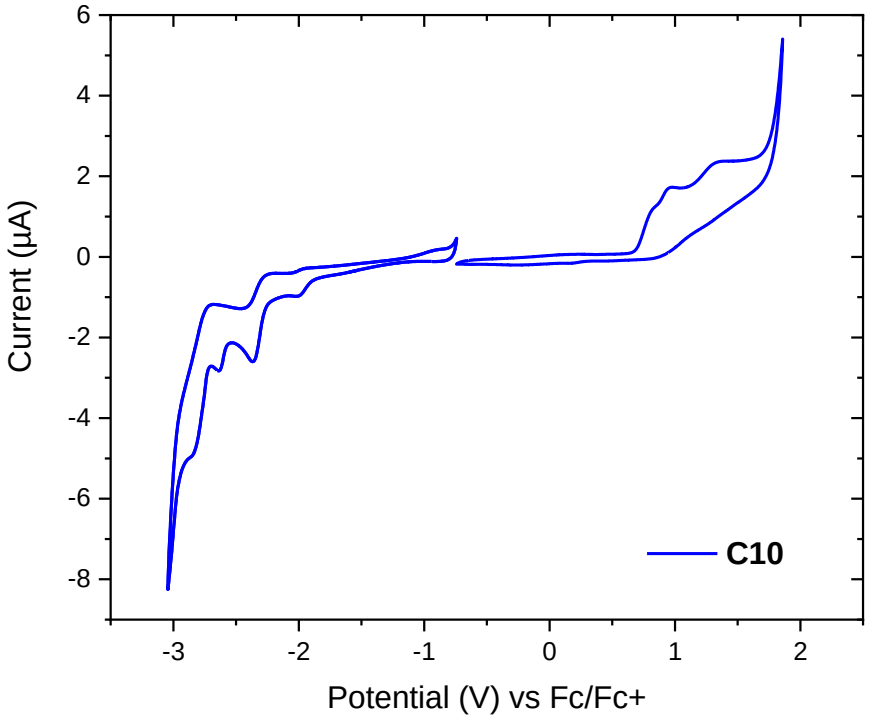

Figure 37: Cyclic voltammetry of complex **C10**, in acetonitrile (0.1 M $TBAPF_6$), scan rate 100 mV/s.

Sample	Eox (V)	E red (V)	HOMO (eV)	LUMO (eV)	$\Delta_{HOMO-LUMO}$ (eV)
C6a	1.15	-2.18	-5.29	-1.96	3.33
C9a	1.22	-2.39	-5.49	-1.85	3.64
C10	1.15	-2.50	-5.32	-1.70	3.62

Table 13: Electrochemical data of the mononuclear complexes **C6a**, **C9a**, **C10** in acetonitrile (0.1M $TBAPF_6$) at room temperature, scan rate 100 mV/s, reported versus ferrocene/ferrocenium potential.

The frontier orbitals HOMO and LUMO are indirectly related to the oxidation and reduction potentials, their values were estimated utilizing the oxidation and reduction potentials of the complexes in respect to the oxidation potential of the ferrocene which is 4.8 eV with respect to zero vacuum level. This value (see **Table 13**) is obtained from the calculated value of $\pm$ 4.6 eV for the standard electrode potential, using a normal hydrogen electrode (NHE) on the zero vacuum level and the value of $\pm$ 0.2 V for Fc vs. NHE.[61]

The HOMO and LUMO values and their gap, reported in the **Table 12** for complex **C6a**, **Table 13** for complex **C9a** and **Table 14** for complex **C10**, are very similar to each other.

Since HOMO-LUMO gap represents the energy absorbed by a photon this value permit to valuate the wavelengths the compounds can absorb.

As we expected to see the HOMO-LUMO gap is lower for these complexes than for the complex **C11a** ($\Delta_{HOMO-LUMO}$ = 4.05 eV).[55] Since energy and wavelength are inversely proportional (see **eq.2**) the increasing in absorption in visible light of the complexes (higher wavelength) is reflected in a decrease of the energy.

$$E = h\nu = h \cdot c/\lambda$$

Equation 2: Planck's equation, where h is Plank's constant, c is light speed and λ wavelength.

In future also the binuclear complexes will be electrochemically characterised.

Moreover, in order to use these complexes as photosensitizers it will be necessary to determine the excited state redox processes. These values will be used to evaluate if a photoinduced electron transfer process, reductive or oxidative quenching, is energetically possible.

4- Experimental Section

4.1- Materials and Methods

Analytical Resources and Apparatus

Nuclear Magnetic Resonance Spectroscopy (NMR)

The NMR spectra of compounds described herein were recorded by a Bruker Avance 300 NMR instrument at 300 MHz for ^{1}H NMR and 75 MHz for ^{13}C NMR, a Bruker Avance 400 NMR instrument at 400 MHz for ^{1}H NMR, 100 MHz for ^{13}C NMR and 162 for ^{31}P NMR, a Bruker Avance 500 NMR instrument at 500 MHz for ^{1}H NMR, 125 MHz for ^{13}C NMR and 202 for ^{31}P NMR.

The NMR spectra were recorded at room temperature in deuterated solvents commercially acquired from Euristop. The chemical shift δ is displayed in parts per million [ppm] and the references used were the ^{1}H and ^{13}C peaks of the solvents themselves: d1-chloroform ($CDCl_3$): 7.26 ppm for ^{1}H and 77.0 ppm for ^{13}C, d6-dimethyl sulfoxide (d5-DMSO): 2.50 ppm for ^{1}H and 39.4 ppm for ^{13}C and d3-acetonitrile (CD_3CN):1.93 ppm for ^{1}H and 1.3 ppm for ^{13}C.

Evaluation of the signals was done according to first order spectra. When describing couplings, the following abbreviations were used: d = doublet, t = triplet, m = multiplet, dd = doublet of doublet, ddd = doublet of doublet of doublet. Coupling constants "*J*" are given in Hertz [Hz] with the largest value first. Couplings are given with their respective number of bindings and binding partners, as far as they could be determined, written as index of the coupling constants

Mass Spectrometry (MS)

Different methods were used for the measurements: Electronic Ionisation (EI), Fast Atom Bombardment (FAB) and Electrospray Ionisation (ESI)**. As equipment** Finnigan *MAT 90* (70 eV) with a matrix of 3-Nitrobenzylalkohol (3-NBA) was used for EI and FAB and Thermo Fisher *LTQ Orbitrap XL Spectrometer* in *NanoESI* modus for the ESI. The source in the *NanoESI* modus was home-made. For characterisation, the mass to charge ratio (m/z) is plotted against the relative intensity, with the base peak set to "100%".

Weight Scale

For weightings of solids and liquids, a Sartorius scale, model LC 620 S was used.

Thin Layer Chromatography (TLC)

TLC Aluminium plates with fluorescence indicator, made by Merck, silica gel 60 F_{254}, thickness 0.2 mm), were used for the analytical thin layer chromatography. UV active compounds were detected with a Heraeus UV-Lamp, model Fluotest, at 254 nm and 366 nm wavelength.

Absorption Spectroscopy

The absorption spectra were recorded with a *PerkinElmer Lambda* 750 UV/Vis spectrometer. The measurements were performed at 20 °C. A correction of spectra was made automatically by the instrument with the absorption of the pure solvent (blank).

Fluorescence Spectroscopy

The measurements were recorded with a *HORIBA-Scientific Fluoromax-4* spectrofluorometer with a *Thermo Scientific* thermostat and the software *FluorEssence V3.5*

S*olvents and Chemicals*

Solvents of p.a. quality (per analysis) were commercially acquired from Sigma Aldrich, Carl Roth or Acros Fisher Scientific and, unless otherwise stated, used without previous purification. Absolutized solvents were either purchased from Carl Roth, Acros or Sigma Aldrich (< 50 ppm H2O over molecular sieve). All reagents were commercially acquired (through ABCR, Acros, Alfa Aesar or Sigma Aldrich) or were available in the working group. Unless otherwise stated, they were used without further purification.

Dry solvents have been taken from an automatic dry machine, SPS model 800 manual of MBRAUN.

Preparative Work

Reactions were carried out under argon atmosphere in previously baked out apparatuses with standard Schlenk techniques. Liquid reagents and solvents were injected with plastic syringes and stainless-steel cannula of different sizes.

Product Purification

Crude compounds were purified by flash chromatography. For the stationary phase of the column, silica gel, produced by Merck (silica gel 60, 0.040 × 0.063 mm, 260 – 400 mesh ASTM), and sea sand by Riedel de Haën (baked out and washed with hydrochloric acid) were used. Solvents used were commercially acquired in HPLC-grade and individually measured volumetrically before mixing.

4.2- Synthesis of starting material.

The starting material necessary to synthetize the quinoline-1*H*-1,2,3-triazole ligands is 2-ethynyl(quinoline). This product can be easily obtained via a two-step synthesis. [56]

Step 1: Synthesis of 2-((trimethylsilyl)ethynyl)quinoline.

The first step to obtain the starting material is a Sonogashira coupling.
In a three-neck flask 0,2094 g (1 mmol, 1 equiv.) of 2-bromoquinoline were reacted with 0,69 mL (4,98 mmol, 5 equiv.) of ethynyl(trimethyl)silane, N-propan-2-ylpropan-2-amine (DIPA) act here as non-nucleophile base and is used in excess as solvent, 20 mL.
The reaction was carried out for 4 h under Argon atmosphere and at room temperature to avoid the breaking of the triple bond. As catalyst is used $Pd(PPh_3)_2Cl_2$ 1% mol (0,0074 g) and as co-catalyst CuI 2% mol (0,0036 g).
After filtration and evaporation under vacuum of the solvent, the product looks like a brown oil.
The reaction was checked with TLC using as eluent Dichloromethane and Cyclohexene 1:1.

2-((trimethylsilyl)ethynyl)quinoline

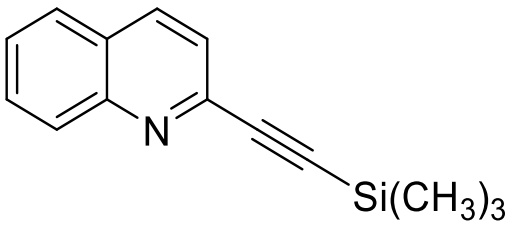

Brown viscous oil

Rf = 0.25 (DCM/CH 1:1), moon-shaped spot

^{1}H-NMR (300 MHz, $CDCl_3$): δ/ppm 8.11 (1H, d, *J* = 3.6 Hz, quinoline), 8.08 (1H, d, J = 3 Hz, quinoline), 7.77 (1H, d, J = 8.1 Hz, quinoline), 7.69 (1H, dd, J = 9 Hz, 6 Hz, quinoline), 7.54 (1H, dd, J = 8.1 Hz, 6.9 Hz, quinoline), 7.52 (1H, d, J = 8.7 Hz, quinoline), 0.29 (9H, s, -$(CH_3)_3$).

Step 2: Synthesis of 2-ethynylquinoline.

The product of the previous reaction was all used for the following step of deprotection.
To remove the TMS group 2-((trimethylsilyl)ethynyl)quinoline was put in a round bottom flask; K_2CO_3 (2 equiv., 0,2689 g) and 10 mL of MeOH were added, the reaction was carried out at room temperature for 2 h. [56]
After completion of the reaction; checked with TLC analysis using as eluent Cyclohexene and Ethyl acetate 1:1; the reaction was quenched with 5 mL of water and diluted with 10 mL of DCM. The organic layer was washed with water and BRINE three times, dried over Na_2SO_4, filtrated and evaporated under vacuum.
The desired product was purified by silica gel chromatographic column using cyclohexene/EtOAc (1:1) as eluent.

2-ethynylquinoline:

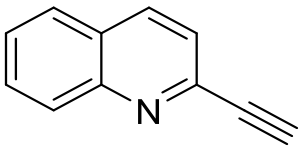

Brown oil

Yield: 60%

Rf = 0,75 (CH/EA 1:1)

^{1}H-NMR (300 MHz, $CDCl_3$): δ/ppm 8.08 (2H, d, J = 8.4 Hz, -CH, quinoline), 7.76 (1H, d, J = 9 Hz, -CH, quinoline), 7.72 (1H, dd, J = 9 Hz, 9 Hz, -CH, quinoline), 7.53 (1H, dd, J = 9Hz, 6Hz, -CH, quinoline), 3.24 (1H, s, -CH aliphatic).

4.3- Synthesis of the ligands.

From the starting material different ligand with different spacer were synthesized. To make a simple and clear presentation these were collected in three groups.

Group 1

Synthesis of quinoline 1,4-di substituted-1,2,3-triazole ligands, spacer = benzyl group.

General procedure:

The typical procedure follows for the synthesis of one of the compounds is described below.

To obtain this group of ligands an easy and cheap Sharpless-click reaction was followed, this procedure lead selectively to the 1,4-disubstituted-1*H*-1,2,3-triazole. [57]

In a 100 mL round flask, under constant stirring, 0.126 g (0.823 mmol, 1 equiv.) of 2-ethynylquinoline were reacted with 0.0545 g (0.206 mmol, 0.5 equiv.) of 1,4-bis(bromomethyl)benzene, 0.121 g (2.2 equiv.) of sodium azide, 0.0815 g of sodium ascorbate, 0.0400 g of copper sulphate penta hydrate and 0.0674 of sodium carbonate, in 10 mL of a solution of ethanol and water 7:3 at room temperature for 24 h.

Warning: azides and nitrogen-rich compounds can be explosive, so it's necessary to handle them with care.

The end of the reaction is checked via TLC analysis using dichloromethane and 1% methanol as eluent. The reaction was quenched with 20 mL of NH_4OH 10%, a yellow/brown precipitate was isolated by filtration and then dissolved in DCM. The organic solution was washed with water and BRINE three time, dried over Na_2SO_4, filtrated and evaporated under vacuum.

The product was purified by silica gel chromatographic column using as eluent DCM and 1% MeOH.

1,3-bis((4’-(quinolin-2’’-yl)-1’*H*-1’,2’,3’-triazol-l’-yl)methyl)benzene

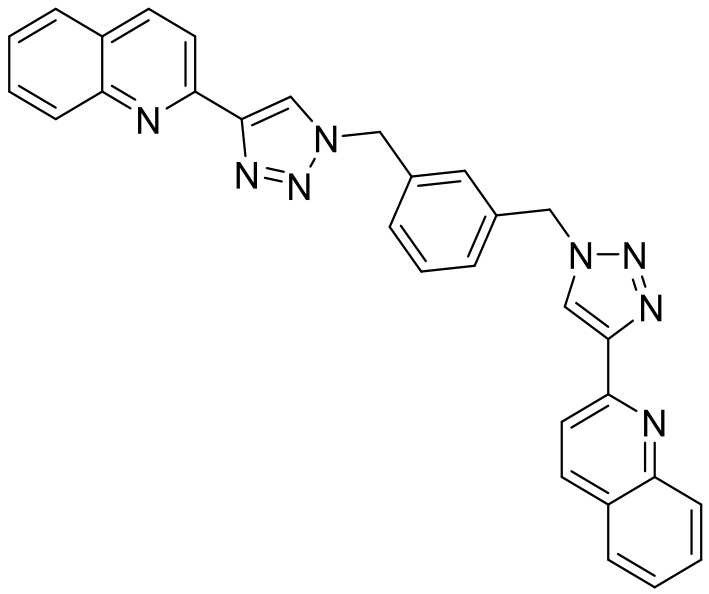

Yellow/brown solid

Yield: 41%

^{1}H-NMR (300 MHz, $CDCl_3$): δ/ppm 8.46 (2H, s, NCHCC), 8.28(2H, d, J = 8.7 Hz, -CH, quinoline), 8.22(2H, d, J = 8.7 Hz, -CH, quinoline). 8.00 (2H, d, J = 8.1 Hz, -CH, quinoline), 7.8 (2H, d, J = 6 Hz, CH, quinoline), 7.67 (2H, dd, J1 = 7.2 Hz, J2 = 7.8 Hz, -CH quinoline), 7.50 (2H, dd, J1 = 6.3 Hz, J2= 8.1, -CH, quinoline), 7.37 (4H, m, CH benzyl group) 5.64 (4H, s, -CH2).

1,4-bis((4’-(quinolin-2’’-yl)-1’*H*-1’,2’,3’-triazol-l’-yl)methyl)benzene

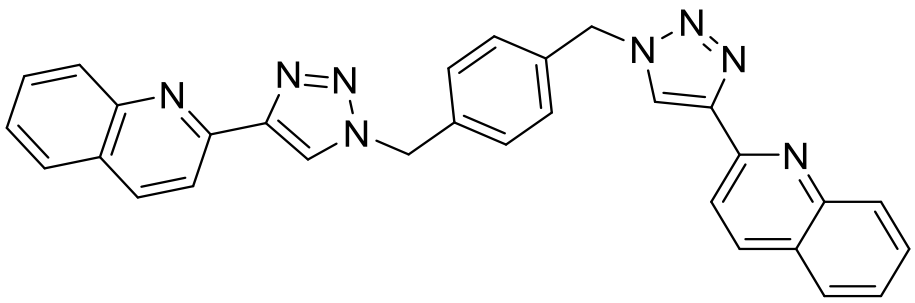

Yellow/brown solid

Yield: 17%

^{1}H-NMR (300 MHz, $CDCl_3$): δ/ppm 8.36 (2H, s, NCHCC), 8.33(2H, d, J not visible, under singlet, -CH, quinoline), 8.27(2H, d, J = 8.7 Hz, -CH, quinoline). 8.05 (2H, d, J = 8.4 Hz, -CH, quinoline), 7.83 (2H, d, J = 8.1 Hz, CH, quinoline), 7.69 (2H, dd, J1 = 9 Hz, J2 = 9 Hz, -CH quinoline), 7.52 (2H, dd, J1 = 6.9 Hz, J2= 8.1, -CH, quinoline), 7.40 (4H, s, CH benzyl group), 5.54 (4H, s, $-CH_2$).

1,2-bis((4’-(quinolin-2’’-yl)-1’*H*-1’,2’,3’-triazol-l’-yl)methyl)benzene

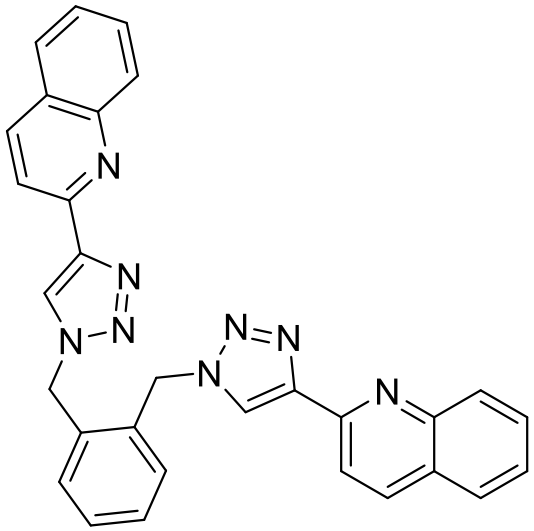

Yellow/brown solid

Yield: 19 %

^{1}H-NMR (300 MHz, CD_3SOCD_3) δ/ppm 8.78 (2H, s, NCHCC), 8.42 (2H, d, J = 7.2, -CH, quinoline), 8.18 (2H, d, J = 8.1 Hz, -CH, quinoline). 7.98 (2H, d, J = 7.8 Hz, -CH, quinoline), 7.93 (2H, d, J = 8.7 Hz, CH, quinoline), 7.72 (2H, dd, J1 = 8.1 Hz, J2 = 7.2 Hz, -CH quinoline), 7.56 (2H, dd, J1 = 7.8 Hz, J2= 7.2, -CH, quinoline), 7.41 (2H, m, CH benzyl group), 7.38 (2H, m, CH benzyl group), 6.00 (4H, s, -CH2).

To study the properties of the complexes it was necessary to study also the mono-substituted complex, therefore also the relative mono-substituted quinoline-1*H*-1,2,3-triazole were synthesised.

2-(1''-benzyl-1'*H*-1',2',3'-triazol-4'-yl)quinoline

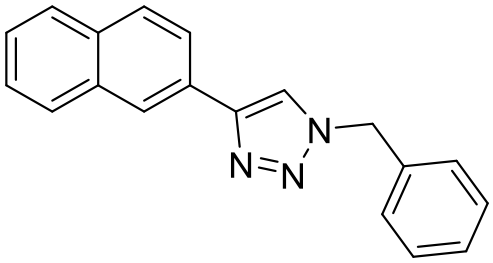

Brown solid

Yield: 82 %

^{1}H-NMR (300 MHz, CD_3Cl) δ/ppm 8.39 (1H, s, NCHCC), 8.36 (1H, d, J = 6.9, -CH, quinoline), 8.23 (1H, d, J = 8.4 Hz, -CH, quinoline), 8.07 (1H, d, J = 9.3 Hz, -CH, quinoline). 7.82 (1H, d, J = 6.9 Hz, CH, quinoline), 7.70 (1H, dd, J1 = 6.9 Hz, J2 = 7.8 Hz, -CH quinoline), 7.51 (1H, dd, J1 = 7.2 Hz, J2= 7.5, -CH, quinoline), 7.37 (5H, m, CH benzyl group), 5.61 (4H, s, $-CH_2$).

Group 2

Synthesis of quinoline 4,5-di substituted-1,2,3-triazole ligand, spacer = phenyl group.

General procedure:

The typical procedure for the synthesis of one compound is described below.
To obtain this group of ligands a two-step synthesis was necessary, first a Sonogashira coupling to synthetize the intramolecular triple bond and then a Huigsen reaction.

Step 1: synthesis of 1,4-bis(quinolin-ylethynyl)benzene.

In a round bottom flask, under argon atmosphere and constant stirring, 0.1374 g of 2-ethynylquinoline (1equiv.), 0.148 g of 1,4-diiodobenzene were added, as catalyst is used 1% mol $Pd(PPh_3)_2Cl_2$ (0.0063 g) and as co-catalyst CuI 2% mol (0.005 g). All was dissolved in 20 mL of DIPA. The reaction was carried out for 3h, with constant stirring at 70°C.
The end of the reaction was checked via TLC analysis, using DCM as eluent.
The reaction mixture was quenched with 10 mL of distilled water and washed with 10 mL of DCM, the organic layers were then washed with water and BRINE 3 times. The organic phase was collected, dried over Na_2SO_4 anhydrous, filtrated and evaporated under vacuum.
The obtained crude product was purified via flash-chromatography on silica gel using first dichloromethane and then dichloromethane and 1% of methanol as eluent.
The product is obtained with 42% yield, 0.1464 g.

1,4-bis(quinolin-ylethynyl)benzene

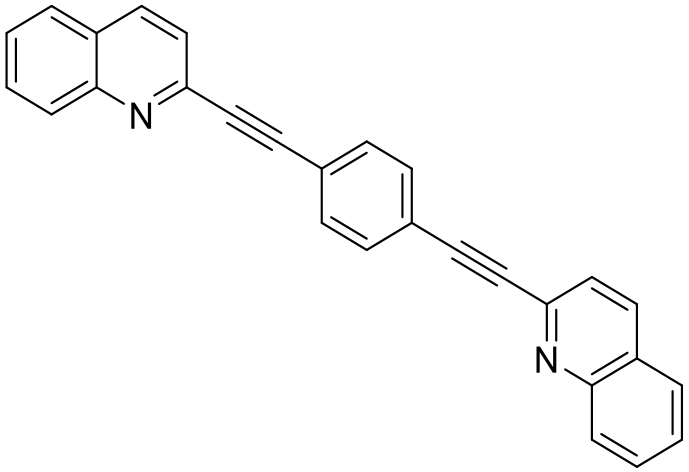

Pale yellow solid

yellow luminescence under 366 nm lamp

Yield: 42%

Rf-value: 0.16 (DCM)

^{1}H-NMR (300 MHz, CD_3Cl) δ/ppm 8.17 (4H, d, J = 8.4 Hz, -CH quinoline), 7.83 (2H, d, J = 8.1 Hz, CH quinoline), 7.75 (2H, dd, J1 = 8.4, J2 = 7.2, CH quinoline), 7.68 (4H, s (d), CH phenyl), 7.63 (2H, d, J = 8.4 Hz, -CH quinoline), 7.57 (2H, dd, J1 = 7.5 Hz, J2 = 7.5 Hz, -CH quinoline).

1,3-bis(quinolin-ylethynyl)benzene

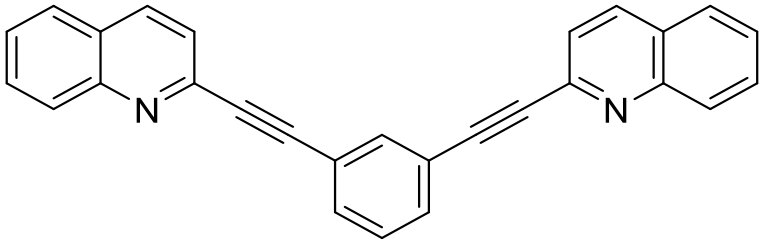

Pale yellow solid

Yellow luminescence under 366 nm lamp.

Yield: 42%

Rf-value: 0.42 (DCM)

^{1}H-NMR (300 MHz, CD_3Cl) δ/ppm 8.13 (2H, d, J = 5.1 Hz, -CH quinoline), 8.10 (2H, d, J = 5.1 Hz, -CH quinoline), 7.92 (1H, s, J = 8.1 Hz, CCHC phenyl), 7.77 (2H, d, J = 8.1, CH quinoline), 7.71 (2H, dd,J1 = 8.4, J2 = 7.2, CH quinoline), 7.67 (2H, d, J = 7.8 Hz, -CH quinoline), 7.58 (2H, d, J = 8.4 Hz, -CH phenyl) 7.52 (2H, dd, J1 = 8.1 Hz, J2 = 8.1 Hz, -CH quinoline), 7.37 (1h, dd, J1= 7.8 Hz, J2= 7.8 Hz, -CH phenyl).

1,2-bis(quinolin-ylethynyl)benzene

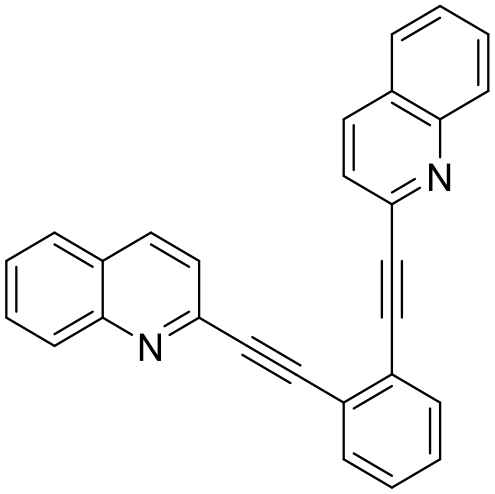

Pale yellow solid

Yellow luminescence under 366 nm lamp.

Yield: 14 %

Rf-value: 0.35 (DCM)

^{1}H-NMR (300 MHz, CD_3Cl) δ/ppm 8.18 (2H, d, J = 8.7 Hz, -CH quinoline), 8.13 (2H, d, J = 8.4 Hz, -CH quinoline), 7.91 (2H, s, J = 8.4 Hz, CH quinoline), 7.75 (6H, m, CH quinoline), 7.54 (2H, dd, J1 = 6.9, J2 = 8.1, CH phenyl), 7.37 (2H, dd, $J_{1,2}$ = 6 Hz, -CH phenyl), , 7.26 (1H, d, J = 4.5 Hz, -CH phenyl), 7.24 (1H, d, J = 5.1 Hz).

2-(phenylethynyl)quinoline

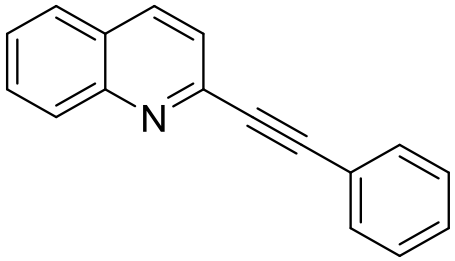

White solid

Yield: 88%

^{1}H-NMR (300 MHz,CDCl3): δ/ppm 8.17 (1H, d, J = 3.3 Hz, quinoline), 8.14 (1H, d, J = 3.3 Hz, quinoline), 7.82 (1H, d, J = 8.1 Hz, quinoline), 7.74 (1H, dd, J1 = 7.2 Hz,J2 = 6.9 Hz, quinoline), 7.69 (1H, d, J = 2.4 Hz, quinoline), 7.67 (1H, d, J = 3.9 Hz), 7.63 (1H, d, J = 8.4 Hz), 7.56 (1H, dd, J1 = 6.9 Hz, J2 = 7.2 Hz), 7.40-7.37 (3H, m, phenyl).

Step 2: Synthesis of 1,3-bis(5'-(quinolin-2''-yl)-1'*H*-1',2',3'-triazol-4'-yl)benzene

In a two neck round bottom flask, under Ar atmosphere the product of the previous reaction was dissolved in 10 mL of dry DMF, under constant stirring 6 equiv. of TMS-N_3 were added. The reaction was left overnight at 70°C.
TLC control (eluent DCM +1% MeOH) showed the presence of the starting material, therefore 3 eq. of TMS-N_3 were added, and the reaction was left for other 4 hours.
The reaction was stopped and lowered to ambient temperature, the solvent was then evaporated under vacuum.
The product look like a brown oil and was obtained with 87% yield, 0.1558 g.

2-(5'-phenyl-1'*H*-1',2',3'-triazol-4'-yl)quinoline

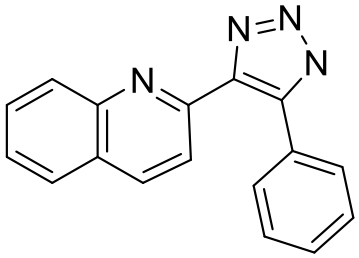

Yellow/white solid

Blue luminescence under 366 nm lamp.

Yield: 89 %

Rf-value: bottom of TLC

^{1}H-NMR (300 MHz, CD_3SOCD_3) δ/ppm 8.15 (1H, d, J = 8.7 Hz, CH quinoline), 7,99 (3H, 3d overlaid signals, CH quinoline), 7.79 (2H, 2d, overlaid signals, J1,2 = 7.2 Hz CH phenyl), 7.60 (1H, dd, J1 = 7.2 Hz J2 = 7.5 Hz, CH quinoline), 7.40 (1H, dd, J1 = 7.5 Hz, J2 = 7.2 Hz, Ch quinoline), 7.25 (2H, 2dd, J1 = 7.5 Hz, J2 = 7.5 Hz, CH phenyl), 7.12 (1H, dd, J1 = 7.2 Hz,J2 = 7.2 Hz, CH phenyl).

1,3-bis(5’-(quinolin-2’’-yl)-1’*H*-1’,2’,3’-triazol-4’-yl)benzene

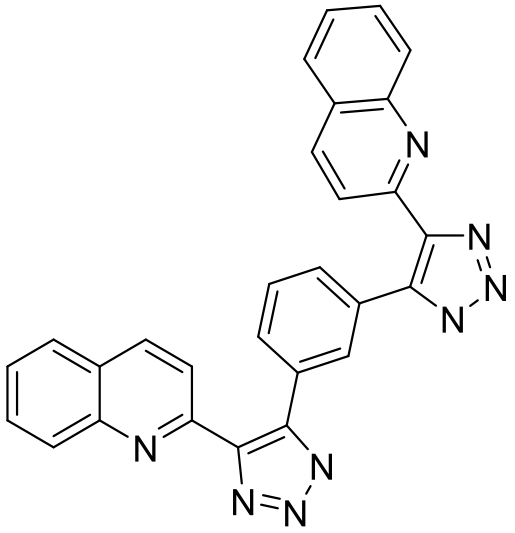

Pale yellow solid

Blue luminescence under 366 nm lamp.

Yield: 60 %

Rf-value: 0.08 (DCM)

^{1}H-NMR (300 MHz, CD_3Cl) δ/ppm 8.38 (1H, s, CH phenyl), 8.02 (4H, m, quinoline), 7.87 (4H, m , CH quinoline), 7.73 (2H, d, J = 8.7 Hz CH phenyl), 7.61 (2H, dd, J1= 8.7 Hz, J2 = 6.3 Hz, CH quinoline), 7.47 (2H, dd, J1 = 6.6 Hz, J2 = 7.2 Hz, Ch quinoline), 7.34 (1H, dd, J1 = 7.8 Hz, J2 = 8.4 Hz, CH phenyl).

1,4-bis(5’-(quinolin-2’’-yl)-1’*H*-1’,2’,3’-triazol-4’-yl)benzene

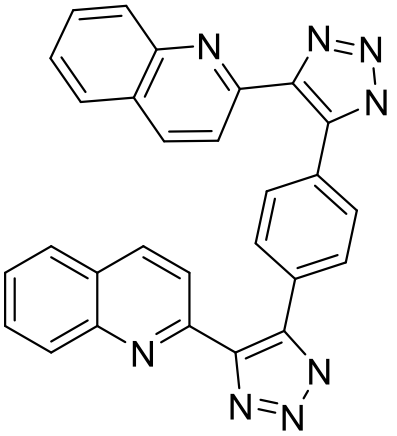

Pale yellow solid

Yellow luminescence under 366 nm lamp.

Yield: 88 %

Rf-value: 0.08 (DCM)

^{1}H-NMR (300 MHz, CD_3Cl) δ/ppm 8.10 (2H, d, J = 8.7 Hz, -CH, quinoline), 7.99 (2H, d, J no visible under DMF signal), 7.90 (2H, d, J = 8.4 Hz, CH quinoline), 7.83 (4H, s, CH phenyl), 7.73 (2H, d, J = 8.1 Hz, CH quinoline), 7.59 (2H, dd, J1 = 7.5 Hz, J2 = 7.5 Hz, CH quinoline), 7.44 (2H, dd, J1 = 8.1 Hz, J2 = 7.8, -CH quinoline).

Group 3:

Synthesis of 2-(1''-phenyl-1'H-1',2',3'-triazol-4'-yl)quinoline

1° procedure.

In a 10 mL flask were added 0.1 mL of iodobenzene (1 equiv.), 0.137 g 2-ethynylquinoline (1 equiv.), 0.0759 g NaN_3 (1.2 equiv.), L-proline (0.2 equiv.), 0.0223 g of Na_2CO_3 (0.2 equiv.), 0.0222 g of sodium ascorbate (0.1 equiv.) and 0.0112 of $CuSO_4 \cdot 5H_2O$ (0.05 equiv.). As solvent is used a solution of DMSO/H_2O 9:1 (2 mL). The reaction mixture was heated to 65°C and stirred overnight.

After completion, the reaction mixture was quenched with 10 mL of NH_3OH (10%) and washed with ethyl acetate, then, the organic layer was washed with water three times. The water layer was washed with DCM two times. The organic phase was dried on Na_2SO_4, evaporated under vacuum and analysed.

The product was purified on a silica gel chromatography.

To obtain a good separation of the different fraction as eluent is first used DCM/cyclohexene 7:3, then DCM, and after DCM with 1% MeOH this percentage was increased to 5% to remove also the last spot. In attempt to understand the structure of the product and of the by-product a preparative TLC is done using DCM as eluent; few milligrams of the desired product were collected but not enough to proceed with the complexation.

2° procedure.

Since the previous reactions haven't given good results, this new method of synthesis was followed. [58] To a stirred solution (EtOH/H2O, 10 mL, 7:3) and iodobenzene (0.447 mmol, 1.0 equiv.) was added NaN_3 (0.0912 g, 0,943 mmol, 2.2 equiv.), CuI (0.0167 g, 0.2 equiv.), N,N'-dimethylethylenediamine (0,014 ml, 0.3 equiv.) and sodium ascorbate (0.0476 g, 0.5 equiv.). The reaction was then heated to reflux under argon atmosphere for 4:30 h. After this time the reaction mixture was cooled to room temperature and 2- ethynylquinoline (0.4354 mmol, 1 equiv.), $CuSO_4 \cdot 5\ H_2O$ (0.0228 g, 0.2 equiv.), and sodium ascorbate (0.0426 g, 0.5 equiv.) were added to the reaction mixture and the resulting suspension was stirred at room temperature for all the weekend

The first part of reaction was checked with TLC using as eluent dichloromethane/cyclohexene (2:8).

The reaction mixture was quenched with 10 mL of NH_3OH 10%. After the addition of DCM, the organic layers were washed with water three times and dried over Na_2SO_4 and evaporated under vacuum.

The obtained crude product was purified by Flash chromatography silica gel using CH_2Cl_2 as eluent; because some difficulties in separating the product from by-product, as eluent was used CH_2Cl_2 with 1% MeOH, the percentage was increased to 5 % but it was not possible to achieve a good separation and again a preparative TLC was necessary.

2-(1''-phenyl-1'*H*-1',2',3'-triazol-4'-yl)quinoline

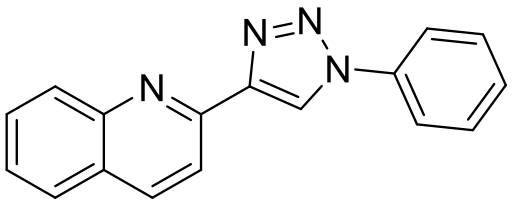

Brown/yellow solid,

Yield: 16 %

^{1}H-NMR (300 MHz, CD_3Cl) δ/ppm 8.82 (1H, s, CH triazole), 8.43 (1H, d, J = 8.4 Hz, CH quinoline), 8.30 (1H, d, J = 8.7 Hz, CH quinoline), 8.11 (1H, d, J = 8.4 Hz, CH quinoline), 7.86 (3H, 2dd, 1 d, CH quinoline, J1 = 7.5 Hz, J2= 6.3 Hz), 7.74 (1H, dd, J1 = 6.9 Hz, J2 = 8.4 Hz, Ch phenyl); 7.60-7.48 (4 H, dd, J1 = 7.5 Hz, J2 = 7.2 Hz, CH phenyl).

4.4- Synthesis of the pre-catalyst.

Copper(I) oxide (2.02 g, 0.014 mol) was mixed with acetonitrile (30mL) in a round bottom flask. Fluoroboric acid diethyl ether (7.6 mL, 55.8 mmol) was added slowly with constant stirring over a 30 minute.

Then the warm mixture was filtered to remove any unreacted copper(I) oxide. The green/blue solution was then cooled to -10 °C in a freezer and left overnight. A white powder crystallized out of solution, which was collected by filtration, washed with cold acetonitrile. The pure tetrakis(acetonitrile) copper(I)tetrafluorophosphate, was then dried in vacuum and stored under argon.

4.5- Synthesis of [Cu(I)(N^N)(P^P)] complexes.

General procedure:

In a Schlenk tube, under Argon atmosphere, $Cu[CH_3CN]_4(BF_4)$ (31.4 mg, 0.1 mmol) was dissolved in 8 ml of dry and freshly distilled CH_2Cl_2. Bis[(2-diphenylphosphino)phenyl] ether (DPEPhos) (53.9 mg, 0.1 mmol, 1 equiv.) was added. The reaction was finished in 30 min, at room temperature, always under inert atmosphere. To reaction mixture was added the ligand (30 mg, 0.1 mmol). The reaction is maintained under argon atmosphere overnight. The reaction mixture is evaporated under vacuum and the product is dissolved in DCM (min) and cyclohexene was added slowly. In order

to obtain a first purification of the complex, the solution was cooled in the freezer and left overnight.

The complex was then purified via silica gel chromatographic column, using DCM + 1% MeOH.

To better understand and facilitate the interpretation of the ^{1}H-NMR of the complexes, the NMR of the phosphine ligand (DPEPhos) was recorded.

(Oxybis(2,1-phenylene))bis(diphenylphosphine)

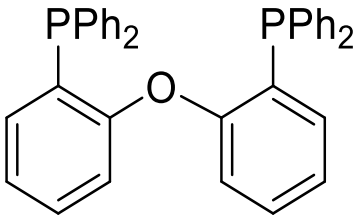

White solid

^{1}H-NMR (300 MHz, $CDCl_3$) δ/ppm 7.30 - 7.17 (22H, m), 6.96 (2H, dd, J1 = 6.6 Hz, J2 = 7.2 Hz), 6.84 - 6.79 (2H, m), 6.71 – 6.67 (2H, m).

Oxydi-2,1-phenylene)bis(diphenylphosphine), 2-(1''-phenyl-1'*H*-1',2',3'-triazol-4'-yl)quinoline, Cu(I)

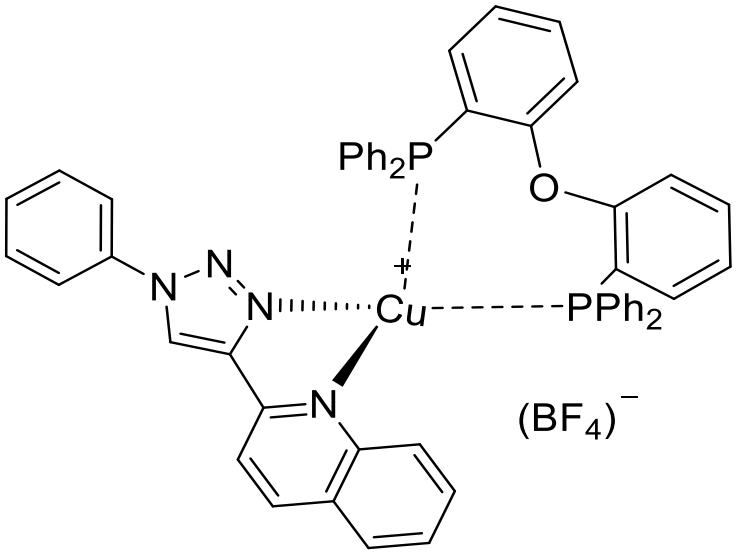

Yellow solid

Yield: 52%

^{1}H-NMR: (500 MHz, $CDCl_3$) δ/ppm 9.48(1H, s, CH triazole), 8.48 (2H, d, CH quinoline, J too little), 7.95 (2H, d, J = 4.5 Hz, CH quinoline), 7.82 (1H, d, J = 4.8 Hz, CH quinoline),7.62 – 7.45 (8H, m, CH quinoline + CH DPEPhos), 7.37 – 7.24 (8H, m, CH DPEPhos), 7.15 (2H, dd, J1,2 = 7.2 Hz, DPEPhos), 7.06 (2H, d, J = 7.8 Hz, DPEPhos), 6.96 – 6.89 (8H, m, DPEPhos), 6.76 – 6.71 (2H, m, DPEPhos), 6.66 – 6.06 (4H, m, DPEPhos).

^{13}C-NMR: (125 MHz, $CDCl_3$) δ/ppm 158.53, 147.68, 146.77, 145.65, 139.48, 136.47, 134.52, 134.32, 132.01, 131.66, 130.33, 130.01, 129.67, 129.63, 129.55, 128.70, 128.51, 128.42, 127.82, 127.23, 124.94, 123.36, 120.72, 120.42, 120.11.

^{31}P-NMR: (162 MHz, $CDCl_3$): δ/ppm -12.59.

HRMS m/z ($C_{53}H_{40}CuN_4OP_2$): 873.20 (calc), 873.20 (found).

Elemental analysis ($C_{53}H_{40}CuN_4OP_2BF_4 \cdot CH_2Cl_2$): N= 5.82, C= 66.09, H= 4.40 (calc); N= 5.34, C= 61.96, H= 4.21 (found).

(Oxydi-2,1-phenylene)bis(diphenylphosphine), 2-(1''-benzyl-1'*H*-1',2',3'-triazol-4'-yl)quinoline, Cu(I)

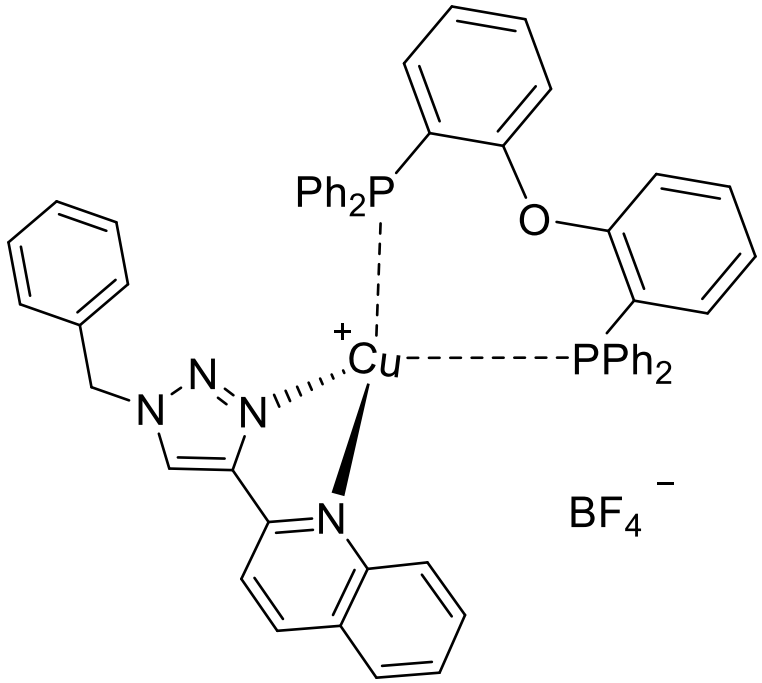

Yellow solid

Yield: 72%

^{1}H-NMR (500 MHz, CD_3CN): δ/ppm 7.92 (1H, s, CH triazole), 7.86 (1H, d, J = 8.4 Hz, CH quinoline), 7.71 – 7.19 (3H, 3d, CH quinoline), 6.76 - 6.42 (25H, m, quinoline + DPEPhos), 6.34- 6.25 (6H, m, DPEPhos), 6.03 – 5.95 (4H, m, DPEPhos), 4.99 (2H, s, CH_2 benzyl).

^{13}C-NMR (125 MHz, $CDCl_3$): δ/ppm 158.55, 147.76, 145.97, 146.60, 139.00, 134.51, 134.56, 131.89, 131.57, 130.93, 130.66, 130.26, 129.62, 129.47, 128.88, 128.68, 128.53, 128.29, 127.72, 127.11, 125.80, 124.88, 120.08, 119.86, 99.99, 26.93.

^{31}P-NMR (162 MHz $CDCl_3$) δ/ppm: -12.73.

HRMS m/z ($C_{54}H_{42}CuN_4OP_2$): 887.21 (calc.), 887.21 (found).

Elemental analysis ($C_{54}H_{42}CuN_4OP_2BF_4$): C = 65.51, H = 4.43, N = 5.74 (calc.); C = 65.53, H = 4.357, N = 5.54 (found).

(Oxydi-2,1-phenylene)bis(diphenylphosphine), 1,4-bis((4'-(quinolin-2''-yl)-1'*H*-1',2',3'-triazol-l'-yl)methyl)benzene,Cu(I)

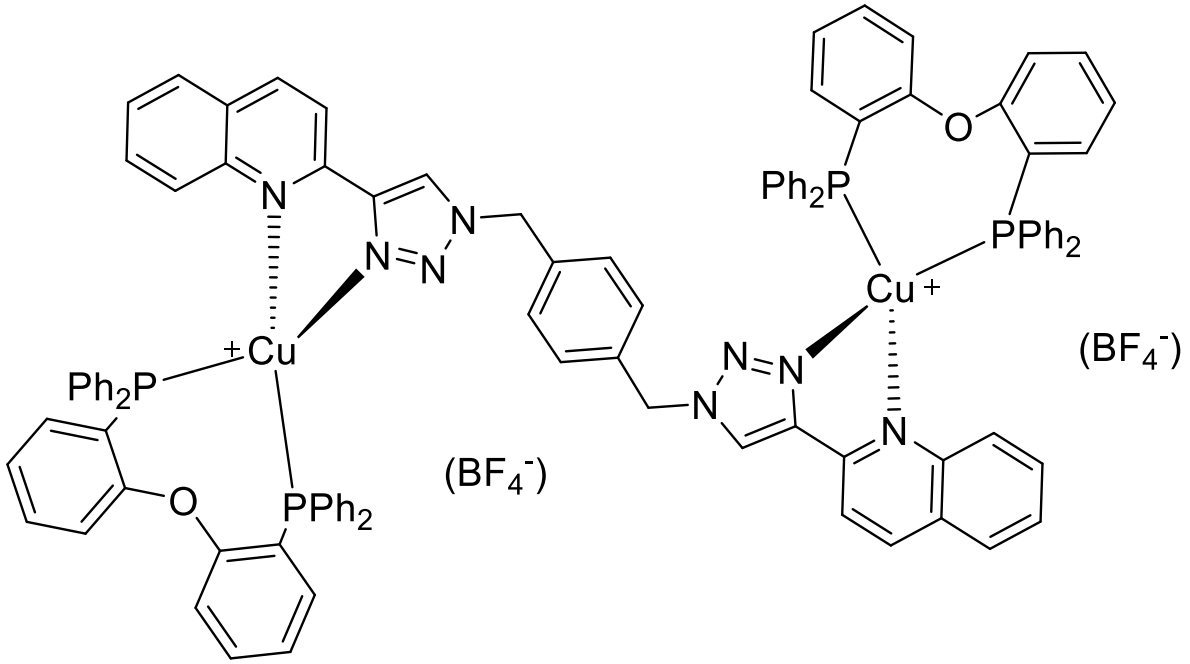

Yellow solid.

Yield: 94 %

^{1}H-NMR (500 MHz, CD_3CN): δ/ppm 8.48 (4H, m, CH quinoline), 7.92 (4H, m, CH quinoline), 7.78 (2H, s,CH triazole), 7.43 – 6.58 (64H, m, CH quinoline and DPEPhos), 5.66 (4H, s, CH_2 benzyl).

^{13}C-NMR (125 MHz, CD_3CN): δ/ppm 158.73, 147.49, 146.53, 146.3, 139.59, 135,63,134.42, 132.47, 131.28, 130.41, 129.10, 128.83, 128.36, 127.88, 125.20, 124.80, 123,98, 123.87, 123.75, 120.69, 119.08, 100.26, 54.61, 30.21.

^{31}P-NMR (162 MHz, CD_3CN): δ/ppm -13.30.

HRMS m/z ($C_{102}H_{78}BCu_2F_4N_8O_2P_4$): 1783.38 (calc), 1785.39 (found, presence of $2H^+$).

Elemental analysis ($C_{102}H_{78}BCu_2F_4N_8O_2P_4B_2F_8$): C = 65.43, H = 4.20, N = 5.98 (calc.); C = 65.28, H = 3.956, N = 6.19 (found).

(Oxydi-2,1-phenylene)bis(diphenylphosphine), 1,3-bis((4'-(quinolin-2''-yl)-1'*H*-1',2',3'-triazol-l'-yl)methyl)benzene,Cu(I)

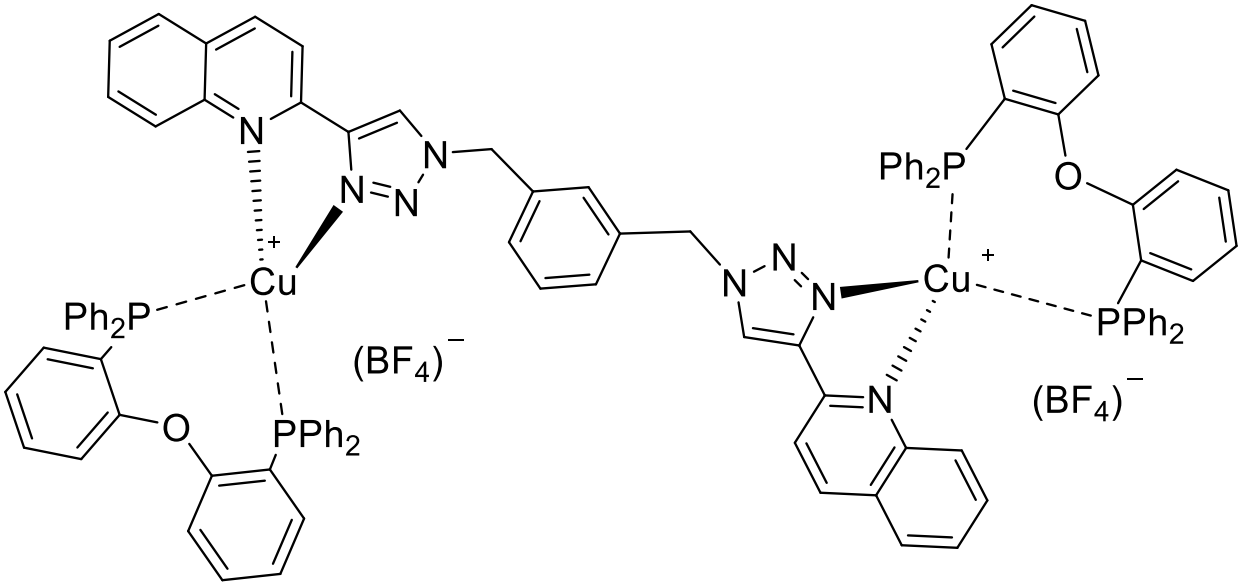

Yellow solid

Yield: 62%

^{1}H-NMR (500 MHz, CD_3CN): δ/ppm 8.50 (2H, s, CH quinoline), 8.46 (2H, d, CH quinoline), 7.94 (4H, m, CH quinoline), 7.80 (2H, m,CH quinoline), 7.46 – 6.60 (64H, m, CH quinoline and DPEPhos), 5.58 (4H, s, CH_2 benzyl).

^{13}C-NMR (125 MHz, CD_3CN): δ/ppm 158.78, 149.87,149.06,147.54,146.125,135.89, 134.50, 132.52, 131.72, 130.43,130.26 ,129.00, 128.92, 128.76, 128.39, 127.86, 125.29, 124.75, 124.05, 123.93, 123.81,120.77, 119.15, 54.66.

^{31}P-NMR (162 MHz, CD_3CN): δ/ppm -13.19.

HRMS m/z ($C_{102}H_{78}Cu_2P_4N_8O_2BF_4$): 1783.38 (calc.), 1785.39 (found, presence of $2H^+$).

Elemental analysis ($C_{102}H_{78}BCu_2F_4N_8O_2P_4B_2F_8$): C = 65.43, H = 4.20, N = 5.98 (calc.); C = 65.29, H = 4.242, N = 5.93 (found).

(Oxydi-2,1-phenylene)bis(diphenylphosphine), 1,2-bis((4'-(quinolin-2''-yl)-1'*H*-1',2',3'-triazol-l'-yl)methyl)benzene, Cu(I)

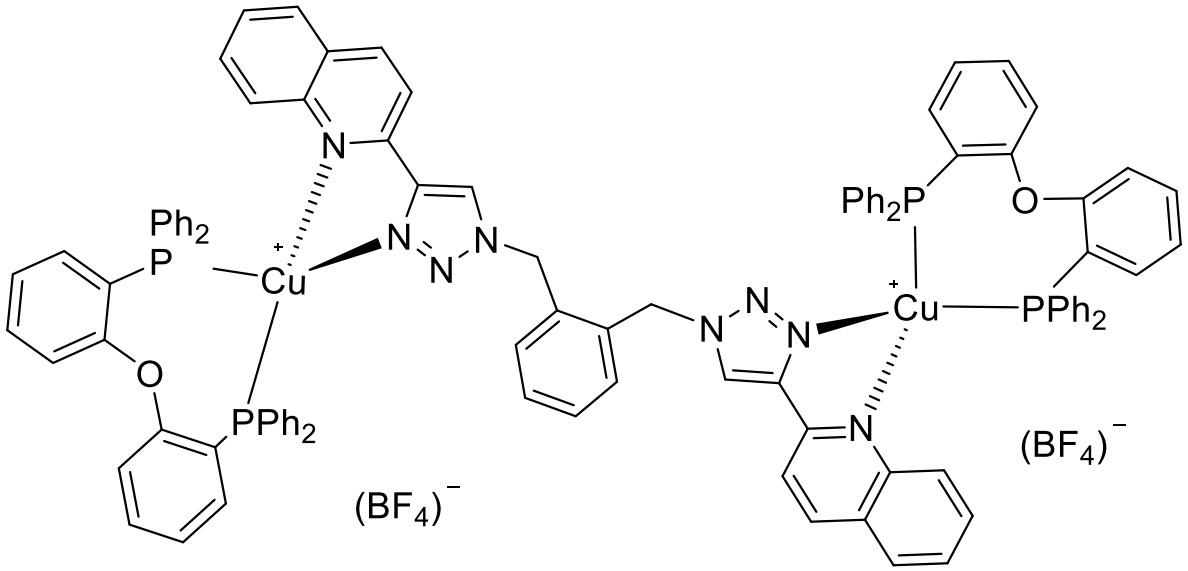

Yellow solid.

Yield: 91%

^{1}H-NMR (500 MHz, $CDCl_3$): δ/ppm 7.07 (2H, s, CH triazole), 8.39 (2H, d, J = 5.1 Hz, CH quinoline), 8.11 (2H, d, J = 5.1 Hz, CH quinoline),7.94 (2H, d, J = 5.1 Hz, CH quinoline),7.81 (2H, d, J = 5.1 Hz, CH quinoline), 7.48 (8H, m, quinoline), 7.35 (2H, dd, J1,2= 4.5 Hz) 7.28 – 7.24 (12H, m, DPEPhos), 7.22 – 7.19 (8H, m, DPEPhos), 7.10 (4H, m, DPEPhos), 7.04 (4H, m, DPEPhos), 6.93 (6H, m, DPEPhos) 6.84 (8H, m, DPEPhos), 6.72-6.69 (4H,m, DPEPhos) , 6.60-6.57(8H, m, DPEPhos), 5.85 (4H, s, CH_2 benzyl).

^{13}C-NMR (125 MHz, $CDCl_3$): δ/ppm 158.62, 147.47, 146.16, 145.67, 139.04, 134.53, 134.09, 132.97, 131.97, 131.73, 131.03, 130.64, 130.35, 129.89, 129.49, 128.34, 128.32, 127.73, 127.35, 125.69, 124.69, 124.23, 120.13, 119.72, 26.93.

^{31}P-NMR (162 MHz, $CDCl_3$): δ/ppm -12.60.

HRMS m/z ($C_{102}H_{78}Cu_2P_4N_8$ BF_4): 1783.38 (calc), 1785.40(found, presence of $2H^+$)

Elemental analysis ($C_{102}H_{78}BCu_2F_4N_8O_2P_4B_2F_8$)**:** C = 65.43, H = 4.20, N = 5.98 (calc.); C = 65.10, H = 4.321, N = 5.91 (found).

(Oxydi-2,1-phenylene)bis(diphenylphosphine), 1,4-bis(5'-(quinolin-2''-yl)-1'*H*-1',2',3'-triazol-4'-yl)benzene,Cu(I)

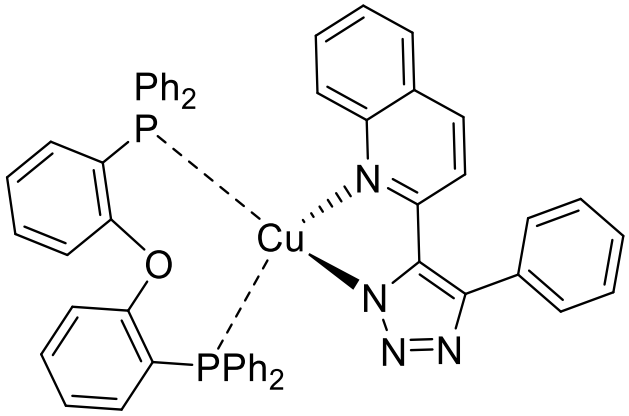

Yellow solid.

Yield: 56%

^{1}H-NMR (500 MHz, CD_3CN): δ/ppm 8.22 (1H, d. quinoline), 7.98 (1H, d, J = 4.8 Hz, quinoline), 7.80 (1H, d, quinoline), 7.47 (8H, m, quinoline), 7.13-6.66 (28H, m, DPEPhos).

^{13}C-NMR (125 MHz, $CDCl_3$) δ/ppm 168.64, 149.62, 146.14, 139.75, 137.54, 134.61, 134.48, 132.00, 131.47, 130.82, 130.14, 129,56, 129.34, 129.12, 129.00, 128.75, 128.09, 127.46, 127.29, 126.79, 124.76, 120.14, 118.08.

^{31}P-NMR (202 MHz, CD_3CN): - δ/ppm -13.59.

HRMS m/z ($C_{53}H_{39}CuN_4OP_2$): 872.19 calc., 873.20 ($+H^+$), 1745,28 (+ DPEPhos, Cu, $2H^+$)

Elemental analysis ($C_{53}H_{39}CuN_4OP_2 \cdot CH_2Cl_2 \cdot DMF$)**:** C = 68,38 H = 4.69, N = 6.79 (calc.); C = 66.38, H = 4.69, N = 5.79 (found).

(Oxydi-2,1-phenylene)bis(diphenylphosphine), 1,4-bis(5'-(quinolin-2''-yl)-1'*H*-1',2',3'-triazol-4'-yl)benzene,Cu(I)

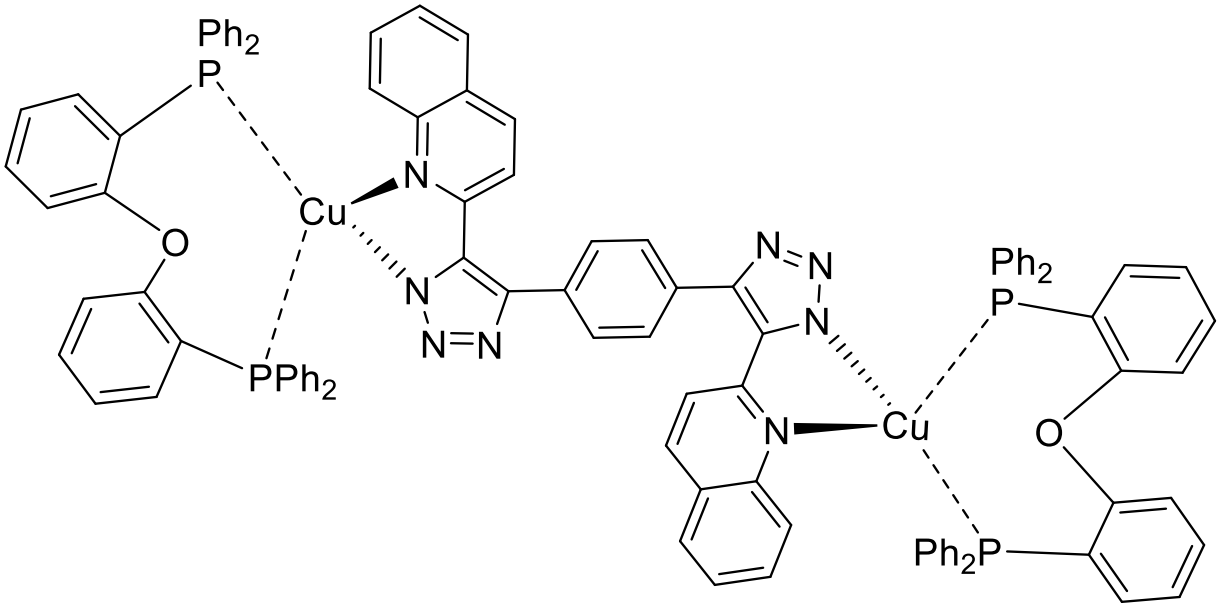

Yellow/orange solid

Yield: 30%

^{1}H-NMR (300 MHz, CD_3CN) δ/ppm 8.26 (2H, d, J = 6.9 Hz, quinoline), 8.00 (2H, d, J = 8.1 Hz, quinoline), 7.815 (2H, d, J = 8.4 Hz, quinoline), 7.65 (4H, m, quinoline), 7.40 – 6.80 (54H, m, 6H, quinoline; 48H DPEPhos), 6.70 – 6.58 (8H, m, DPEPhos).

^{13}C-NMR (125 MHz, $CDCl_3$): δ/ppm 158.82, 158.65, 158.47, 157.59, 146.45, 146.23, 139.41, 137.57, 135.04, 133.46,132.23, 131.82, 131.40, 130.36, 129,87, 129.43, 128.90, 128.57, 128.18, 127.97, 127.33, 126.81, 124.88, 124.57, 120.10, 119.76.

^{31}P-NMR (162 MHz, CD_3CN): δ/ppm -15.78.

HRMS m/z ($C_{100}H_{72}Cu_2N_8O_2P_4$):1666.33 calc., 1668.35 ($2H^+$), 2270.42 (+ DPEPhos, Cu, $3H^+$)

(Oxydi-2,1-phenylene)bis(diphenylphosphine), 1,3-bis(5'-(quinolin-2''-yl)-1'*H*-1',2',3'-triazol-4'-yl)benzene,Cu(I)

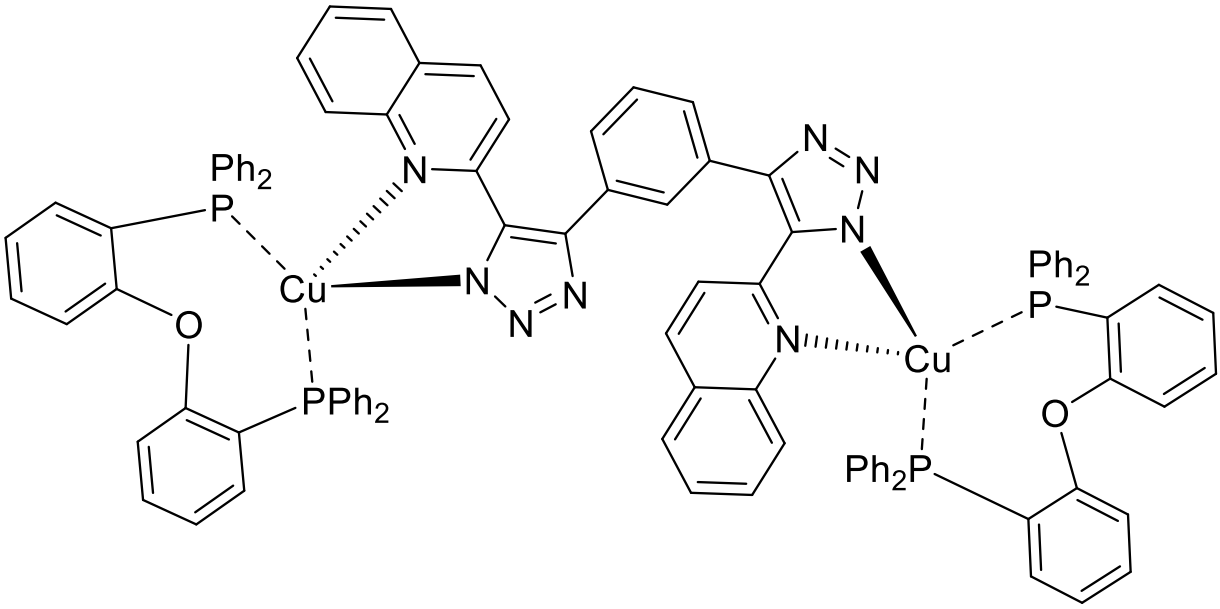

Yellow solid

Yield: 72%

^{1}H-NMR (500 MHz, CD_3CN): δ/ppm 7.93 (2H, d, J = 5.1 Hz, CH quinoline), 7.67 (8H, m, quinoline), 7.30-7.27 (5H, m, quinoline), 7.25-6.75 (43H, m, DPEPhos), 6.65-6.53 (13H, m, DPEPhos).

^{13}C-NMR (125 MHz, $CDCl_3$): δ/ppm 159.00, 152.84, 146.56, 139.73, 137.21, 135.30, 134.85, 132.45, 131.86, 131.03, 130.80, 129,87, 129.25, 128.84, 128.76, 128.62, 128.07, 127.25, 127.16, 125.29, 124.64, 120.28, 119.35.

^{31}P-NMR (202 MHz, CD_3CN): δ/ppm – 14.44.

HRMS m/z ($C_{100}H_{72}Cu_2N_8O_2P_4$):1666.33 calc., 1669.32 (+ $3H^+$), 2270.39 (+ DPEPhos, Cu, $3H^+$)

5- Conclusion and Outlook

In this work, three mononuclear and five binuclear heteroleptic copper(I) complexes based on quinolin-yl-1*H*-1,2,3-triazole as diimine chelating ligand and DPEPhos as chelating diphosphine were successful synthesised. These complexes are of high interest because their properties make them suitable photosensitizers in the photocatalytic reduction of carbon dioxide.

The presence of the quinoline instead of pyridine, not only increases the structural rigidity, leading to a less reorganisation in the excited state, but also increases the π-conjugation of the diimine ligand, lowering the HOMO-LUMO energy gap and shifting the absorption in the visible region (^{1}MLCT absorption max ≈ 410 nm). For these reasons, these complexes possess good luminescence properties in solution at room temperature, with high PLQY and long lifetime of the excited state, which for most of the binuclear complexes is much longer than for the mononuclear compounds.

Of course, further optimisation of the synthetic approach towards the N^N ligands is suitable. In particular, further study on the synthesis of ligands with 1,4-disubstituted -1*H*-1,2,3-triazole and phenyl group as spacer is necessary (structure of the ligands in **Fig. 38**). These ligands can lead to complexes with high π-conjugation and high degree of electronic communication between the metal centres, therefore we expected to see a great influence and improvement on the luminescence properties.

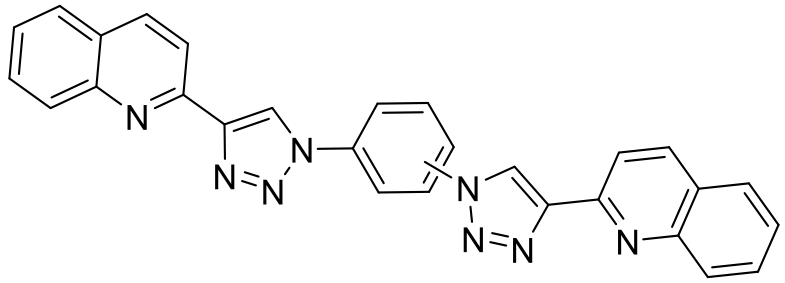

Figure 38: Chemical structure of bis(4-(quinolin-2-yl)-1*H*-1,2,3-triazol-1-yl)benzene ligands.

Moreover, new N^N ligands with different electron withdrawing or donating groups or different triazoles can be synthesised to study the stability, as well as the flattening behaviour of Cu(I) complexes during the excited state and how the resulting luminescent properties of the complexes change. Furthermore, different bridging unit can be used, to evaluate the effect of

the π-conjugation on the luminescent properties of the new compound and also the phosphine ligands can be changed.

In future will be possible to synthetize and study the use of the triazole ring as bridging ligand or to build multicomponent (PS+CAT) systems (possible structure in **Fig. 39**).

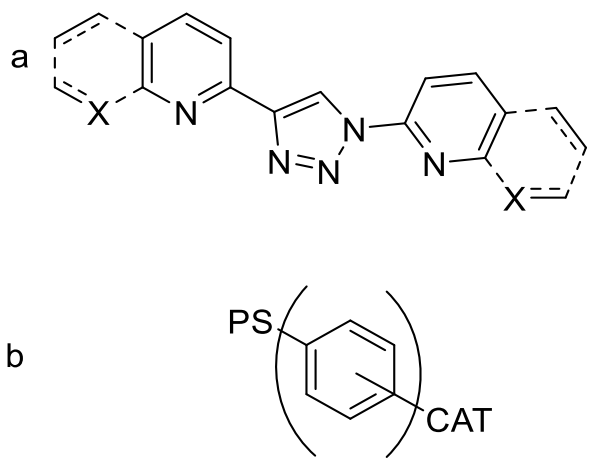

Figure 39: Chemical structure of possible future compounds that can be used in the photoreduction of CO_2, **a**) triazole as bridging unit; **b**) multifunction systems.

The new complexes will have to be fully studied. Photophysical and electrochemical characterisation of the new complexes, in fact, plays a very important role to understand the mechanism of energy and electron transfer, which might occur in photocatalytic processes. In particular, it is important to establish if a PS undergoes oxidative or reductive quenching in a specific system and if this quenching is thermodynamically favoured.

The most promising complexes, which show adequate photophysical characteristics, such as high PLQY and long luminescence lifetimes will be used to prove their activity in the photocatalytic reduction of CO_2.

6- Bibliography

[1] V. Armaroli, N. Balzani, *Energia per l'astronave terra,* Zanichelli, **2017**, 39. (Italian version).

[2] M. Roser and E. Ortiz-Ospina, *World Population Growth, at OurWorldInData.org.*, **2018**.URL: https://ourworldindata.org/world-population-growth (last consulted 5/09/2018)

[3] BP, *Statistical Review of World Energy*, **2018.**
URL: https://www.bp.com/statistical-review-of-world- energy (last consulted 5/09/2018)

[4] a) http://www.iea.org/topics/climatechange/ (last consulted 05/09/2010);
b) A. Rosas-Hernández, C. Steinlechner, H. Junge, M. Beller, *Green Chemistry*, **2017**, *19*, 2356-2360.

[5] N. Armaroli, V. Balzani, *Chem. Eur. J.*, **2016**, *22*, 32 – 57;

[6] a) S. Berardi, S. Drouet, L. Francàs et others, *Chem. Soc. Rev*., **2014**, *43*, 7501-7519.
b) L. Zhao, H. Odaka, H. Ono, S. Kajimoto, K. Hatanaka, J. Hobley, H. Fukumura, *Photochem. Photobiol. Sci*., **2005**, *4*, 113-118.

[7] D. Gust, T. A. Moore, *Acc. Chem. Res.*, **2001**, *34*, 40–48.

[8] DOE/Brookhaven National Laboratory, *Molecular system for artificial photosynthesis*, ScienceDaily, **2017**.
https://www.sciencedaily.com/releases/2017/06/170602112848 (last consulted 13/09/2018)

[9] J. Marshall, *Nature*, **2014**, *510*, 22-24.

[10] Ș. Neațu, J. A. Maciá-Agulló and H. Garcia *Int. J. Mol. Sci.* **2014**, *15*, 5246-5262.

[11] E. E. Benson, C. P. Kubiak, A. J. Sathrum and J. M. Smieja, *Chem. Soc. Rev*., **2009**, *38*, 89–99.

[12] A. J. Morris, G. J. Meyer and E. Fujita, *Accounts of Chemical Research*, **2009**, *12*, 1983-1994.

[13] E. Fujita, *Coordination Chemistry Reviews*, **1999**, *185-186*, 373 – 384.

[14] W. Wang, S. Wang, X. Ma and J. Gong, *Chem. Soc. Rev*., **2011**, *40*, 3703-3727.

[15] M. S. Jeletic, M. T. Mock, A. M. Appel and J. C. Linehan, *J. Am. Chem. Soc*., **2013**, *135*, 11533-11536.

[16] C. D. Windle and R. N. Perutz, *Coord. Chem. Rev*.,**2012**, *256*, 2562-2570.

[17] a) B. Kumar, M. Llorente, J. Froehlich, T. Dang, A. Sathrum and C. P. Kubiak, *Annu. Rev. Phys.Chem*, **2012,** *63*, 541–69;
b) J. Barber, *Chem. Soc. Rev*., **2009**, *38*, 185-196.

[18] T. Yui, Y. Tamaki, K. Sekizawa, O. Ishitani, *Top Curr Chem*, **2011**, *303*, 151–184.

[19] a) J. Bonin, M. Robert, M.Routier, *J. Am. Chem. Soc*., **2014**, *136* (48), 16768-16771;
b) C. Costentin, M. Robert, J. M. Savéant, A. Tatin, *Proc. Natl. Acad. Sci*., **2015**, *112* (22), 6882-6886.

[20] A. Juris, V. Balzani, F. Barigelletti, S. Campagna, P. Belser, A. von Zelewsky, *Coordination Chemistry Reviews* **1988**, *84*, 85-277.

[21] H. Takeda, C. Cometto, O.Ishitani, M. Robert, *ACS Catalysis*, **2017**, *7*, 70-88.

[22] C. Bizzarri, F. Hundemer, J. Busch, S. Bräse, *Polyhedron* **2018**, *140*, 51-66.

[23] C. L. Linfoot, M. J. Leitl, P. Richardson, A. F. Rausch, O. Chepelin, F. J. White, H. Yersin, N. Robertson, *Inorganic Chemistry* **2014**, *53*, 10854-10861.

[24] F. Brunner, L. Martinez-Sarti, S. Keller, A. Pertegas, A. Prescimone, E. C. Constable, H. J. Bolink, C. E. Housecroft, *Dalton Transactions* **2016**, *45*, 15180-15192.

[25] S. Paria, O. Reiser, *ChemCatChem* **2014**, *6*, 2477-2483.

[26] N. Armaroli, G. Accorsi, F. Cardinali, A. Listorti, in *Photochemistry and Photophysics of Coordination Compounds I* , Springer Berlin Heidelberg, **2007**, 69-115.

[27] A. K. Ichinaga, J. R. Kirchhoff, D. R. McMillin, C. O. Dietrich-Buchecker, P. A. Marnot, J.P. Sauvage, *Inorg. Chem.*, **1987,** *26*, 4290–4292.

[28] S. Tschierlei, M. Karnahl, N. Rockstroh, H. Junge, M. Beller, S. Lochbrunner, *ChemPhysChem* **2014**, *15*, 3709-3713.

[29] Y. Zhang, M. Schultz, M. Wachtler, M. Karnahl, B. Dietzek, *Coordination Chem. Rev*., **2018**, *356*, 127-146.

[30] M. W. Mara, K. A. Fransted, L. X. Chen, *Coordination Chem. Rev.* **2015**, *282-283*, 2-18.

[31] a)R. M. Everly, D. R. McMillin, *Photochem. Photobiol.*, **1989**, *50*, 711–716.
b) S. Kuang, D.G. Cuttell, D.R. McMillin, P.E. Fanwick, R.A. Walton, W. Lafayette, *Inorg. Chem.*, **2002**, *41*, 3313–3322.

[32] C.E. McCusker, F. N. Castellano, *Inorg. Chem.*, **2013**, *52*, 8114–8120.

[33] S. Daly, M. F. Haddow, A. G. Orpen, G. T. A. Rolls, D. F. Wass, R. L. Wingad, *Organometallics* **2008**, *27*, 3196-3202.

[34] R. H. Crabtree, *Carbonyls, Phosphine Complexes, and Ligand Substitution Reactions***,** in *The Organometallic Chemistry of the Transition Metals*, Wiley, **2005,** *4*, 87-124**.**

[35] R.A. Rader, D.R. McMillin, M.T. Buckner, T.G. Matthews, D. J. Casadonte, R. K. Lengel, S.B. Whittaker, L.M. Darmon, F. E. Lytle, *J. Am. Chem. Soc.*, **1981,** *103*, 5906–5912.

[36] C. E. A. Palmer, D. R. McMillin, C. Kirmaier, D. Holten, *Inorg. Chem.*, **1987,** *26*, 3167–3170.

[37] M.K. Eggleston, D.R. McMillin, K.S. Koenig, A.J. Pallenberg, *Inorg. Chem.*, **1997,** *36*, 172–176.

[38] S. Tschierlei, M. Karnahl, N. Rockstroh, H. Junge, M. Beller, S. Lochbrunner, *Chem. Phys. Chem.*, **2014,** *15*, 3709–3713.

[39] R. Czerwieniec, M.J. Leitl, H. H. H. Homeier, H. Yersin, *Coord. Chem. Rev*, **2016,** *325*, 2–28.

[40] D.G. Cuttell, S.M. Kuang, P.E. Fanwick, D.R. McMillin, R. a Walton, *J. Am. Chem. Soc.*, **2002,** *124*, 6–7.

[41] E. Mejía, S. Luo, M. Karnahl, A. Friedrich, S. Tschierlei, A. Surkus, H. Junge, S. Gladiali, S. Lochbrunner, M. Beller, *Chem. Eur. J.*, **2013,** *19*, 15972–15978.

[42] M. Nishikawa, S. Sawamura, A. Haraguchi, J. Morikubo, K. Takao, T. Tsubomura, *Dalton Trans.*, **2015,** *44*, 411–418.

[43] a) H. Wamhoff, *In Comprehensive Heterocyclic Chemistry*, A.R. Katritzky, C. W. Rees, *Oxford*, **1984,** *5*, 669;

b) W.Q. Fan, *In Comprehensive Heterocyclic Chemistry II*, A. R. Katritzky, C.W. Rees, E. F. V. Scriven, *Elsevier: Oxford*, **1996,** *4*, 1.

[44] N. Belskaya, J. Subbotina, S. Lesogorova, *Top. Heterocycl. Chem.*, **2015**, *40*, 51–116.

[45] H. Wamhoff, *1,2,3-Triazoles and their benzo derivatives*, A.R. Katritzky, S.W. Rees, E.F.V. Scriven, *Comprehensive heterocyclic chemistry*, Pergamon, *Oxford*, ***1996***, *4*, 669–732.

[46] F. Tomas, J.-L. M. Abboud, J. Laynez, R. Notario, L. Santos, S.O. Nilsson, R. Catalan, R. M. Claramunt, J. Elguero, *J. Am. Chem. Soc.*, **1989**, *111*, 7348.

[47] R. Huisgen, *Angew. Chem. Int. Ed.*, **1963**, *2*, 565 – 598.

[48] Z.Y. Cheng, W.J. Li, F. He, J.M. Zhou, X.F. Zhu, *Bioorg. Med. Chem.*, **2007**, *15*, 1533–1538.

[49] R. Huisgen, R.Grashey, J. Sauer, *Chemistry of Alkenes*, Interscience, **1964**, 806-877.

[50] V. V. Rostovtsev, L. G. Green, V. V. Fokin, K. B. Sharpless Angew. *Chem. Int. Ed.* **2002**, *41*, 2596 – 2599.

[51] J. Kosmrly , *Click triazoles*, *Springer*, New York, **2012**, 1–236

[52] H. C. Kolb, M. G. Finn, K. B. Sharpless, *Angew. Chem. Int. Ed*., **2001**, *40*, 2004 -2021.

[53] a) R. Breinbauer, M. Kohn, *Chem. Bio. Chem*, **2003**, *4*, 1147 – 1149;

b) W. G. Lewis, L. G. Green, F. Grynszpan, Z. Radic´, P. R. Carlier, P. Taylor, M. G. Finn, K. B. Sharpless, *Angew. Chem*., **2002**, *114*, 1095 – 1098.

[54] B. T. Worrell, J. A. Malik, V.V. Fokin, *Science*, **2013**, *340*, 457-460.

[55] C. Bizzarri, A. P. Arndt, S. Kohaut, K. Fink, M. Nieger, *Journal of Organometallic Chemistry*, **2018**, *871*, 140-149.

[56] N. Niamnont, N. Kimpitak, K. Wongravee, P. Rashatasakhon, K. K. Baldridge, J.S. Siegel, M. Sukwattanasinitt, *Chem. Commun*.**, 2013**, *49*, 780-782.

[57] A. K. Feldman, B. Colasson, V. V. Fokin, *Org. Lett*., **2004,** *6*, No.22, 3897-3899.

[58] J. D. Crowley, P.H. Bandeen, *Dalton Trans*., **2010**, *39*, 612-623.

[59] G. J. Kubas, *Inorganic Syntheses* **1979**, *19*, 90.

[60] A. M. Brouwer, *Pure Appl. Chem*, **2011**, *83*, No. 12, 2213-2228.

[61] M. Thelakkat, H.-W. Schmidt, *Adv. Mater*., **1998**, *10*, 219.

7- List of Abbreviations

bpy	Bipyridyl
DCM	Dichloromethane
DMF	N,N-dimethylformamide
DPEPhos	Bis[(2-diphenylphosphino)phenyl] ether
DSSC	Dye-sensitized solar cell
ESI	Electrospray Ionisation
°C	Grad Celsius
g	Gramm
h	Hour
HOMO	Highest occupied molecule orbital
HRMS	High resolution mass spectroscopy
ISC	Intersystem crossing
λ	Lambda
L	Liter
LC	Ligand-centered transition
LECs	Light-emitting electrochemical cells
LUMO	Lowest unoccupied molecule orbital
τ	Luminescence lifetime
M	Molarities in mol/L
MLCT	Metal-ligand charge transfer
m/z	Masse to charge ratio
MeOH	Methanol
mg	Milligramm
min	Minute

mL	Milliliter
mmol	Millimol
mol	Mol
MS	Mass spectroscopy
(N^N)	Diimine ligand
NMR	Nuclear magnetic resonance
OLEDs	Organic light-emitting diodes
(P^P)	Diphosphine ligand
π	Pi
phen	1,10-Phenantroline
PPh_3	Triphenylphosphine
PJT	Pseudo Jahn-Teller
PLQY	Photoluminescence quantum yield
PS	Photosensitizers
R.T.	Room temperature (25 °C)
σ	Sigma
S_0	Ground state
TADF	Thermally activated delayed fluorescence
TLC	Thin layer chromatography
UV	Ultra violet
VIS	Visible light
Xantphos	4,5-Bis(diphenylphosphino)-9,9-dimethylxanthene